TECHNISCHE UNIVERSITÄT MÜNCHEN

Wissenschaftszentrum Weihenstephan für Ernährung, Landnutzung und Umwelt (WZW)

Lehrstuhl für biochemische Pflanzenpathologie

Nitric oxide affects histone acetylation by inhibiting histone deacetylase activity in *Arabidopsis*

Wilhelm Alexander Mengel

Vollständiger Abdruck der von der Fakultät Wissenschaftszentrum Weihenstephan für Ernährung, Landnutzung und Umwelt der Technischen Universität München zur Erlangung des akademischen Grades eines

Doktors der Naturwissenschaften

genehmigten Dissertation.

Vorsitzender:	Univ.-Prof. Dr. E. Grill
Prüfer der Dissertation:	1. Univ.-Prof. Dr. J. Durner
	2. Univ.-Prof. Dr. B. Poppenberger-Sieberer

Die Dissertation wurde am 26.11.2015 bei der Technischen Universität München eingereicht und durch die Fakultät Wissenschaftszentrum Weihenstephan für Ernährung, Landnutzung und Umwelt am 29.02.2016 angenommen.

Publications related to this thesis:

Mengel A, Chaki M, Shekariesfahlan A, Lindermayr C.
"Effect of nitric oxide on transcription – S-nitrosylation of nuclear proteins."
Front Plant Sci., 2013, **4**:293

Chaki M, Shekariesfahlan A, Ageeva A, **Mengel A**, von Toerne C, Durner J, Lindermayr C.
"Identification of nuclear target proteins for S-nitrosylation in pathogen-treated Arabidopsis thaliana cell cultures." *Plant Sci*., 2015, **238**: 115-126

Other publications:

Leitner L, Shaposhnikov D, **Mengel A**, Descot A, Julien S, Hoffmann R, Posern G.
"MAL/MRTF-A controls migration of non-invasive cells by upregulation of cytoskeleton-associated proteins." *J. Cell Sci*., 2011, **124**(Pt 24):4318-31

Table of content

Summary

NO is a ubiquitous signaling molecule operating in different species across the kingdoms. In plants it regulates developmental transitions but is also an important modulator of the plant´s response to biotic and abiotic stresses. However, the molecular mechanisms underlying these functions remain largely elusive. Evidence accumulates that NO exerts most of its effects through covalent modification of cysteine residues on target proteins, resulting in the formation of S-nitrosothiols. S-nitrosylation of histone deacetylases is an important mechanism of transcriptional regulation in animals, however has not been investigated in plants. The aim of this thesis was to elucidate whether and how NO affects histone acetylation in *Arabidopsis* and to infer possible physiological roles of this mode of regulation.

A ChIPseq-experiment revealed that treatment with a chemical NO-donor (GSNO) induced specific changes in the H3K9/14 acetylation pattern in seedlings. Most of these alterations were found within genes involved in the response to biotic and abiotic stresses and the proteasome-mediated degradation of proteins. The majority of NO-regulated H3K9/14ac sites were similarly regulated in the TSA treatment (a strong inhibitor of RPD3/HDA1-like HDACs), indicating that these changes might be induced by NO-dependent inhibition of HDAC activity. Supporting this, a slight but significant increase in total H3ac was observed upon treatment of *Arabidopsis* suspension cells with GSNO. To analyze HDAC activity in response to endogenous NO production an HDAC activity assay in protoplasts was established. Salicylic acid (SA) induced a rapid and strong NO production in protoplasts, which correlated with a decrease in HDAC activity. Scavenging of the NO rescued HDAC activity. Treatment of protoplasts with chemical NO-donors (GSNO and SNAP) similarly resulted in a decrease of HDAC activity, which was reversible upon treatment with a reducing agent, indicating that the inhibition was mediated by S-nitrosylation. The effect of NO on HDAC activity in protoplasts might be caused by either direct modification of HDAC complexes or indirectly by S-nitrosylation of upstream regulatory proteins. To distinguish between these scenarios, HDAC-activity in nuclear extracts was analyzed. GSNO and SNAP strongly and reversibly inhibited nuclear HDAC activity, suggesting that S-nitrosylation of HDACs or directly associated HDAC-regulators might have caused the inhibition of deacetylase activity and hence the H3K9/14ac changes observed in the initial ChIPseq-experiment. To identify the HDAC-isoform(s) targeted by NO, candidates were selected based on sequence homology to human HDAC2, which is a well characterized example for an HDAC regulated by S-nitrosylation. The HDAC domains of *Arabidopsis* HDA6 and HDA19 show high sequence identity to HDAC2 and the cysteines demonstrated to be S-nitrosylated in HDAC2 are conserved in both isoforms. An *hda6* suspension cell line did not show increased H3ac after GSNO treatment and HDAC activity in nuclear extracts prepared from *hda6* could not be inhibited by GSNO. In contrast, HDAC activity in nuclear extracts prepared from *hda6* seedlings was sensitive towards S-nitrosylation, indicating that additional NO-

sensitive HDACs exist. Recombinant HDA6 was S-nitrosylated *in vitro*, however this modification did not affect its basal activity, indicating that S-nitrosylation of other members of the HDA6-complex might be needed to block the activity of the complex. Further, the beneficial effect of a NO-pretreatment on subsequent salt-stress was completely abrogated in the *hda6* mutant, indicating that NO exerts parts of its function during salt-stress through acting on HDA6.

In summary, this work revealed a new function of NO as an inhibitor of HDAC activity, probably by direct S-nitrosylation of HDAC-complexes. This mechanism might play a role during the plant´s stress response to enhance transcription of stress-related genes by inducing histone acetylation at the corresponding loci. In conclusion, this work provides a mechanistic insight into stress-mediated alterations of histone acetylation and demonstrates that NO regulates transcription not only by modifying transcription factors but also by modulating the chromatin structure.

Abbreviations

BCIP	5-Bromo-4-chloro-3-indoxylphosphate
BDNF	Brain derived neurotrophic factor
Bis-Tris	Bis- Tris(hydroxymethyl)aminomethane
ChIP	Chromatin immunoprecipitation
ChIPseq	Chromatin immunoprecipitation followed by deep-sequencing
cPTIO	2-(4-Carboxyphenyl)-4,4,5,5-tetramethylimidazoline-1-oxyl-3-oxide
Cys	Cysteine
DAF-FM DA	4-amino-5-methylamino-2´,7´-difluorofluoresceine diacetate
DMSO	Dimethylsulfoxide
DNA	Deoxyribonucleic acid
DTT	Dithiothreitol
E. coli	Escherichia coli
EDTA	Ethylenediaminetetraacetic acid
FDR	False discovery rate
Flg22	Flagellin 22
GSH	Glutathione
GSNO	S-Nitrosoglutathione
GSSG	Glutathione disulfide
GST	Glutathione-S-transferase
H1,2,3,4	Histone 1, 2, 3, 4
H3K9/14ac	Histone 3 lysine 9 and lysine 14 acetylation
HAT	Histone acetyltransferase
HDAC	Histone deacetylase
HDT	Plant specific histone deacetylase family
HEPES	4-(2-hydroxyethyl)-1-piperazineethanesulfonic acid
His_6-tag	Hexa-histidine-tag
INA	2, 6-Dichloro-isonicotinic acid
ko	knock-out
LC-MS	Liquid chromatography coupled to mass spectrometry
LPS	Lipopolysaccharide
MAPK	Mitogen associated protein kinase
MES	2-(N-morpholino)ethanesulfonic acid
MS-medium	Murashige-Skoog medium
MW	Molecular weight
NADPH	Nicotinamide adenine dinucleotide phosphate
NBT	Nitroblue tetrazolium
NEM	N-ethylmaleimide
NIBA	Nuclei isolation buffer A
NLB	Nuclear lysis buffer
NO	Nitric oxide
NOS	Nitric oxide synthase
NRBT	Nuclei resuspension buffer with Triton-X100
N-terminal	Amino-terminal
PAGE	Polyacrylamide gel electrophoresis

PBS	Phosphate buffered saline
PCD	Programmed cell death
PHD	plant homeodomain
PR-gene	Pathogenesis related gene
PS I	Photosystem I
PS II	Photosystem II
PTM	Posttranslational modification
RNS	Reactive nitrogen species
ROS	Reactive oxygen species
RPD3-like	Reduced potassium deficiency 3 like
SA	Salicylic acid
SDS	Sodium dodecyl sulfate
SEM	Standard error of the mean
SNAP	S-Nitroso-N-acetylpenicillamine
S-phase	Synthesis phase of cell cycle
TBS	Tris-buffered saline
TBS-T	Tris-buffered saline with Tween
TF	Transcription factor
TMV	Tobacco mosaic virus
Tris	Tris(hydroxymethyl)aminomethane
TSA	Trichostatin A
TSS	Transcriptional start site
wt	wild-type

List of Figures and Tables

Figures

Tables

Supplementary figures

1 Introduction

1.1 Concepts of redox-signaling

Cells maintain a reducing intracellular environment since oxidizing conditions - due to production of radicals - are potentially very harmful. Radicals are involved in many deleterious processes in cells like lipid peroxidation, DNA crosslinking and formation of disulfide bonds in proteins [4]. Under stress conditions but also during developmental transitions the intracellular redox environment can undergo temporal fluctuations changing from reducing to oxidizing conditions. Initially considered to be solely harmful, it was soon recognized that these redox changes fulfill important signaling functions, leading to the concept of redox-signaling. Classical signaling cascades rely on the transient association and dissociation of macromolecular complexes converging on transcription factors and leading to transcriptional responses. In contrast, during redox-signaling small redox-molecules (reactive oxygen (ROS) or nitrogen species RNS) covalently modify target proteins resulting in structural changes and altered activities of these proteins. Plants produce a variety of ROS and RNS each with distinct chemical properties and the nature of the redox-molecule as well as the temporally and spatially controlled synthesis of these species determines the signaling output. Superoxide (O_2^-) is produced in PS I and II during the light reaction as well as by plasma membrane located NADPH oxidases. O_2^- can be converted to hydrogen peroxide (H_2O_2) by peroxidases or – in the presence of certain metal ions – to the highly reactive hydroxyl radical $OH^\cdot$ (Fenton reaction) [5]. Nitrix oxide (NO) and the reaction product of NO with O_2^-, peroxynitrite (ONO_2^-), are examples of RNS with distinct signaling functions. Each type of ROS and RNS has preferred and largely distinct perception mechanisms determined by the different redox-potentials: O_2^- preferentially reacts with iron-sulfur clusters, H_2O_2 and NO modify cysteine residues and ONO_2^- binds covalently to tyrosine residues. Among these, cysteine modification seems to be particularly important. Under non-stressed conditions cysteines are reduced but upon changes towards a more oxidizing environment they can - depending on the nature and concentration of the redox-molecules as well as the microenvironment and accessibility of the cysteine - undergo different posttranslational modifications ranging from S-nitrosylation to S-glutathionylation, hydroxylation and oxidation to sulfinic, sulfenic or sulfonic acid [6]. With the exception of fully oxidized cysteines, all of these PTMs are reversible (either enzymatic by thioredoxins and glutaredoxins, or non-enzymatically by light or heavy metal ions), thereby fulfilling a critical prerequisite as a cellular signal. One prototypic example of a protein which senses and signals ROS and RNS is the bacterial transcription factor OxyR. Specific cysteine residues of OxyR can undergo redox-dependent posttranslational modifications like oxidation to sulphinic acid, S-glutathionylation or S-nitrosylation. Each of these modifications affects binding affinity and specificity of OxyR to DNA thus resulting in distinct transcriptional

responses [7]. In eukaryotes, redox signaling is often more complex than the simple one-component systems found in bacteria. For instance, redox-sensors can modulate classical signaling pathways like the MAPK phosphorylation cascade resulting in a very complex interplay between both types of signaling [8].

Redox-signaling in plants occurs in various physiological as well as pathophysiological contexts. Many developmental transitions (for instance flowering or root development) are marked by changes in the intracellular redox-potential associated with extensive redox-signaling and in tight interplay with plant phytohormones [9, 10]. Moreover, ROS and RNS signaling regulate cell cycle progression and cell differentiation offering the possibility to integrate environmental signals and adjust the cellular response to external biotic or abiotic cues [5]. Redox-signaling also plays a fundamental role in the perception and transduction of environmental stresses like salt, drought, heat or cold stress [11-13]. Finally, the plant´s immune response is modulated by redox-mediated posttranslational modifications of key regulators, like NONEXPRESSOR OF PATHOGENESIS RELATED 1 (NPR1), TGA1 or the MAPK *Arabidopsis* NPK1-like protein kinase (ANP1) [8, 14, 15].

1.2 NO-signaling in plants

NO is a very important redox-signaling molecule in all kingdoms, operating in many different physiological processes (**Fig. 1**). In plants, NO modulates the response to biotic and abiotic stresses like drought, heat, cold and pathogen-infection but is also a crucial developmental regulator involved in root development, germination and flowering.

1.2.1 Physiological functions of NO-signaling

The first reports about NO in plants described its role in the plant´s defense response. Pharmacological NO-donors potentiated the induction of the hypersensitive disease response in soybean cells in response to pathogen infection, whereas inhibitors of NO-synthase (derived from the animal field) compromised this response [16]. Independently, Durner et al. demonstrated that NOS activity (section 1.2.2) increased after infection of tobacco with TMV and that the subsequent induction of defense genes involved NO, cyclic GMP and cyclic ADP-ribose [17]. NO production in response to elicitor treatment could also be detected in tobacco plants [18]. A knockout mutant of one of the central NO metabolizing enzymes (S-nitrosoglutathione reductase, GSNOR) showed increased disease susceptibility, highlighting the central role of NO and S-nitrosothiols (section 1.2.3.3) in the plant´s disease response [19]. NO also controls the subcellular localization of a master regulator of systemic defense, NPR1, although the exact molecular details of this mechanism still remain controversial [14, 15, 20]. Interestingly, NO modulated the activity of RESPIRATORY BURST OXIDASE HOMOLOG D (RBOHD) in the later stages of the hypersensitive response, possibly

indicating that NO functions in a negative feedback loop to control the amplitude of the cell death response [21]. Together, several lines of evidence suggest a critical role of NO during the plant´s immune response, probably through crosstalk with SA and other reactive oxygen species signaling pathways.

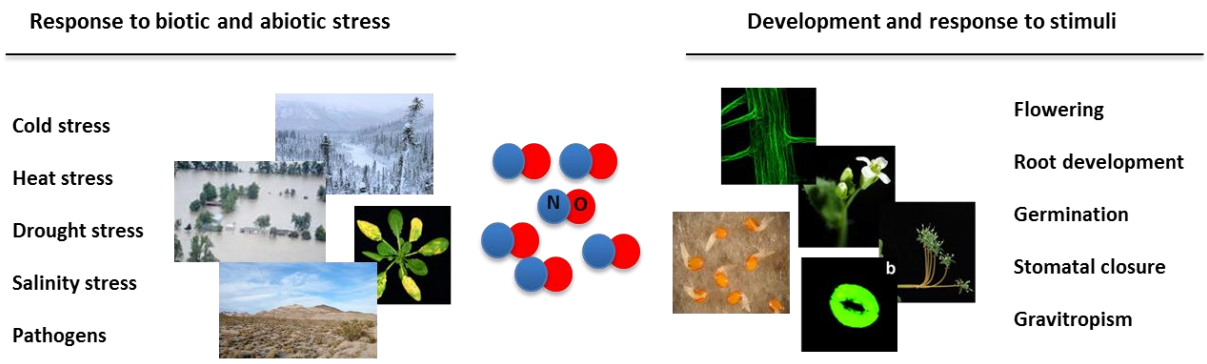

Figure 1: Physiological functions of NO. NO is involved in the plant´s response to stress (left) but is also an important regulator of developmental processes (right). See text for details. The references for the pictures are listed in Suppl. References.

Soon, NO was recognized to be a key regulator of the abiotic stress response. The plant hormone abscisic acid (ABA) induced NO synthesis in guard cells - presumably via intermediate production of H_2O_2 - and NO-scavengers impaired ABA mediated stomatal closure, implying a critical role of NO/ABA crosstalk in stomata regulation [22] [23]. Given the role of NO in stomatal closure it is not surprising that mutants impaired in NO synthesis showed increased susceptibility towards water stress (drought and salt stress). Moreover, salt stress induced S-nitrosylation in mitochondrial proteins from pea which were involved in respiratory and photorespiratory pathways, indicating that NO might regulate these processes under salt stress [24]. During cold stress, NO both served as an antioxidant to scavenge reactive oxygen species but also participated in signaling by activating the expression of the master cold regulators CBF1 and CBF3 (CRT/DRE binding factor 1 and 3) [12, 25]. Another example for NO as a key regulator of abiotic stress response is heat stress. A mutant which was defective in the catabolism of SNOs showed increased susceptibility towards higher temperatures, which could be rescued by addition of NO scavengers [26].

NO further functions as an important developmental regulator. NO was demonstrated to be required for proper root development in cucumber explants and *Arabidopsis* roots by directly modulating root meristem morphology and activity [27, 28]. Another study showed that gravitropic bending in soybean roots was dependent on the synthesis and proper distribution of NO and cGMP [29]. Based on the observation that mutants with higher endogenous NO levels showed a delayed transition towards reproductive development, He et al. inferred a critical role of NO in the regulation of flowering time. The proposed mechanism involved the transcriptional repression of key flowering inducers (CONSTANS and GIGANTEA) as well as the induction of the floral repressor FLOWERING LOCUS C (FLC) by NO

[30]. Modulation of flower development by NO was also reported [26]. Moreover, an important role of NO during germination was uncovered by using chemical NO donors and scavengers [31].

In summary, NO has emerged as an important modulator of many processes in plants, ranging from stress response to development. However, until now no strict requirement for NO in any physiological process has been reported in plants, which is in contrast to the animal field.

1.2.2 Pathways for NO biosynthesis in plants

In mammals, NO synthesis is accomplished by three cell-type specific NO synthases (NOS), which oxidize L-Arginine to citrulline thereby releasing NO. Although no structural homologue could be identified in higher plants, several studies indicate the presence of a NOS-like activity. First, mammalian NOS inhibitors reduced NO production during the nitrosative burst after pathogen attack [16, 17]. This NOS-inhibitor sensitive activity could be detected in many other studies. Furthermore, an arginine-dependent NO synthase activity in pea was detected, which was differentially regulated throughout the developmental stages and different tissues [32]. These data are supported by a commonly used NO mutant (nox1) which has elevated arginine, citrulline and NO levels [30]. Other possible substrates for oxidative NO production involve polyamines and hydroxylamine, however, the molecular details and specifically the involved enzymes are still elusive (**Fig. 2**).

Reduction of nitrite to NO constitutes the second main route of NO production (**Fig. 2**). Nitrate reductase usually catalyzes the reduction of nitrate to nitrite. Under special conditions i.e. low oxygen concentrations, light and high nitrite levels, an alternative reaction mechanism has been described, namely the reduction of nitrite to NO [33]. This pathway only constituted a minor part of nitrate reductase activity, however, has been implicated in the endogenous NO production in several processes like elicitor induced NO production in tobacco protoplasts or stomatal closure [34, 35]. At very low oxygen concentrations, nitrite can also be reduced to NO via cytochrome c oxidase / reductase in the inner mitochondrial membrane, but the biological significance of this mechanism has to be determined [36]. Finally, NO can be produced non-enzymatically at acidic conditions and high nitrite levels, but this mechanism is unlikely to operate in physiological conditions. In summary, NO production in plants is a debated and rather unresolved issue with many open questions. Important information like spatial and temporal control of NO synthesis is still lacking and the unambiguous detection of NO is rather challenging.

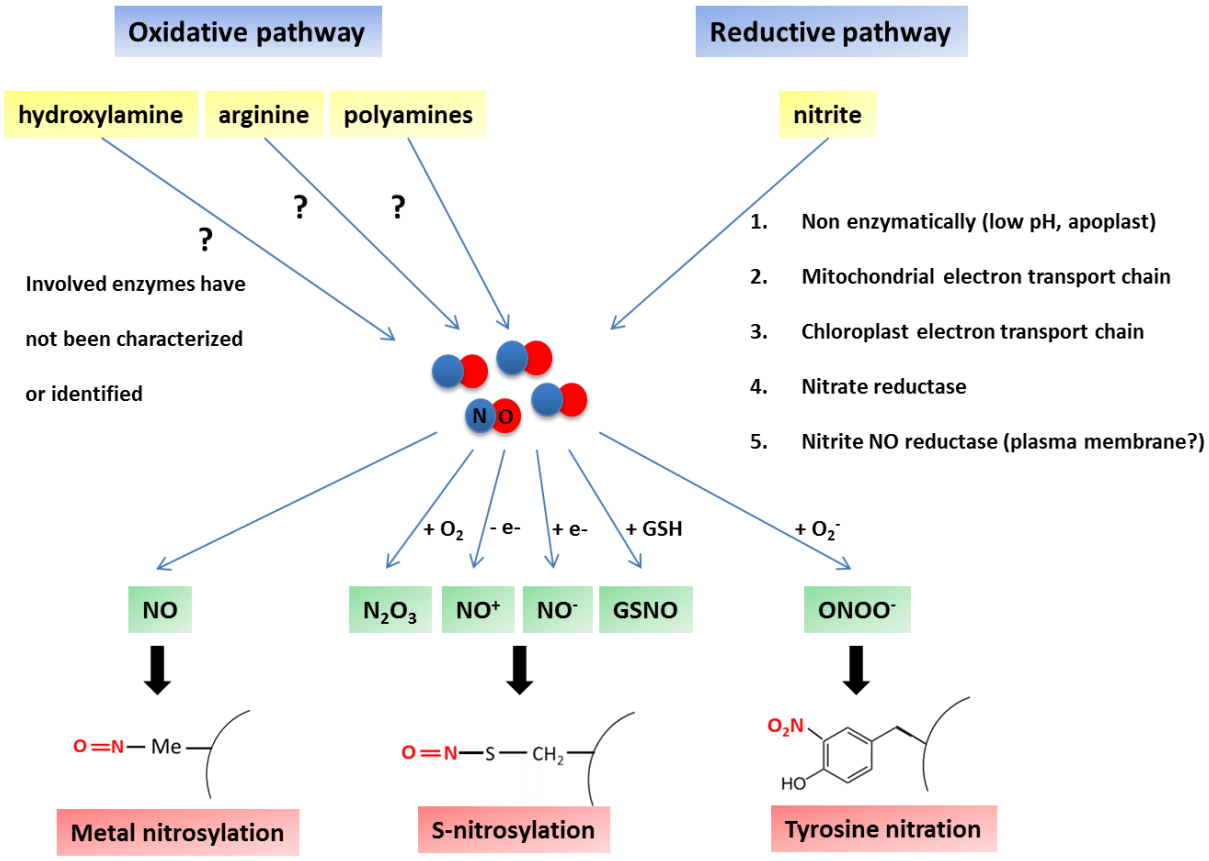

Figure 2: Routes of NO production in plants and transduction of its bioactivity by posttranslational modifications. The oxidative pathway uses arginine, polyamines or hydroxylamine as substrates for NO production. The enzymes catalyzing these reactions have not been found. The reductive pathway is based on Nitrate reductase activity, which can reduce nitrite to NO under defined conditions. Other pathways described to reduce nitrite to NO include the electron transport chains in the chloroplast and mitochondria. NO then either directly binds metal centers in metalloproteins (metal nitrosylation) or further reacts to give species that bind to cysteine (S-nitrosylation) or tyrosine residues (tyrosine nitration). Symbols: NO: nitric oxide, e- : electron, GSH: glutathione, N_2O_3: Dinitrogen trioxide, NO^+: nitroxyl cation, NO^-: nitrosonium anion; O_2^-: superoxide radical, $ONOO^-$: peroxynitrite.

1.2.3 Transduction of NO bioactivity

As mentioned before, redox-signaling molecules transduce their bioactivity by direct covalent binding to target proteins. NO exerts most of its functions by reacting with cysteine residues in proteins (S-nitrosylation). However, NO can also be ccordinated to metal-ion cofactors (metal nitrosylation) or bind to tyrosine residues (tyrosine nitration).

1.2.3.1 Signal transduction via metal-nitrosylation

Metal nitrosylation refers to the dative binding of NO to the metal center of metallo-proteins (**Fig. 2**). NO acts as electron donor (Lewis acid), the metal ion is the corresponding electron acceptor (Lewis base). In mammals, NO produced by NOS proteins can bind to the iron atom in a heme moiety of soluble guanylate cyclase, which induces a conformational switch of the protein, resulting in the activation and production of the second messenger cGMP [37]. In plants, information about metal-nitrosylation is rather sparse. It was early demonstrated

that the non-heme iron of soybean Lipoxygenase-1 could coordinate NO, which displaced the substrate linoleic acid. The physiological role of this competitive inhibition remained unresolved [38]. When grown in the absence of nitrate, soybean root nodules accumulated a symbiotic leghemoglobin-NO adduct [39] and later it was demonstrated that oxy-leghemoglobin can scavenge NO and peroxynitrite formed during the nodulation, thereby possibly preventing the induction of defense responses [40]. Moreover it was shown that class I hemoglobins can bind NO and catalyze the conversion to nitrate [41]. Finally, the activites of cytochrome c oxidase [42], aconitase [43], catalase and ascorbate peroxidase [44] were reversibly inhibited by binding of NO to the catalytic metal ion.

1.2.3.2 Signal transduction via tyrosine nitration

Tyrosine nitration refers to the covalent attachment of peroxynitrite to tyrosine residues in ortho-position to the hydroxyl-group. Peroxynitrite is the product of the reaction of superoxide (O_2^-) with NO and is formed during severe oxidative and nitrosative stress conditions [45]. Tyrosine nitration preferentially occurs in solvent accessible regions and acidic residues promote this modification [46]. Total protein nitration increased strongly during the defence response in *Arabidopsis* or in response to salt stress in the root tips of sunflower seedlings [47-49]. Protein nitration exclusively inhibited protein activity in all the examples reported so far. For instance, some superoxide dismutases, which are important antioxidants during the defence response, were inhibited by peroxynitrite, possibly via blocking the access to the active site [50]. Other examples include the inhibition of ferredoxin NADPH oxidoreductase from sunflower [51], glutamine synthetase 1 from *Arabidopsis* [52] and O-acetylserin-thiol ligase from *Medicago* [53]. Moreover, a role in modulating MAPK signaling was discussed since tyrosine nitration precludes phosphorylation of this tyrosine [54]. Initially, protein nitration was considered to be an unavoidable consequence of oxidative and nitrosative stress, but recently a signaling function of this modification is emerging. However, it has to be stated that the reversibility of tyrosine nitration - a critical prerequisite for any signaling pathway – has not been demonstrated so far.

1.2.3.3 Signal transduction via S-nitrosylation

Most of the proteinogenous cysteine residues are buried in the inner hydrophobic core of the protein, thereby being shielded from posttranslational modifications. However, a small subset is located at the outer, solvent accessible surface and these are often characterized by an atypically low pKa-value. The low pKa-value correlates with a high nucleophilicity of the corresponding sulfur atom and this in turn is a prerequisite to react with various redox-molecules [55]. These redox-switchable cysteines can undergo different posttranslational modifications, depending on the nature and concentration of the specific redox-molecule present around the cysteine [6]. Among these, S-nitrosylation, which formally describes the covalent attachment of NO to cysteine residues, is emerging as one of the most important redox-modifications. In addition to low pKa-values the targeted cysteines are often

embedded within hydrophobic pockets with positively and negatively charged amino acids nearby [56].

The exact mechanism of S-nitrosothiol formation is still not entirely understood. The direct formation of NO with thiol-groups is too slow to occur *in vivo* and therefore other NO-derived species have been proposed to mediate S-nitrosylation. Among these, N_2O_3 which is the reaction product of NO and O_2, appears to be the most promising candidate [57]. Because the formation of N_2O_3 is accelerated in hydrophobic environments, this could explain why S-nitrosylated cysteines often lie within hydrophobic pockets. Other S-nitrosylating species include the nitroxyl and nitrosonium ion, which derive from NO by removal or addition of one electron, respectively [58]. Since plant cells contain millimolar concentrations of GSH it is assumed that a major part of NO first reacts with this cysteine-containing tripeptide [59]. Indeed, S-nitrosylated GSH (GSNO) is considered to be a stable reservoir of NO bioactivity. In a process called trans-nitrosylation GSNO can then transfer its NO-moiety to susceptible cysteine residues on target proteins. This process has been well characterized in animals [58, 60], in plants, however, only indirect evidence for trans-nitrosylation is available: An *Arabidopsis* mutant lacking an enzyme catabolizing GSNO (GSNO reductase, GSNOR) shows globally increased protein S-nitrosylation accompanied by developmental defects and increased susceptibility towards abiotic and biotic stresses, highlighting the diverse functions of S-nitrosothiols in plants [19, 26, 61].

Similar to other PTMs like phosphorylation, S-nitrosylation can affect protein-function in different ways. I) Effect on enzyme activity. Examples include the inhibition of members of the S-adenosylmethionine cycle [62], modulation of peroxiredoxin II E activity [63] and inhibition of SA-BINDING PROTEIN 3 (AtSABP3) carbonic anhydrase activity [64]. II) Subcellular localization. For instance, the redox status of NPR1 controls the nuclear/cytosolic distribution of this protein [14, 15] and S-nitrosylation of GAPDH mediated its nuclear translocation in mammalian cells [65] where it initiated apoptotic cell death. III) Association with binding partners. For instance, S-nitrosylated GAPDH bound to Siah1, an E3 ubiquitin ligase, which triggered its nuclear import [65]. As expected from the ubiquitous function of NO, S-nitrosylated proteins have been detected in many physiological processes in the plant, including immune response, abiotic stresses like cold, heat or salt stress and after heavy metal application [24, 66, 67] (see also 1.2.1).

1.3 Epigenetic regulation of transcription

What defines the identity of a cell? It cannot be the DNA itself since every cell of an organism contains the same DNA molecules. Moreover, once differentiation of a cell is achieved, progenitors of these cells are usually from the same cell type. How is this cell identity inherited? This is the field of epigenetics, which describes heritable patterns of phenotypic variation, which are not just caused by changes in the DNA sequence [68]. Very

often this strict definition is relaxed by including changes in the chromatin state (histone modifications), which are not always heritable into the epigenetic toolbox. In this work, the term epigenetic will be used in its relaxed definition, including stable, heritable changes (DNA methylation, histone variants, some miRNA based effects) as well as transient alterations in the chromatin state (most histone modifications, **Fig. 3**). In the past decades it has emerged that epigenetic mechanisms constitute a second layer of transcriptional control, which – in many cases – excels transcriptional regulation by classical transcription factors.

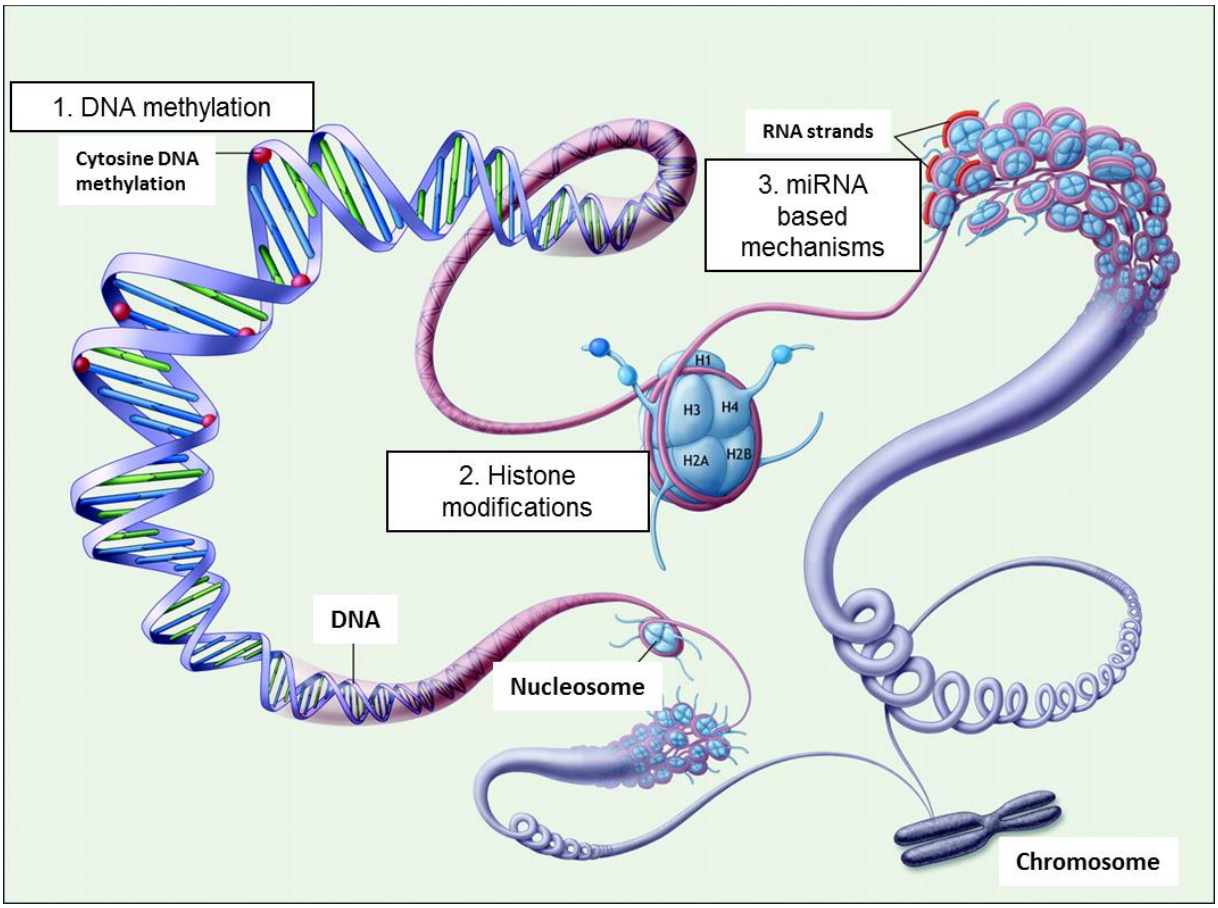

Figure 3: Chromatin structure and epigenetic mechanisms of gene regulation. See text for details. Modified from [69].

1.3.1 Hierarchical organization of the chromatin structure

In eukaryotes, the genetic information is stored in the cell nucleus. The total length of *Arabidopsis* DNA in each cell is approximately 4.6 cm, but has to fit in the cell nucleus, which is around 5 µM in diameter. To achieve this, DNA has to be folded into higher order structures, resulting in a strongly decreased contour length of the DNA but allowing the temporally and spatially controlled access of the transcriptional machinery and other transcriptional regulators to specific regions. The basic packaging unit of chromatin is the so called nucleosome in which a stretch of DNA is wrapped around a protein core consisting of eight histone proteins. Histones are small, basic proteins which show a remarkable structural conservation throughout evolution, indicating the importance and functional specification of

this protein group. There are four different core histone proteins, H2A, H2B, H3 and H4. Despite their sequence divergence, all histones have a very similar 3D fold consisting of a large central α-helix and two smaller helices at each end connected to the central helix by small loops. H2A/H2B and H3/H4 form heterodimers and two of each dimers form the histone octamer around which DNA is wrapped. Conserved arginine residues stick out from this protein core promoting binding of the negatively charged phosphate backbone of the DNA. In a nucleosome, 146 bp of DNA are wrapped in 1.7 negative superhelical turns around the protein core. Importantly, DNA is mainly bound via its phosphate backbone and no sequence specific interactions are formed. From the central protein core, the N-termini of histones are protruding [70]. These regions are rich in lysine, arginine, serine and threonine residues and also participate in DNA binding. Moreover, these residues are extensively modified by phosphorylation, ubiquitination, ADP-ribosylation, methylation and acetylation (see below). Each nucleosome is separated by the next through a 50 bp DNA stretch called linker DNA (beads on a string structure). Nucleosomes are then arranged into higher order structures with the help of linker histones (H1) and other proteins giving rise to the solenoid-like shaped 30 nm fibre and after further looping to the mitotic chromosome representing a 50 000 fold compaction of the original DNA molecule [70] (**Fig. 3**).

Under the light microscope, two different appearance forms of interphase chromosomes can be distinguished. Heterochromatin represents highly condensed, transcriptionally inactive chromatin (for instance pericentromeric or telomeric DNA), whereas euchromatin appears as loosely packed, transcriptionally active chromatin. Both euchromatin and heterochromatin are defined by specific histone modification and DNA methylation patterns, which will be detailed in the following section. Moreover, several functional ultrastructural chromatin domains have been identified. Lamina-associated domains (LADs) represent chromatin fragments of varying sizes, which mediate the attachment to the nuclear lamina [71]. Topologically associated domains (TADs) are developmentally and cell-type specific stable units of transcription and replication timing regulation [72]. These domains are typically separated by the insulator-protein CCCTC-BINDING FACTOR (CTCF) and/or distinct DNA methylation patterns [71].

1.3.2 Determinants of the chromatin state

Chromatin structure is not static but undergoes significant alterations during development or biotic and abiotic stresses [73, 74]. The chromatin state is determined by different post-translational modifications of histones as well as by the usage of histone variants and DNA methylation [75]. Together, these features determine the local structure of the chromatin and thus control the accessibility of certain regulatory proteins to the DNA, in turn controlling important molecular processes like transcription or replication.

1.3.2.1 DNA methylation

DNA methylation at cytosine residues (5-methylcytosine, 5mC) has clearly been established as one of the major determinants for epigenetic gene silencing and hence heterochromatin formation. In plants, 5mC is found in three different sequence contexts, namely within CG, CHG and CHH motifs (H stands for A, T or C) which differs from mammalian cells, in which this modification is almost exclusively found in CG sites. 5mC is mainly located within repetitive regions of the genome including centromeric regions or rDNA repeats. Only a minority was found in promoters or within gene bodies, the latter potentially being important during pre-mRNA splicing [76].

In plants, DNA methylation patterns are established during development by siRNA directed de novo methylation (RNA directed DNA methylation, RdDM) and maintained throughout replication by maintenance methyltransferases. Plants possess homologs of all families of mammalian methyltransferases (for instance MET1, DRM) and additionally a plant specific group called chromomethylases, which is characterized by the presence of a methyl-histone binding chromodomain [75]. This implies the presence of a crosstalk between histone patterns and DNA methylation in which repressive histone modifications recruit enzymes for DNA methylation thus reinforcing the repressive chromatin state [77]. DNA-methylation is a reversible process. In *Arabidopsis* active demethylation is catalyzed by REPRESSOR OF SILENCING 1 (ROS1), DEMETER (DME) and DEMETER-LIKE proteins (DML2, -3) which are characterized by a DNA glycosylase domain cutting out the 5mC [78]. Besides active demethylation, 5mC can be passively lost if not properly established on the daughter strand during replication or after DNA repair [75].

5mC constitutes a mark for gene repression. The exact details how this mark is transduced into a repressive chromatin state are unknown. However, several proteins have been identified which bind to 5mC; this is accomplished by specialized modules like METHYL-C-BINDING DOMAIN (MBD) or SET and RING-finger ASSOCIATED (SRA) domains. These proteins serve as adapters for other proteins, which then cooperatively promote changes in the chromatin structure.

1.3.2.2 Histone variants

Together with histone modifications, histone variants determine the physical stability of nucleosomes as well as the propensity to be replaced or relocated along the DNA. Eukaryotes have evolved variants of H2A and H3, which are inserted into nucleosomes during interphase by large ATP-dependent remodeler complexes (canonical histones are incorporated during S-phase of the cell cycle). These remodeler complexes also displace and remove histones from the DNA, thereby critically regulating the chromatin state.

H2AX contains a unique serine residue in its C-terminus, which is phosphorylated at sites of DNA damage. This probably serves as a signal for other DNA repair enzymes to be recruited to these places [79]. The primary sequence of H2A.Z differs from H2A at many positions,

however, amino acid substitutions accumulate at the C-terminus. Immunoprecipitation followed by deep sequencing (ChIPseq) revealed that this variant was primarily located in nucleosomes flanking the transcriptional start sites where it possibly regulates transcription of the corresponding genes [80]. Centromeric chromatin is characterized by the presence of the H3 variant CenH3, which serves as a platform for kinetochore assembly and microtubule attachment thereby regulating segregation of sister chromatids during mitosis [79]. Another H3 variant, H3.3, is primarily located in regulatory regions and expressed genes, but the functional significance has not been resolved so far. In contrast to the core histones, linker histones (H1) display significant diversity including stress-induced variants. Disturbed expression of these genes resulted in hypomethylation of DNA and diverse phenotypic defects [81].

1.3.2.3 Histone modifications

The N-terminal tails of histones are rich in lysine, arginine and serine residues which are subjected to diverse posttranslational modifications (acetylation, methylation, ubiquitination, phosphorylation and ADP-ribosylation). Each of these modifications introduces negative and/or neutralizes positive charges on the histone, resulting in a weakening of the interaction with DNA. Histone modifications not only alter the interaction with DNA but also serve as binding sites for proteins. These proteins contain specific domains which recognize and bind certain modified histone residues. For instance: chromodomains, CW-domains and PHD-domains recognize methylated whereas bromodomains bind acetylated lysine residues of histones. By combining several of these domains, for example in large multiprotein complexes, distinct modification patterns, the so called histone-code, can be translated into distinct transcriptional or epigenetic responses. Since ADP-ribosylation is not well described in plants, only ubiquitination, phosphorylation, methylation and acetylation will be detailed in the following sections.

1.3.2.3.1 Ubiquitination and phosphorylation

Ubiquitination occurs on all histones, however, most of the studies focused on H2A and H2B monoubiquitination (H2Aub1 and H2Bub1). In contrast to K48 linked polyubiquitin chains, attachment of a single ubiquitin molecule is not a signal for degradation via the proteasome, but fulfills important signaling functions. H2Aub1 is installed by POLYCOMB REPRESSIVE COMPLEX1 – like complexes (RING finger E3) and results in transcriptional silencing of the corresponding locus. It was shown that PRC1-like complex mediated H2A-ubiquitination was important to suppress embryonic and stem cell regulators, thereby defining and keeping cell identity [82]. In contrast, H2Bub1 is rather associated with transcriptional activation of genes. For example, H2Bub1 of the FLOWERING LOCUS C chromatin resulted in expression of FLC and repression of the floral transition [83]. This modification is catalyzed by the E3 enzymes HISTONE MONOUBIQUITINATION1 (HUB1) and HUB2 in cooperation with the E2 enzymes AtUBC1, AtUBC2 and AtUBC3. Deubiquitination is catalyzed by ubiquitin proteases

(UBPs). Among the putative *Arabidopsis* homologs, only UBP26 was identified to cleave H2Bub1 labels. This protein was demonstrated to be involved in the suppression of transgenes and transposons as well as in the heterochromatin formation at particular genes [84].

In plants, serine 10 and 28 of H3 are subjected to phosphorylation specifically in the pericentromeric region during mitosis and meiosis. In contrast, phosphorylation of threonine 3 and 11 occurs along the whole chromosome arm, correlating with the condensation of mitotic and meiotic chromosomes [85]. The functional significance of these modifications has not been resolved so far, although a model has been proposed in which the different histone phosphorylations identify different regions on the chromosome, allowing to monitor these regions through the progression of the cell cycle [85]. Histone phosphorylation is likely mediated by Aurora kinases, which are highly expressed in dividing cells, localize to centromeres and the mitotic spindle and show *in vitro* phosphorylation of H3S10 [86].

1.3.2.3.2 Methylation

Methylation is one of the most important posttranslational modifications of histones. In contrast to other PTMs like acetylation, the effect of methylation on transcription depends on the specific lysine or arginine residue and the number of attached methyl-groups (for instance, lysines can be mono-, di- or trimethylated). H3K4me2 and H3K4me3 are strongly enriched at the 5´ end of transcriptionally active genes. Similarly, H3K9me3 is primarily found at expressed euchromatic genes. In contrast, H3K27me3 is distributed broadly through the gene body of inactive, repressed genes. Finally, H3K9me2 is associated with transposons embedded in highly compacted facultative heterochromatin [87, 88].

Histone methytransferases are characterized by a conserved SET-domain (Suppressor of variegation (Su(var)3-9), Enhancer of Zeste (E(z)), Trithorax (TRX)). SET-domains catalyze the nucleophilic attack of the deprotonated lysine substrate on the S-adenosylmethionine cofactor thereby generating a methylated lysine residue. Three different subclasses of SET-domain containing proteins can be distinguished in plants and other organisms. Members of the Su(var)3-9 subgroup use H3K9 as substrate, whereas E(z) subgroup proteins preferentially methylate H3K27. The latter group comprises Polycomb (PcG) proteins, which are important transcriptional suppressors in eukaryotes. In contrast, TrxG proteins mainly act on H3K4 and H3K36, thereby establishing key marks associated with active transcription [89]. Methylation is one of the most stable histone PTMs, however, can be removed by the action of demethylases. Two classes of demethylases have been identified (lysine specific histone demethylase-LIKE (LDL) proteins and JUMONJI-C-DOMAIN (JmjC) proteins), which are characterized by different catalytical mechanisms [75].

Mutants defective in histone methylation often show severe and pleiotropic phenotypes highlighting the exceptional role of this modification for gene expression. Phenotypes range

from abnormal development (for instance early flowering) to root and leaf morphological defects and disturbed responses to biotic and abiotic stresses [90].

1.3.2.3.3 Acetylation

One of the most important determinants for chromatin structure is histone acetylation. This modification neutralizes the positive charge of the ε-amino group of lysines, thereby weakening the interaction with the negatively charged phosphate backbone of the DNA resulting in an opening of the chromatin and facilitated access of transcriptional regulators or polymerases. Accordingly, histone acetylation strongly correlates with transcriptionally active chromatin, whereas heterochromatin or silenced genes are generally characterized by hypoacetylated histones. Several lysines on H3 and H4 have been identified to undergo acetylation. Most of these modifications are strongly enriched at promoter regions of actively transcribed genes and are absent from silenced loci. Moreover, histone acetylation is found more often in longer genes than in short ones [87].

Histone acetylation is controlled by two enzyme families. Histone acetyltransferases (HATs) use acetyl-CoA as cofactor to transfer acetyl groups on histone-lysines. They can be classified into four distinct families, harboring different substrate specificities [91]. For instance, HAG1 from the GCN5-like family almost exclusively acetylated H3K14, whereas HAG2 from the same family showed specificity for H4K12. HAM1 and HAM2 belonging to the Myst-like family of HATs both acetylated H4K5, whereas HAC1, 5 and 12 from the CBP-like family had multiple target lysines on H3 and H4 [92]. The fourth group called $TAF_{II}250$-like has not been characterized in plants. Histone deacetylases (HDACs) catalyze the reverse reaction by polarizing a water molecule, which then serves as nucleophile to attack the nitrogen of the ε-peptide bond, resulting in hydrolysis of the amide-bond and the release of an acetyl-group. HDACs are categorized into three families [91]. The largest family consists of 12 members characterized by a highly conserved N-terminal HDAC domain with a catalytic zinc ion and diverging C-termini. This REDUCED POTASSIUM DEFICIENCY-like (RPD3-like) family has close homologs in human, worm, fly and yeast. The structurally diverse family of Sirtuins (2 members in *Arabidopsis*) is homologous to yeast SILENT INFORMATION REGULATOR 2 (SIR2) and has a different catalytic mechanism using NADH as a cofactor. The HD2-like family (HDT1, 2, 3 and 4, also named HD-tuins) seems to be plant-specific since no homologs have been identified in other organisms so far [93]. However, evidence accumulates that these family members probably do not possess HDAC activity, instead they might serve as scaffolding proteins since some of them do interact with RPD3-like HDACs, for instance HDA6 and HDA19 [94]. In general, HDACs are subunits of large multiprotein repressor complexes. Since most HDACs do not show substrate specificity in vitro, it is likely that components of these complexes target them to specific genes. Moreover, recombinant HDACs show much weaker deacetylase activity as compared to the same enzyme in its native complex, indicating that the interaction with specific subunits of the complex enhances HDAC activity [95].

HDA6 and HDA19 from the RPD3-family are two of the best-characterized HDACs in *Arabidopsis*. HDA6 was originally identified to affect transgene silencing [96] and is a key player in nucleolar dominance maintaining gene silencing of rDNA repeats [97, 98]. By interacting with the DNA-methyltransferase MET1, HDA6 also modulates DNA-methylation to suppress transposon transcription [99]. This is an example of a self-reinforcing loop - a common theme in epigenetics - in which repressive histone modifications and DNA methylation enforce each other thereby creating a silenced chromatin state. Moreover, HDA6 is involved in the response to abscisic acid (ABA), salt and cold stress implying an important role as an abiotic stress regulator [100, 101]. Finally, together with HDA5, HDA6 regulates proper flowering induction [102]. HDA19 is an important modulator of the plant´s response to biotic stresses - like pathogen infection by P. syringae or A. brassicicola - by repressing the expression of pathogenesis related genes PR1 and PR2 [103, 104]. This prevents overstimulation of the immune response in challenged conditions as well as unwanted activation of defense in unchallenged conditions. HDA19 is an important developmental regulator. By interacting with TOPLESS, HDA19 defines the apical shoot pole in the embryo and different floral organs of *Arabidopsis* [105, 106]. Moreover, this HDAC is involved in the repression of embryonic properties after germination (together with HDA6) and the repression of seed maturation [107, 108]. Furthermore, proper photomorphogenesis requires HDA19 activity at specific light regulated genes [109]. Two other HDACs are characterized in *Arabidopsis*. HDA18 is a key HDAC during patterning of the root epidermis by controlling the acetylation status of kinase genes involved in the signaling mechanisms underlying root morphogenesis [110, 111]. Finally, HDA9 represses seedling traits in dry seeds and regulates flowering by repressing AGL19 expression [112, 113]. Information about sirtuins is limited and partially contradictory. AtSRT2 was implicated in suppression of basal defence by silencing PAD4, EDS5 and SID2 [114]. On the other hand, AtSRT2 was demonstrated to localize to the mitochondria where it was responsible for the acetylation of certain metabolic proteins and protein complexes [115], implying a rather indirect function of this protein in basal defense.

In summary, although many biological processes are described in which HDACs are crucial regulators, information on how HDACs themselves are regulated is sparse. In particular, mechanisms of posttranslational regulation of this enzyme family are currently unknown in plants. The effect of histone modifications and DNA-methylation as well as the involved enzymes on the chromatin state are summarized in **Fig. 4**.

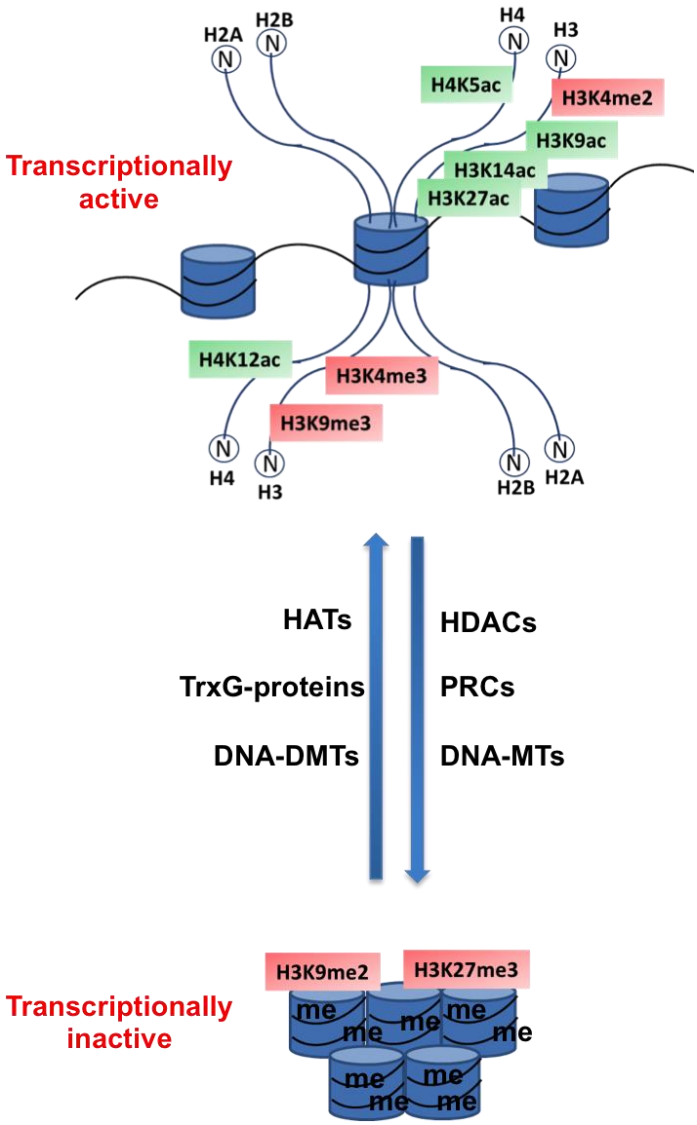

Figure 4: Characteristics of transcriptionally active and silenced chromatin. Transcriptionally active chromatin is usually characterized by histone hyperacetylation and activating histone methylation marks, whereas transcriptional inactive chromatin contains repressive histone methylation marks and DNA-methylation. HAT: Histone acetyltransferase, TrxG: Histone methyltransferase from the Trithorax subfamily, DNA-DMT: DNA-Demethylase, HDAC: Histone-deacetylase, PRC: Polycomb repressive complex, contains PcG group histone methylases, DNA-MT: DNA-Methyltransferase.

1.4 Impact of S-nitrosylation on transcription

Exogenous application of NO resulted in profound transcriptional reprogramming in *Arabidopsis* as demonstrated early by microarray analysis and AFLP-transcript profiling [116, 117]. Partly, this effect is mediated indirectly by modulating other phytohormone signaling cascades. For instance, NO interferes with cytokinin signaling through S-nitrosylation of Cys115 of the histidine phosphotransfer protein AHP1, which represses AHP1 phosphorylation and subsequent transfer of the phosphate to downstream proteins [118]. Further, NO induces the degradation of the auxin transporter PIN1, resulting in improper

auxin distribution, morphological abnormalities in root meristems and delayed root growth in *Arabidopsis* [28]. Moreover, NO inhibits gibberellin signaling by stabilizing the signaling repressor DELLA [119]. Finally, it was demonstrated that S-nitrosylation of the auxin receptor TIR1 at Cys140 enhanced auxin signaling by accelerating the degradation of AUX/IAA [120]. However, NO also affects transcription by directly modifying transcription factors.

1.4.1 S-Nitrosylation of transcription factors

Several members of the MYB-family of transcription factors are targeted by S-nitrosylation. DNA binding activity of AtMYB2 is inhibited by S-nitrosylation of the highly conserved Cys53, which is located in the DNA-recognition helix of this protein [121]. Similarly, AtMYB30 showed reduced DNA binding activity upon incubation with NO-donors, which was dependent on S-nitrosylation of two cysteine residues. This modification induced structural changes in the arrangement of secondary structure elements as proven by circular dichroism and temperature induced denaturation profiles [122]. In contrast, S-nitrosylation of Cys260 and Cys266 of TGA1 – a key regulator of systemic acquired resistance – enhanced its binding to the activating sequence 1 element found in the promoters of defense genes in the presence of NPR1 [14]. Another example of NO sensitive transcription factors are members of the TCP family. TCP proteins contain a conserved cysteine residue in the DNA binding and dimerization domain, which is sensitive towards different redox-modifications including S-glutathionylation and S-nitrosylation. Again, these oxidative modifications prevented binding to DNA [123].

1.4.2 S-Nitrosylation of epigenetic regulators

Several reports document the influence of NO on the epigenetic landscape in animals. The primary epigenetic target proteins of NO are HDACs. S-nitrosylation of HDAC2 controls its association with chromatin, which induces chromatin remodeling at certain loci in neurons [1]. The inhibitory effect of NO on HDAC2 activity is explored in therapies against Duchenne muscular dystrophy [124]. Moreover, HDAC6 and HDAC8 activities are inhibited by S-nitrosylation [125]. Finally, the nucleo-cytoplasmic shuttling of HDAC4 and HDAC5 is controlled by S-nitrosylation of one of their interaction partners [126]. In plants, the epigenetic effects of NO have not been investigated until now.

1.5 Aim of the project

NO-signaling is associated with extensive transcriptional reprogramming, resulting in the expression of a variety of genes involved in different physiological processes. In eukaryotes, transcription is mainly regulated by transcription factors (TFs), which recruit the transcriptional machinery to promoter regions and epigenetic mechanisms, which determine the local chromatin structure and thus control the accessibility of proteins to the DNA. The influence of NO on transcription is partially mediated by S-nitrosylation of TFs, like NPR1, TGA1, TCPs or Myb-proteins. In animals, NO has also been implicated in epigenetic regulation – mainly by S-nitrosylation of HDACs –, in plants, however, the effect of NO on epigenetic regulators has not been investigated.

In an attempt to identify S-nitrosylated nuclear proteins after pathogen-treatment of *Arabidopsis* cell cultures, our lab previously identified members of the HDT-family of HDACs [127], suggesting that these proteins might be regulated by NO. Moreover, sequence analysis of HDACs from plants and animals indicated, that cysteine residues shown to be redox-regulated in animal proteins, are conserved in plant HDACs.

Based on this, the role of NO on histone acetylation was to be studied in this work. Therefore, a combination of different biochemical, molecular biology and genetic methods was applied. First, genome-wide histone acetylation changes were analyzed by chromatin-immunoprecipitation followed by deep sequencing (ChIPseq) after treatment of seedling cultures with a natural NO-donor (GSNO). To find a mechanistic explanation for the observed histone acetylation changes, *in vivo* and *in vitro* HDAC-activity measurements were conducted to determine the influence of NO on HDAC activity. To accomplish this, HDAC-activity assays had to be established, which allowed the measurement of HDAC-activity in protein extracts as well as living cells. Based on these results, a NO-affected HDAC-isoform (HDA6) was identified and the *in vitro* effect of NO on this enzyme was studied. Furthermore a possible role of NO-mediated HDA6 regulation during salt stress was uncovered.

2 Results

NO is well known to influence the epigenetic landscape and especially histone acetylation in mammals. For instance, HDAC6 and HDAC8 are both S-nitrosylated *in vitro* [3, 125], the subcellular localization of HDAC4 is controlled by S-nitrosylation of an interaction partner [126], and S-nitrosylation of HDAC2 leads to its dissociation from chromatin, which is important for neuronal development [1]. Recently, a new class of HDAC inhibitors has been introduced, which relies on the presence of a NO emitting chemical group. Very often, S-nitrosylation is conserved across the biological kingdoms. Moreover, a screen for potential, S-nitrosylated nuclear proteins in *Arabidopsis* identified several members of the plant-specific HDT-family of HDACs [127]. We therefore asked, whether NO might also affect histone acetylation in *Arabidopsis*.

2.1 NO-induced genome-wide changes of H3K9/14 acetylation

2.1.1 Experimental design

To test the effect of NO on histone acetylation, chromatin immunoprecipitation followed by deep sequencing (ChIPseq) was applied (**Fig. 5**). This technique allowed for profiling of genome-wide histone modification patterns with a very high resolution, thus providing the possibility to quantify even subtle differences of histone modification patterns across different conditions. We decided to analyze H3K9/14 acetylation (H3K9/14ac) since this modification is associated with active transcription and is located in rather sharp peaks in regulatory regions in the genome [128]. The latter characteristic greatly facilitates downstream quantitative analysis of multiple treatment comparisons. Other histone modifications like H3K9me3 are distributed broadly throughout the gene body and the availability of tools to quantify changes in these patterns is strongly limited.

GSNO is considered to be a mobile rather stable natural reservoir of NO. Therefore, GSNO treatment is widely used to study NO-mediated effects because elevated SNO levels correlate with higher NO concentrations. Compared to plant literature rather low GSNO concentrations (250 µM) were used to ensure that the increase in total S-nitrosothiol levels in the plant tissue was comparable to the increase observed in physiological conditions, for instance pathogen attack (**Supp. Fig. 1**) [19]. To separate NO-mediated effects from others after GSNO treatment, cPTIO was used since this compound is described to be a potent NO scavenger [129]. Moreover, GSH was applied, which structurally resembles GSNO, however, lacks the NO moiety. In contrast to GSNO, GSH is a strong reducing compound thus allowing to compare the effect of an oxidizing (GSNO) and reducing cellular environment (GSH) on histone acetylation. Finally, Trichostatin A was used as positive control, which inhibits RPD3-

type HDACs and possibly HD-tuins thus leading to a global increase in histone acetylation [130].

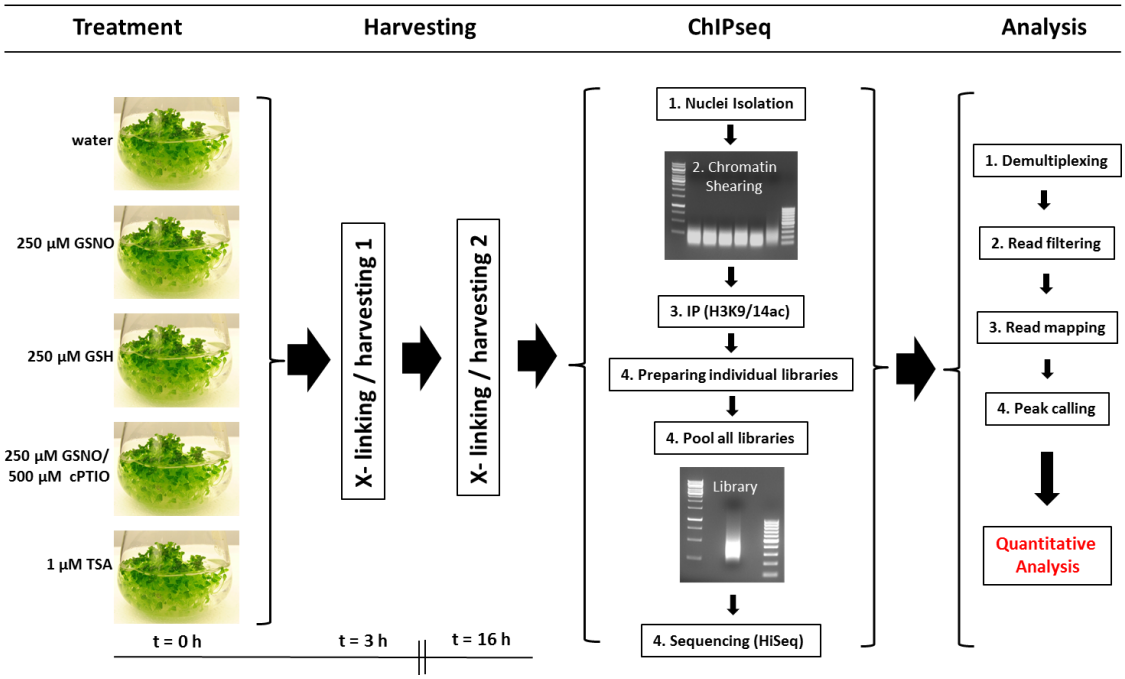

Figure 5: Workflow and experimental design of the conducted ChIPseq analysis

Seven day old liquid grown *Arabidopsis* seedlings were treated with water (solvent control), 250 µM GSNO, 250 µM GSNO / 500 µM cPTIO, 250 µM GSH and 1 µM TSA. Three and 16 h after stimulation, the tissue was cross-linked with formaldehyde and stored for later ChIPseq analysis. The experiment was repeated once (two biological replicates) resulting in a total of 20 samples. For each sample chromatin was prepared, sheared to 200 bp fragments and subjected to immunoprecipitation with an antibody against H3K9/14 acetylation. An aliquot of sheared chromatin was kept to serve as input control. Libraries for all ChIP and input samples were prepared using the Microplex Library Preparation Kit (Diagenode) using 1 ng of DNA as starting material. Equal volumes of all individual libraries were then pooled, purified and the pooled library was sequenced on an Illumina HiSeq. Reads were demultiplexed and mapped using the *Arabidopsis* TAIR10 reference genome. Only uniquely mapped reads were kept for subsequent steps. Peaks were called using the CLC genomics workbench algorithm with stringent settings (P-value < 0.01). Details about antibody quality control experiments, shearing and library preparation as well as mapping and peak calling are provided in **Suppl. Fig. 2 – 6A**.

2.1.2 General features of H3K9/14 acetylation

The distribution of peaks along the A. thaliana chromosomes is illustrated in **Fig. 6**. H3K9/14ac was absent from centromeric and pericentromeric regions and the peak density

increased towards the ends of the chromosomes. Peak density was similar for the different chromosomes.

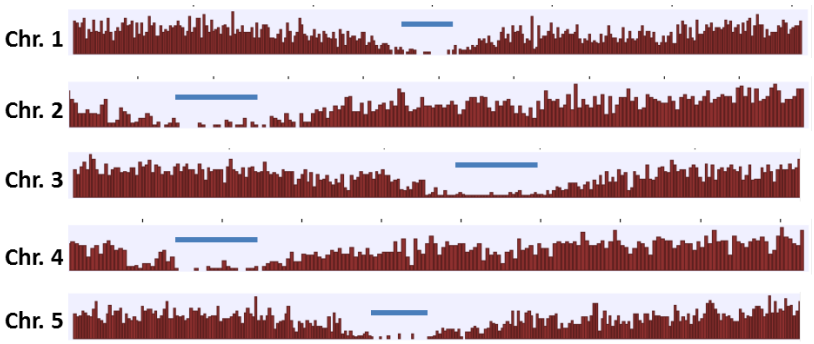

Figure 6: H3K9/14ac distribution along *A. thaliana* chromosomes. Each bar represents the number of peaks in the corresponding chromosomal bin. Blue lines mark the approximate centromeric and pericentromeric regions. Shown are representative snapshots of the CLC-genome browser.

To further investigate general features of H3K9/14ac, peaks were annotated and analyzed using ChIPSeek software [2]. Location annotation revealed that most of the peaks were located within exons, followed by triplex target DNA sites (TTS), promotor regions around the transcriptional start site (TSS) and introns. Only a minority of peaks was located in 5`- or 3`- untranslated or intergenic regions (**Fig. 7B**). A histogram of the distance to the nearest annotated TSS illustrated that more than 95% of all peaks were found within 1 kb downstream of the TSS. The maximum of this distribution was located 400 bp downstream of the TSS (**Fig. 7A**). Motif analysis of the peak regions identified target sequences for numerous transcription factors (**Suppl. Fig. 15**). The most significant motif was found in 49% of all regions and showed strong similarities to the consensus binding sequence of ARR10 and AGP1 (P-value = E-168, **Fig. 7C**). As expected, no differences in these general H3K9/14ac features across the different treatments could be identified.

2.1.3 Quantitative comparison of H3K9/14 acetylation after GSH, GSNO and GSNO/cPTIO treatment

Since peak calling is highly dependent on sequencing depth and background noise, which can vary from sample to sample, qualitative comparison of peak lists for different treatments/conditions is not recommended [131]. Therefore, a quantitative analysis using DiffBind software was conducted in order to identify differentially regulated H3K9/14ac sites. DiffBind allows for multiple treatment comparisons and considers biological replicates as well as the corresponding input controls thereby providing major advantages over other programs like SICER or ChIPDiff [132]. DiffBind needs the read mappings (ChIP and input) as well as the list of called peaks for each sample as input. First, peaks from all treatments are combined to define regions for quantification. Then, DiffBind counts normalized reads within

these regions in the ChIP- and the corresponding input sample, the latter being subtracted from the ChIP counts. Then, groups to be compared (contrasts) are defined (i.e. pairwise comparison) and based on the fold changes of ChIP counts between these groups hypothesis testing and statistical analysis are accomplished. The following contrasts were defined in this specific case: control vs. TSA (3h), control vs. GSNO (3h and 16h), control vs. GSH (3h and 16h), control vs. GSNO/cPTIO (3h and 16h). To verify the quantitative analysis several identified differentially regulated sites were confirmed by ChIP-qPCR (**Suppl. Fig. 6B**). All six tested loci faithfully reproduced the ChIPseq results. Moreover, the read densities at differentially regulated sites reflected the results obtained by DiffBind, demonstrating that the algorithm used by DiffBind was suitable to detect differences in the H3K9/14ac pattern in these datasets (**Fig. 8**).

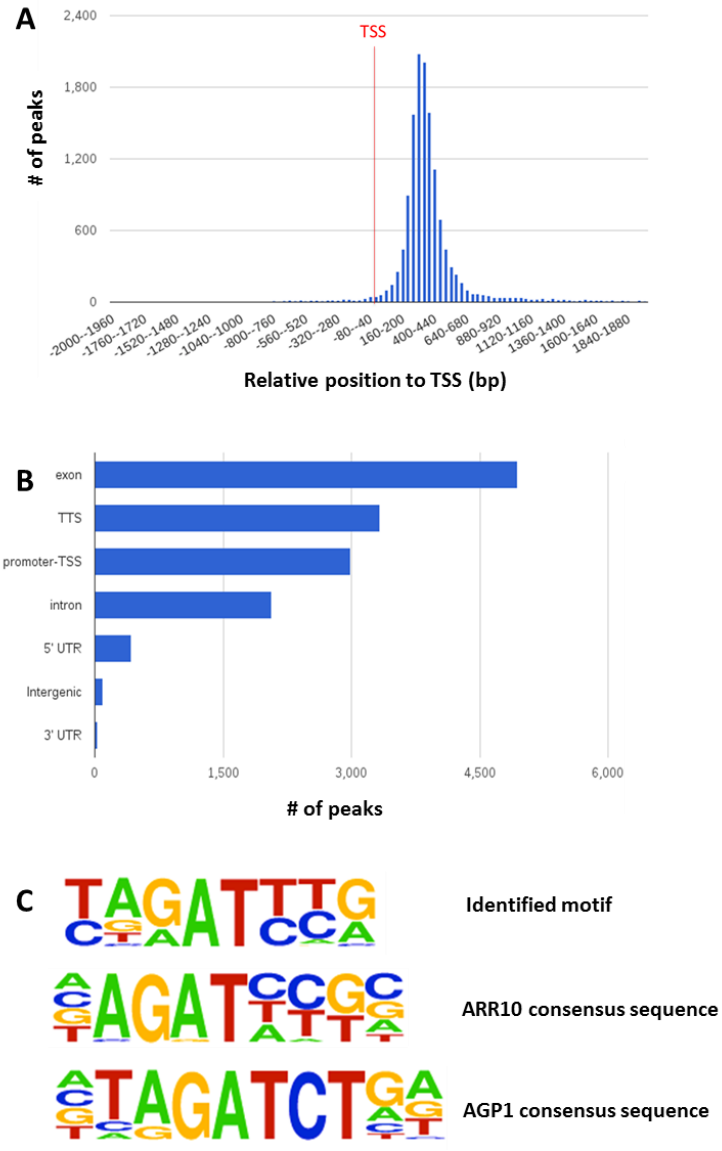

Figure 7: General features of H3K9/14ac. A) Histogram of distance of peaks to the nearest annotated transcriptional start-site (TSS). The distribution shows a maximum at around 400 bp downstream of the TSS. B) Location annotation of peaks. Peaks were annotated to functional cis DNA elements. TTS: triplex target DNA sites, TSS: transcriptional start site, UTR: untranslated region. C) Motif analysis of peak regions. Shown is the most significant motif (P-value = E-168) and the ARR10 and AGP1 consensus sequences for comparison. The identified motif strongly resembles the consensus sequences of both transcription factors. All figures were prepared using the ChIPseek software portal [2, 3].

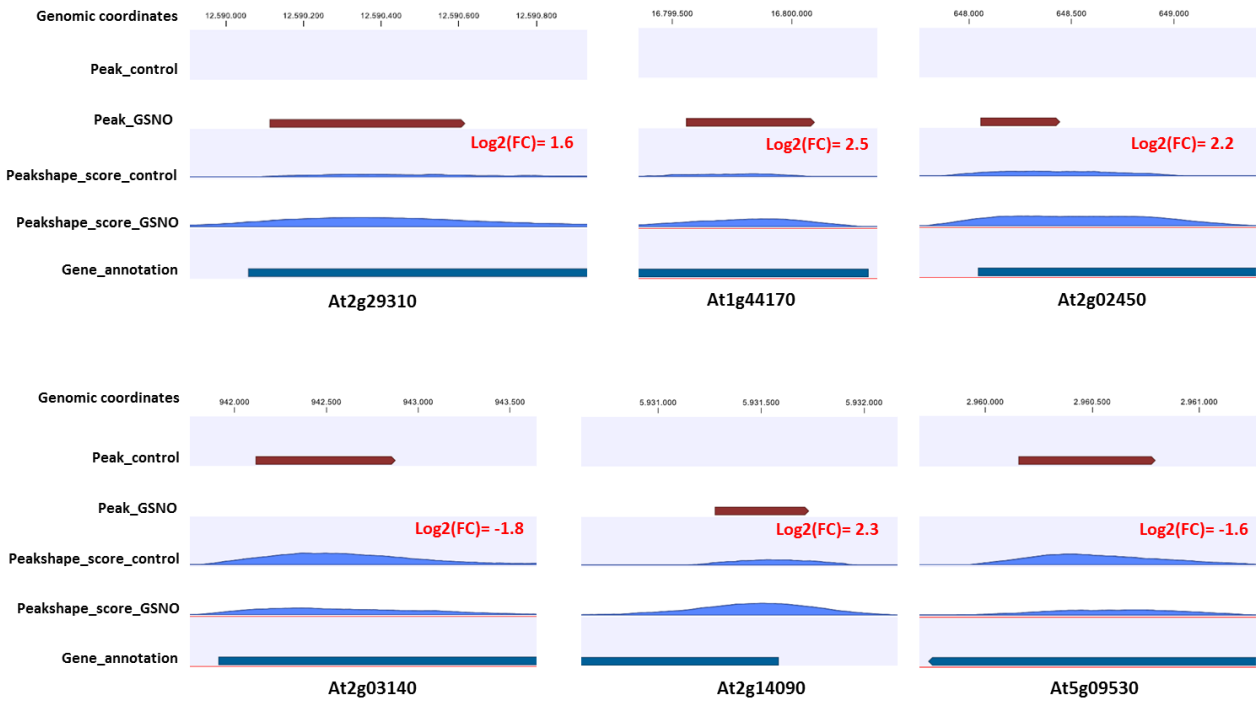

Figure 8: CLC-genome browser snapshots of representative GSNO-regulated H3K9/14ac sites. Brown arrows indicate whether a peak was found in this region during peak-calling for water (second line: Peak_control) or GSNO (third line: Peak_GSNO) treatment. The peak-shape score (fourth and fifth line) is a measure for how well the read distribution fits to the peak shape filter applied for peak identification. The peak-shape score correlates with the read density in the corresponding region. The numbers in red indicate the predicted log2 fold change (treatment-control) as computed by DiffBind.

A summary of all significantly regulated ($P < 0.05$) H3K9/14ac sites for the different treatments is presented in **Fig. 9**. The number of significantly regulated H3K9/14ac sites was several-fold higher for the 16h time point than for the 3h time point, irrespective of the treatment. For the GSNO and GSH treatment, most of the sites showed enhanced acetylation. In contrast, in the GSNO/cPTIO treatment the number of sites with decreased histone acetylation was higher than (3h) or almost similar (16h) to the number of sites with increased acetylation. As expected, a significant number of acetylation sites was significantly regulated in more than one treatment, however, a considerable number of sites was still unique to one specific treatment. To illustrate these observations for the GSNO treatment at 16h: in total 943 H3K9/14ac sites were significantly regulated. 223 sites (23%) showed decreased histone acetylation, 720 sites (77%) were hyperacetylated compared to the control treatment. In contrast only 310 sites were found to be regulated after three hours of treatment, among which 76% showed increased acetylation. Out of the 720 hyperacetylated sites, 132 (14%) were unique to the GSNO treatment, whereas 565 (60%) and 312 (33%) sites overlapped with the GSH and GSNO/cPTIO treatment, respectively. 289 sites (31%) showed enhanced histone acetylation in all three treatments.

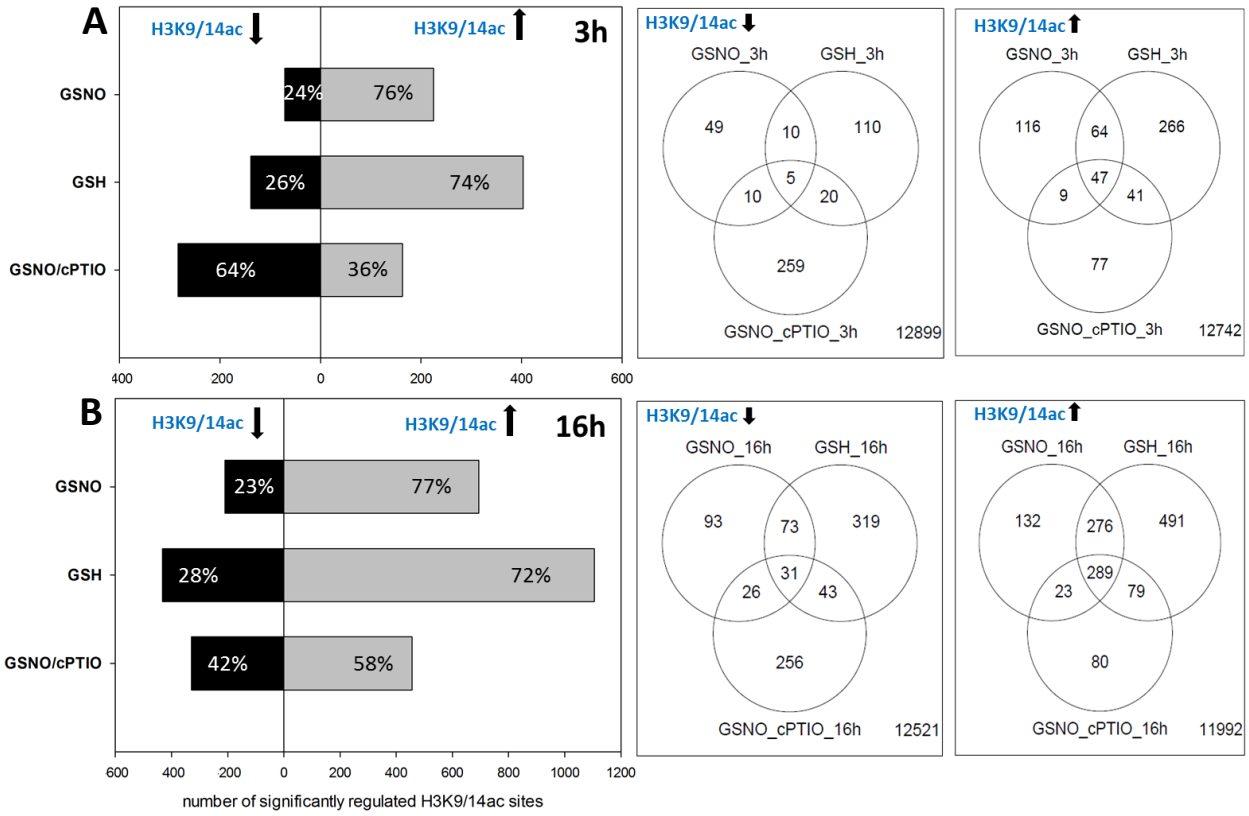

Figure 9: **Summary of GSNO, GSH and GSNO/cPTIO induced H3K9/14ac changes**. For each treatment significant H3K9/14ac changes (P<0.05) were determined in comparison to water (control) treatment using DiffBind software. The graphs in the left panel summarize the number of sites which show enhanced (grey bars) or decreased (black bars) H3K9/14ac after three (A) and 16h (B) of treatment. The Venn-diagrams on the right illustrate the overlap between the treatments separated for peaks with enhanced (right) or decreased (left) H3K9/14ac. The graphs were prepared with the help of Elisabeth Georgii.

2.1.4 Comparison of the 3h and 16h time point

As outlined in 2.1.1, seedlings were crosslinked and harvested 3h and 16h after stimulation with GSNO, GSH, GSNO/cPTIO or TSA in order to compare rapid histone acetylation changes with those occurring at later stages of the treatment. **Fig. 10** summarizes these time point comparisons for the GSNO, GSH and GSNO/cPTIO treatment. H3K9/14ac sites, whose acetylation was significantly changed at the 3h and 16h time point (or at both) were combined and sorted for increasing log2(FC) at the 16h time point (dotted lines in **Fig. 10 A, B, C**). The continuous line reflects the log2(FC) for those peaks at the 3h time point. Sites which showed strongly enhanced or decreased histone acetylation at one of the time points showed no or rather low changes in histone acetylation at the other time point, indicating that the early and later response for one treatment differed qualitatively from each other. Accordingly, the overlap of significantly regulated H3K9/14ac sites for both time_points within one treatment was very low (**Fig. 10 D, E**).

2.1.5 Identification of NO-regulated H3K9/14ac sites

To illustrate the global effects of GSNO, GSH and GSNO/cPTIO treatment on H3K9/14ac volcano-plots were prepared in which the log2(FC) of each acetylation site is plotted versus the negative decadic logarithm of the corresponding P-value (**Fig. 11**). Acetylation sites lying in the red area showed significantly enhanced H3K9/14ac in comparison to water treatment (FC > 1.5, P-value < 0.05). Peaks in the blue area displayed significantly decreased H3K9/14ac (FC < 1.5, P-value < 0.05). In general, many more peaks were found in the red regions than in the blue regions after GSNO and GSH treatment. This observation was highly statistically significant. In contrast, after GSNO/cPTIO application, a majority of acetylation sites displayed decreased H3K9/14ac and most of the sites, which were hyperacetylated after GSNO treatment, showed no or only weak hyperacetylation after GSNO/cPTIO application. This demonstrated that NO was responsible for or at least contributed to the increased histone acetylation levels of those sites.

To identify NO-regulated H3K9/14ac sites, the GSNO and GSNO/cPTIO treatments were compared. Acetylation sites, which showed greater absolute log2(FC) than 0.58 after GSNO application, but smaller absolute log2(FC) than 0.26 in the GSNO/cPTIO treatment (or if this peak was not significantly regulated in the GSNO/cPTIO treatment) were considered to be regulated by NO. This filtering step was applied for both the 3h and 16h time point. In total, 194 NO-regulated H3K9/14ac sites were identified after three hours of treatment (representing 62.6% of the GSNO-regulated acetylation sites), among which 46 sites (23.7%) displayed decreased and 148 sites (76.3%) showed increased histone acetylation. For the 16h time point, 552 NO-regulated sites were found (58.5% of GSNO-regulated sites). Among these, 159 (28.8%) sites were hypoacetylated and 393 sites (71.2%) were hyperacetylated in comparison to the control treatment (**Fig. 12**).

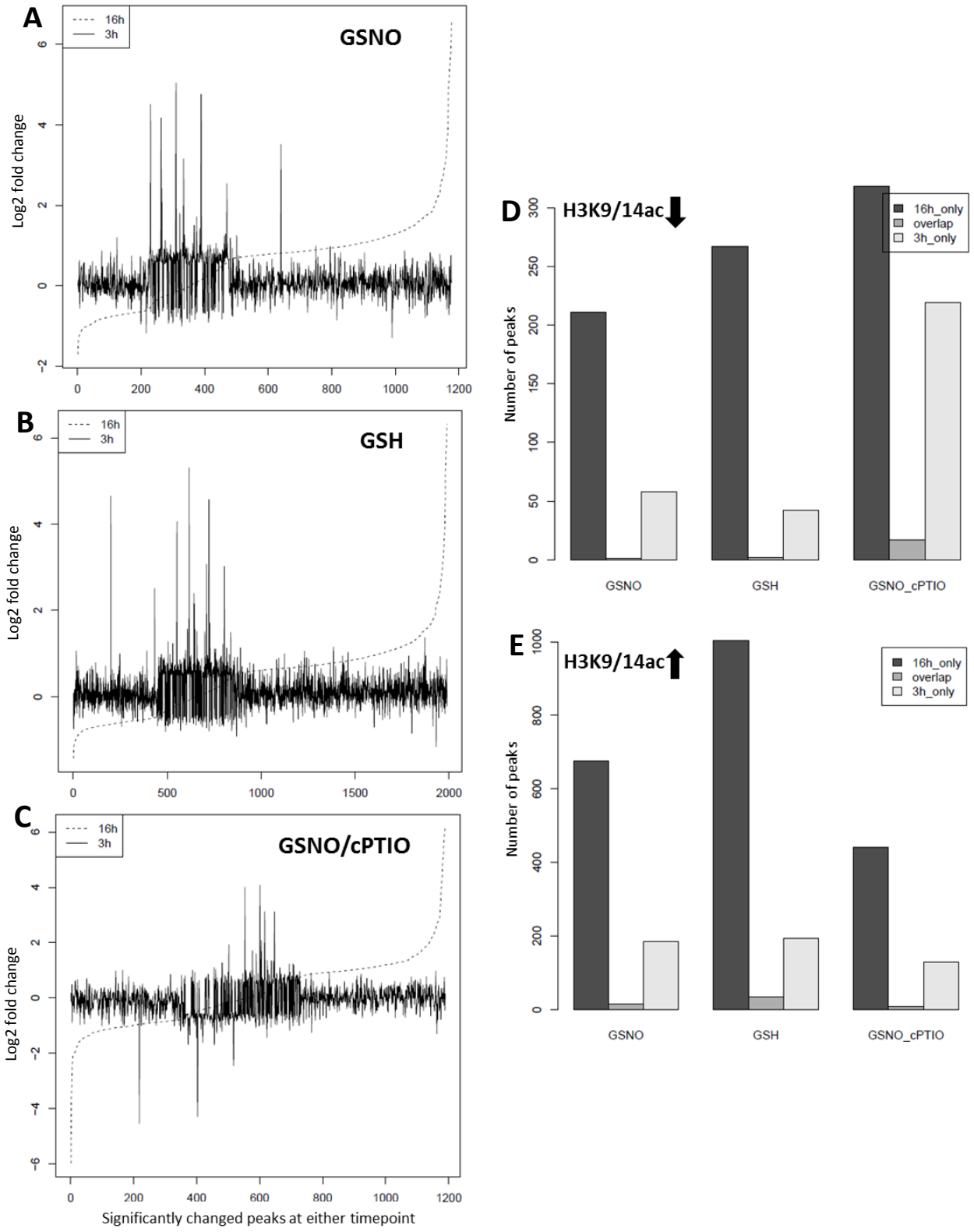

Figure 10: Time point comparison of GSNO -, GSH - and GSNO/cPTIO - induced H3K9/14ac changes. A – C: Peaks showing altered H3K9/14ac with P < 0.05 in the 3h or 16h time point were combined and sorted for increasing log2(FC) in the 16h time point (dotted line). The continuous line reflects the log2(FC) for the corresponding peaks after 3h of treatment. These line-plots indicate that peaks which show strong H3K9/14ac changes in either time point are not or only slightly regulated at the other time point arguing for substantially different responses after 3h and 16h of treatment. D and E: Number of significantly changed H3K9/14ac peaks (P<0.05), which are found after 16h or 3h only (dark grey and light grey bars) or at both time points (grey bars) separated for peaks showing enhanced (E) or decreased H3K9/14ac (D). Graphs were prepared with the help of Elisabeth Georgii.

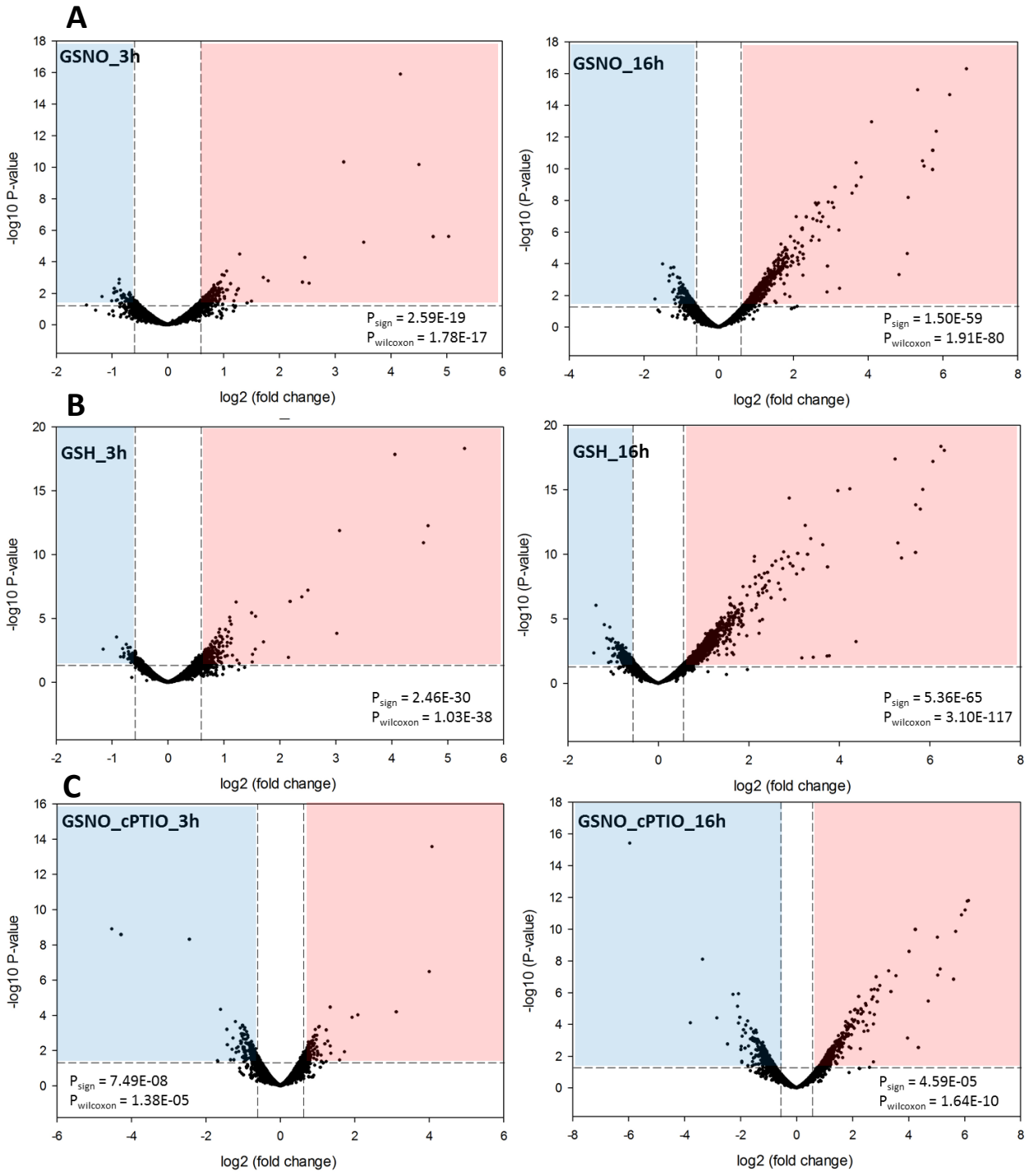

Figure 11: Volcano-Plots illustrating H3K9/14ac changes induced by GSNO (A), GSH (B) and GSNO/cPTIO (C) after 3h and 16h of treatment. Fold changes are defined as treatment over control (water). The horizontal dashed line represents a P-value of 0.05, the two vertical dashed lines mark absolute fold changes of 1.5. Dots in the red regions have P-values < 0.05 and fold changes > 1.5. Dots in the blue regions have P-values < 0.05 but fold changes < -1.5. To test for significant differences in the number of peaks with enhanced or decreased H3K9/14ac among the peaks with p-values < 0.05, a sign-test was performed (P_{sign}). To test whether peaks with increased H3K9/14ac show higher absolute fold changes compared to peaks with decreased H3K9/14ac, a Wilcoxon signed rank test was performed ($P_{wilcoxon}$).

Next, NO-regulated H3K9/14ac sites were compared to the TSA treatment. Unfortunately, one TSA-treated replicate for the 16h time point only produced very few reads during sequencing, which resulted in very low RSC and NSC values, making it impossible to reliably identify peaks. Therefore, this sample was omitted from further analysis. The same problem occurred with one biological replicate of the control sample (16 h). DiffBind can identify differentially regulated peaks if there is just one biological replicate available for one condition but at least two for the other condition, but not if there is only one biological replicate for each condition. Therefore, we couldn´t identify TSA-regulated peaks for the 16h time point.

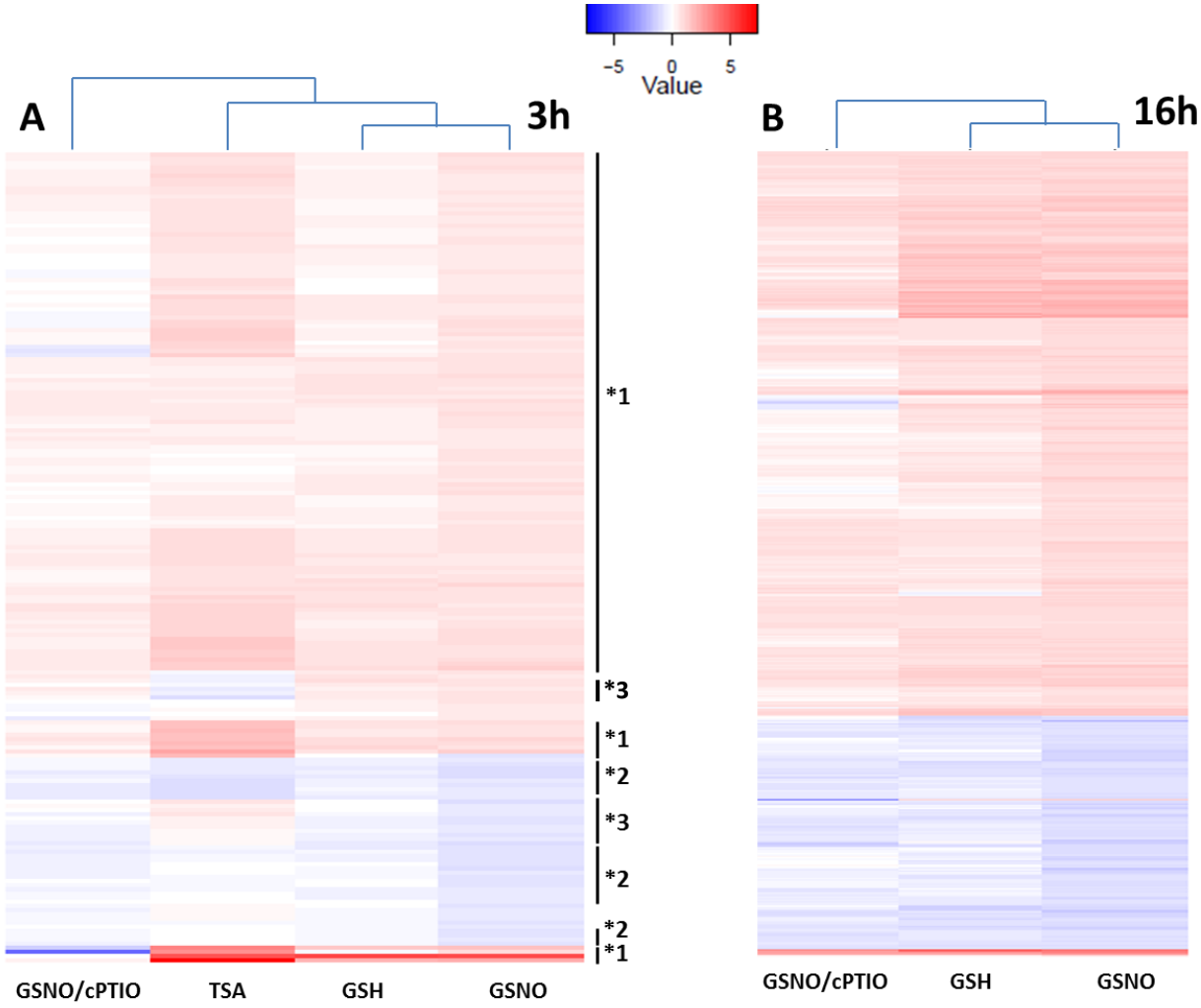

Figure 12: Overview of different classes of NO-regulated H3K9/14ac sites. NO-regulated peaks were identified by comparison of the GSNO and GSNO/cPTIO treatments (see text for details). Each line represents one NO-regulated H3K9/14ac site. The change of H3K9/14ac after GSNO, GSH, TSA and GSNO/cPTIO treatments is colour-coded. A) NO-regulated H3K9/14ac sites after three hours of treatment. Different classes of NO-regulated H3K9/14ac sites are marked with numbers (see text for details). B) NO-regulated H3K9/14ac sites after 16h of treatment. Graphs were prepared with the help of Elisabeth Georgii.

In general, TSA affected many more acetylation sites than NO (4477 significantly altered H3K9/14ac sites, in comparison to 194 NO-regulated sites). However, most of the NO-regulated acetylation sites were similarly regulated in the TSA treatment (Clusters marked with 1 or 2 in **Fig. 12A**). In contrast, only a minority of NO-regulated sites was inversely regulated in the TSA treatment (Clusters marked with 3). This might indicate that NO primarily inhibits a subset of TSA-sensitive HDACs, whereas inhibition of HATs only plays a minor role.

Interestingly, many of the NO-regulated acetylation sites were similarly regulated after GSH application (**Fig. 12**). Analysis of the GSH-regulated H3K9/14ac sites revealed the presence of several H_2O_2 marker genes (ETR2, 2OG-dependent (FeII) oxygenases, syntaxin, xyloglucan endotransglycosylases) [133], indicating that GSH treatment resulted in the accumulation of H_2O_2. H_2O_2 in turn is known to induce the production of NO [134]. It is therefore possible that GSH stimulated NO production, which is supported by the fact that we observed increased SNO-levels after GSH application (**Suppl. Fig. 1**).

2.1.6 GO-enrichment analysis of genes associated with NO-regulated H3K9/14ac sites

NO-regulated H3K9/14ac sites were annotated using PAVIS. Acetylation sites within a 5kb window upstream of the TSS or a 1 kb window downstream of the transcriptional termination site of a gene were ascribed to that gene. Other acetylation sites were defined to be intergenic. All NO-regulated acetylation sites were located within genes, mainly in the first exon, in the promoter or in intronic regions. We then identified significantly enriched GO-terms among genes displaying NO-mediated regulation of histone acetylation (**Fig. 13**). The analysis was performed separately for genes with enhanced or decreased histone acetylation and for both time points. Several interesting GO-terms were identified, including some processes in which NO plays a well established role, for instance “response to cold stress”, “positive regulation of absicisic acid activated signaling pathway”, “cellular iron ion homeostasis” and “defense response” (**Table 1**). The diversity of these processes reflects the multiple functions of NO in the plant. Among the category “molecular function” we found a significant enrichment of genes involved in proteasome-mediated protein degradation, which might indicate that NO induces the degradation of specific proteins by upregulation of the corresponding E3-ubiquitin ligases (**Table 1**).

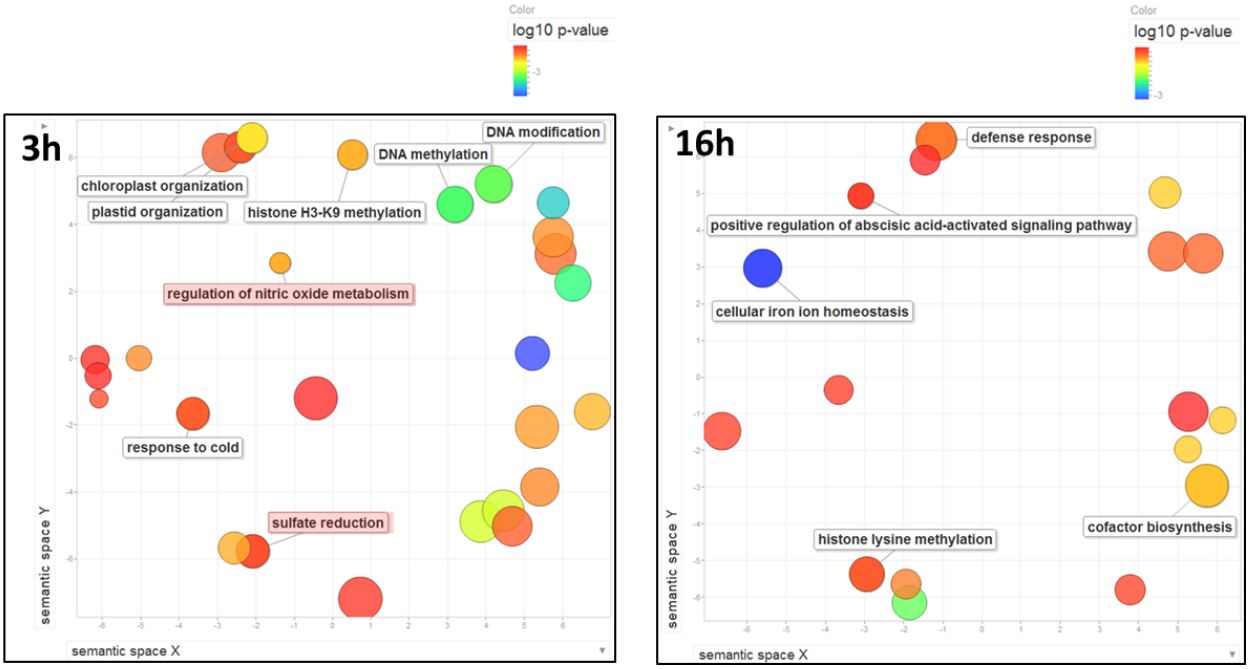

Figure 13: GO-enrichment analysis of genes with NO-regulated H3K9/14ac. Significantly enriched GO terms were visualized using the REVIGO tool. Every circle represents one specific GO-term, the size of the circle is proportional to the number of genes within the corresponding GO-term. The P-value for the enrichment is colour coded. The distance between circles represents the distance of these GO-terms in the GO hierarchical tree. Interesting categories are labeled. White labels mark categories which were significantly enriched in the group of genes showing increased H3K9/14ac, red labels mark GO-terms which were enriched in the group of genes showing decreased H3K9/14ac.

The ChIPseq-data (3h time point) was also compared to a recently published RNAseq-study, in which *Arabidopsis* plants grown in hydroponic culture were treated with 1 mM GSNO and the transcriptomic changes after 3h of treatment were analyzed separately in roots and in leaves [135]. Although we could not detect a clear correlation between histone acetylation levels and expression, we found that several of the genes (approximately 8%) which displayed increased or decreased histone acetylation levels were up- or downregulated after GSNO treatment, respectively (**Suppl. Fig. 17**). Given the strong differences in the experimental setups in both studies these data nicely confirm the reliability of the ChIPseq-experiment.

In summary, it was found that NO induced specific changes in the H3K9/14ac pattern of several genes mainly involved in the response to biotic and abiotic stresses and proteasome mediated protein degradation. Most of the NO-regulated H3K9/14ac sites were similarly regulated in the TSA treatment, whereas only a small set was oppositely regulated. We therefore hypothesized, that NO might inhibit the activity of a subset of TSA sensitive, nuclear HDACs. Therefore, the effect of NO on *Arabidopsis* HDAC activity was investigated *in vitro* and *in vivo*.

Table 1: Examples of significantly enriched GO-terms among genes, which display NO-regulated H3K9/14ac. The most interesting GO-terms were chosen from Fig. 13 and are listed together with a selection of the associated genes. The shown GO-terms were enriched among genes which showed enhanced histone acetylation after 16h of treatment.

GO-term	ATG-number	Gene_name	description
Defense response (biological process)	AT2G38870		PR-6 proteinase inhibitor family protein
	AT3G25510		putative TIR-NBS-LRR class disease resistance protein
	AT4G08450		TIR-NBS-LRR class disease resistance protein
	AT5G11250		TIR-NBS-LRR class disease resistance protein
	AT5G15730		probable leucine-rich repeat receptor-like serine/threonine-protein kinase
	AT4G29810	MKK2	mitogen-activated protein kinase kinase 2
	AT5G27520	PNC2	peroxisomal adenine nucleotide carrier 2
	AT2G46240	BAG6	BCL-2-associated athanogene 6
	AT3G28930	AIG2	avrRpt2-induced protein AIG2
	AT5G42980	TRX3	thioredoxin H3
	AT4G23810	WRKY53	putative WRKY transcription factor 53
	AT5G52830	WRKY27	WRKY DNA-binding protein 27
	AT5G06950	TGA2	transcription factor TGA2
	AT5G06960	TGA5	OCS-element binding factor 5
Ubiquitin ligase activity (molecular function)	AT1G20780	SAUL1	senescence-associated E3 ubiquitin ligase 1
	AT2G16920	UBC23	putative ubiquitin-conjugating enzyme E2 23
	AT2G32950	COP1	E3 ubiquitin-protein ligase COP1
	AT3G05545		RING/U-box domain-containing protein
	AT3G24800	PRT1	E3 ubiquitin-protein ligase PRT1
	AT3G29270		RING/U-box superfamily protein
	AT3G54650	FBL17	ubiquitin protein ligase FBL17
	AT3G55530	SDIR1	E3 ubiquitin-protein ligase SDIR1
	AT3G58040	SINAT2	E3 ubiquitin-protein ligase SINAT2
	AT4G07400	VFB3	VIER F-box protein 3
	AT5G02310	PRT6	proteolysis 6
	AT5G18340		U-box domain-containing protein 48
	AT5G37490		U-box domain-containing protein 21
	AT5G50430	UBC33	ubiquitin-conjugating enzyme 33
	AT5G61560		U-box domain-containing protein 51
Iron ion homeostasis (biological process)	AT2G40300	FER4	ferritin 4
	AT4G04770	ABC1	ATP binding cassette protein 1
	AT5G26820	IREG3	iron-regulated protein 3

2.2 Effect of NO and S-nitrosylation on HDAC activity

2.2.1 Inhibition of HDAC activity in protoplasts by NO

To analyze the effect of NO on HDAC activity a protoplast system was established, which allowed us to measure HDAC activity in response to certain stimuli. Briefly, cells were incubated with a lysine-acetylated substrate in which the acetyl-group quenched a fluorophore. Upon deacetylation the fluorophore could be detected and used as readout to quantify HDAC activity. Protoplasts were chosen since the assay relies on the diffusion of a

membrane permeable substrate into the cells, which was not possible in cell cultures or other tissue due to cell-surrounding cell walls (not shown). Moreover, protoplasts provide a simple model which has been proven to be useful for studying signal transduction mechanisms [136]. Protoplasts were prepared from dark grown suspension cells to eliminate assay interference by chlorophyll.

Several potential inducers of NO production (salicylic acid (SA), di-chloro-isonicotinic acid (INA), flagellin 22 (flg22), lipopolysaccharide (LPS)) were screened for their capability to induce NO production using the protoplast system described above. Therefore, protoplasts were incubated with DAF-FM DA (Di-amino-fluorescein diacetate), which is a cell permeable, NO specific dye [137]. Upon binding of NO the fluorescence quantum yield of this dye strongly increases, resulting in green fluorescence. 1h after stimulation, protoplasts were analyzed by microscopy using DAF-FM DA specific excitation and emission wavelengths.

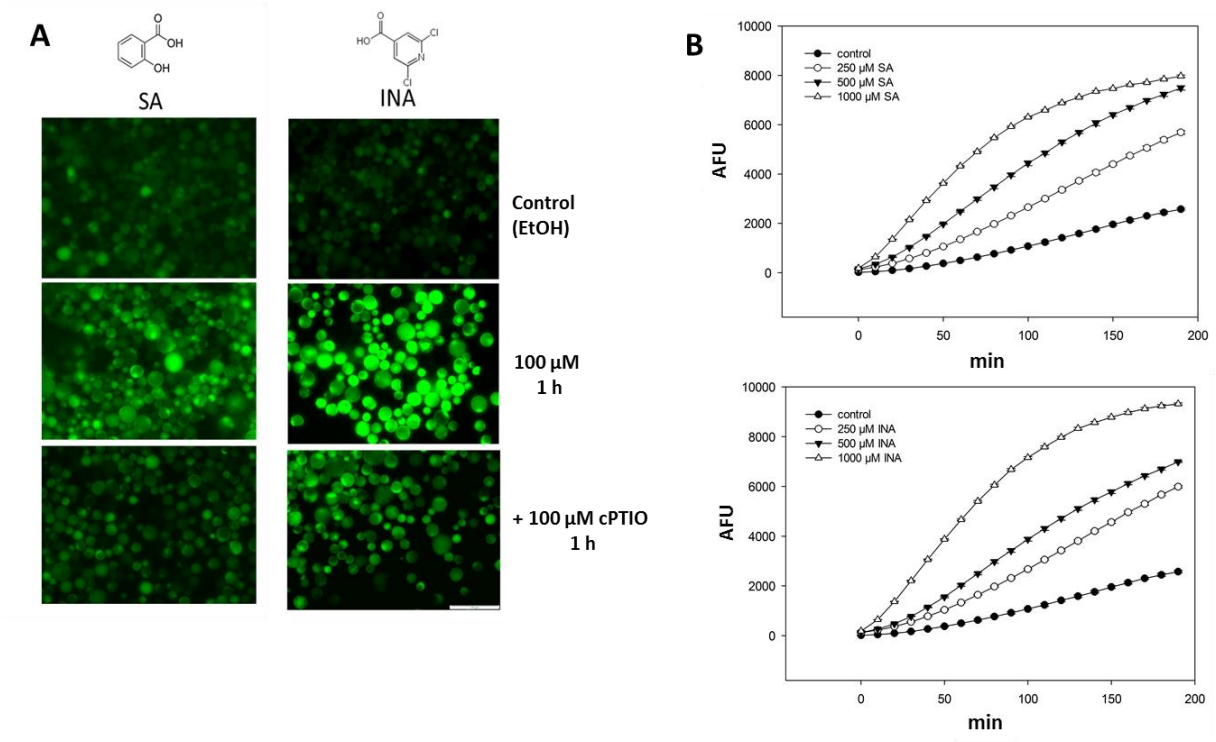

Figure 14: SA/INA-induced NO production in *A. thaliana* protoplasts. A) Micrographs of DAF-FM DA stained protoplasts after stimulation with ethanol (control), 100 µM SA/INA and 100 µM SA/INA + 100 µM cPTIO. Pictures were taken after 1h using identical microscope settings. Scale bar: 100 µM. B) Quantification of DAF-FM fluorescence after SA/INA treatment of protoplasts using a fluorescence microplate reader. The experiments were repeated twice with similar results.

Consistent with other studies [138-141], it was found that SA and its functional analogue INA strongly induced NO synthesis in a concentration dependent manner, whereas simultaneous treatment with the NO scavenger cPTIO showed clearly reduced fluorescence accumulation demonstrating the specificity of DAF-FM DA (**Fig. 14A**). The microscopy data was quantified by measuring fluorescence development after SA/INA stimulation over time using a

fluorescence microplate reader with the appropriate settings (**Fig. 14B**). This revealed that the rate of NO production as well as the total amount of NO was proportional to the concentration of SA or INA.

Next, the effect of SA/INA on HDAC activity was analyzed. A significant decrease of HDAC activity was observed with increasing SA and INA concentrations (around 20 % inhibition for 500 µM SA/INA, **Fig. 15**). Strikingly, this inhibition could be completely (SA) or almost completely prevented (INA) upon cPTIO pretreatment, clearly demonstrating, that the reduction of HDAC activity was caused by higher intracellular NO levels. To strengthen that NO inhibits HDAC activity, protoplasts were incubated with different concentrations of GSNO and SNAP (S-nitroso-penicillamine). SNAP is a non-natural NO donor, which is chemically distinct from GSNO, however, is also capable of transferring its NO-moiety to susceptible cysteines of target proteins.

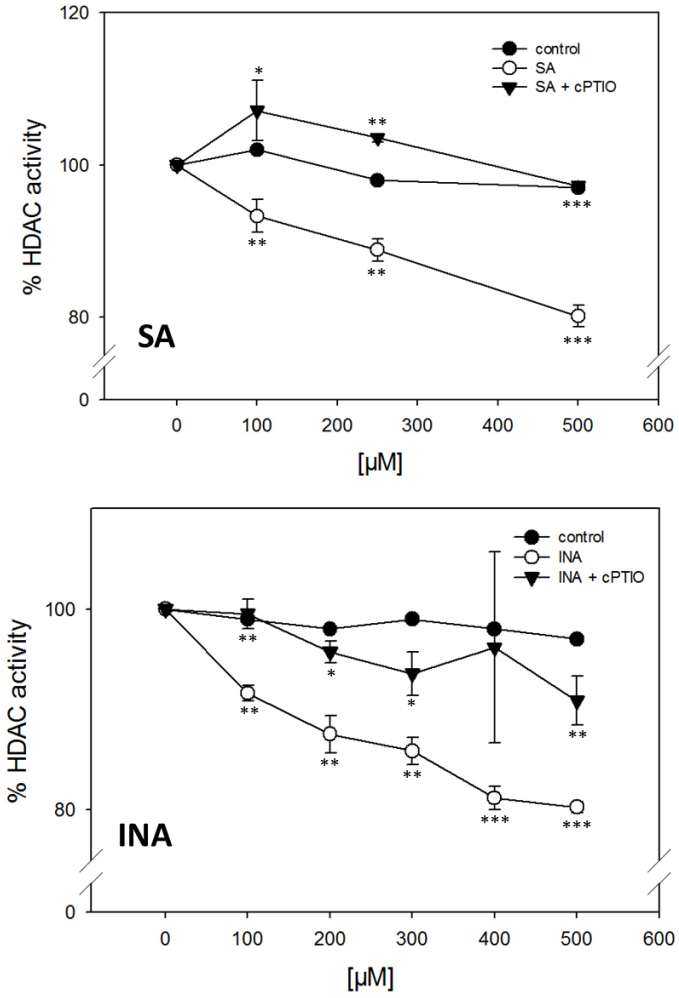

Figure 15: Inhibition of HDAC activity by SA/INA-induced NO production. Protoplasts were treated with different concentrations of SA/INA with or without pretreatment of cPTIO and HDAC activity was determined within the next 30 min. Shown is the mean ± SEM of three independent experiments. Values are expressed as percentage of HDAC activity in untreated protoplasts. * $P < 0.05$, ** $P < 0.01$, *** $P < 0.001$, student´s t-test. Asterisks below open circles indicate statistically significant inhibition in comparison to control treatment, whereas asterisks below triangles (cPTIO preincubation) indicate significant differences compared to SA or INA treatment.

Both GSNO and SNAP application inhibited HDAC activity in a concentration dependent manner (**Fig. 16A**). Importantly, simultaneous treatment with DTT – a strong reducing agent

– restored HDAC activity, indicating that the inhibitory effect of NO might be mediated by reversible, posttranslational cysteine modifications (**Fig. 16B**).

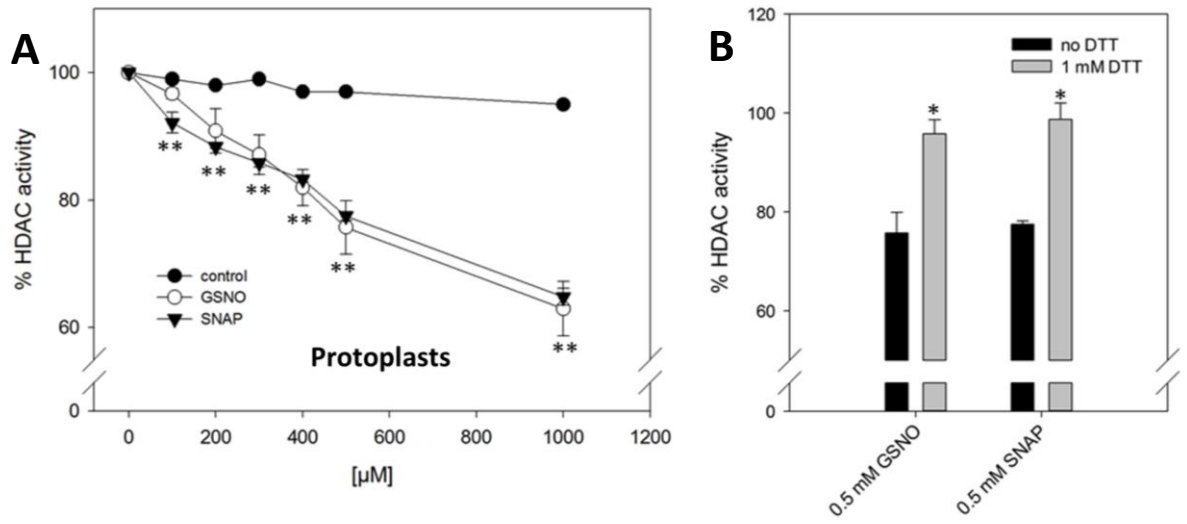

Figure 16: Reversible inhibition of HDAC activity by GSNO and SNAP in protoplasts. A) Protoplasts were treated with water (control), GSNO or SNAP and HDAC activity was measured. Values are expressed as percentage of HDAC activity in untreated protoplasts. B) DTT restored HDAC activity after GSNO and SNAP treatment. Protoplasts were first incubated with GSNO and SNAP before addition of DTT. Subsequently, HDAC activity was measured. Values are normalized to control treatment. Values are mean ± SEM of three independent preparations of protoplasts. * $P < 0.05$, ** $P < 0.01$, student´s t-test.

Further control experiments were conducted. First, SA, INA, GSNO and SNAP did not induce protoplast death within the concentration range used as measured by simultaneous staining of protoplasts with propidium iodide (stains non-viable cells) and fluorescein diacetate (stains viable cells, **Fig. 17**). Furthermore, usage of diluted HCl (at a pH similar to an aqueous solution of SA/INA) revealed, that NO production and HDAC inhibition was not caused by a shift of the pH (**Suppl. Fig. 7A**). Moreover, the SA-mediated inhibition of HDAC activity could be mirrored using 2,3- and 3,4-dihydroxy-benzoic acid (2,3-DHBA and 3,4-DHBA) but not 2,5-DHBA, illustrating that the observed effect is specific and not a chemical artefact (**Suppl. Fig. 8**). Application of the kinase inhibitor K252-A in combination with SA or INA did not show a further reduction or rescue of HDAC activity indicating that phosphorylation cascades did not contribute to the inhibition (**Suppl. Fig. 7B**). Since SA is known to directly bind to proteins thereby modulating their activity the effect of SA on HDAC activity in nuclear extracts was tested. However, no significant changes of HDAC activity could be detected in these experiments excluding that the observed phenotype was caused by direct binding of SA to HDACs (**Suppl. Fig. 7C**).

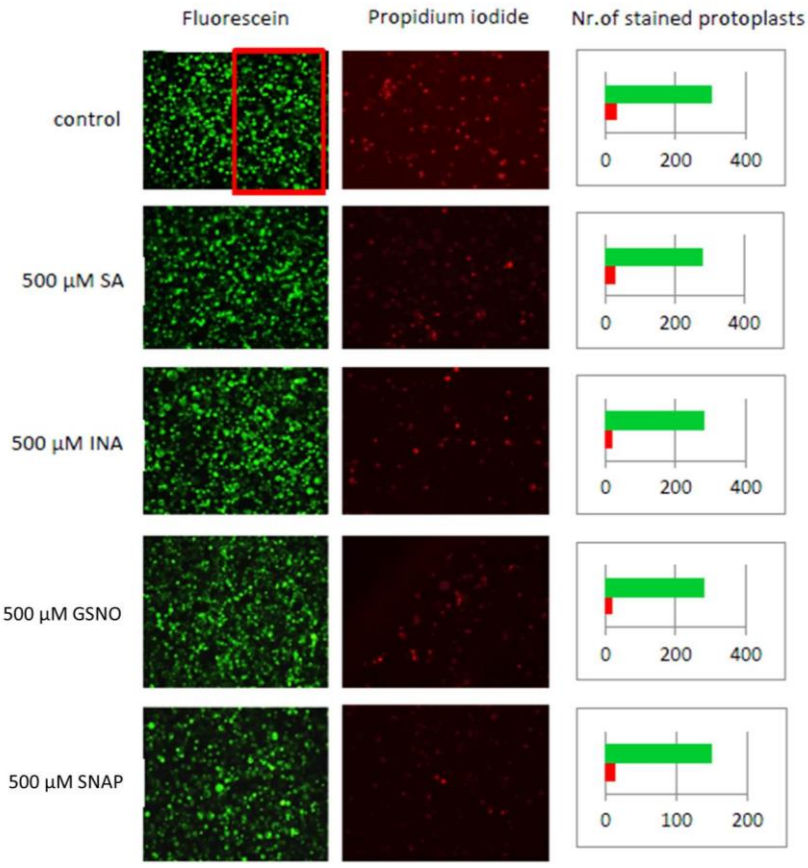

Figure 17: Viability of protoplasts after SA, INA, GSNO and SNAP treatment. Protoplasts were stained simultaneously with fluorescein diacetate and propidium iodide. Viable (accumulation of fluorescein in the cytosol, green) and non - viable (accumulation of propidium iodide in the nucleus, red) cells were counted in one half of the images (red square), the respective numbers are depicted in the diagrams on the right. Green bars represent viable, red bars represent non-viable cells.

Taken together, these data suggest that NO modulates HDAC activity, thereby influencing histone acetylation at specific genomic loci. Two alternative scenarios are conceivable how NO could accomplish this. First, the effect of NO might be indirect, i.e. NO acts upstream of HDACs. Second, NO might affect HDACs directly by S-nitrosylation. To analyze whether HDACs are directly modified by NO, the influence of NO on purified nuclear extracts was investigated since signaling cascades rely on the spatially and temporally controlled association of macromolecules which should be disrupted in protein extracts.

2.2.2 Inhibition of HDAC activity in nuclear extracts by NEM

Since NO mainly acts on cysteine residues, the importance of cysteine residues for HDAC activity was characterized. Nuclear extracts were incubated with NEM (N-ethylmaleimide), a chemical, which alkylates cysteines thereby blocking them for catalytic functions. To measure HDAC activity, a commercial fluorescence based assay was adapted to be used for plant extracts. Briefly, an acetylated peptide was incubated with nuclear extract and the deacetylated product was recognized by a specific antibody. A secondary antibody coupled to a fluorescent reporter then allowed the direct fluorometric quantification of HDAC activity. All chemicals used were tested for interference with the assay by performing standard curves in the presence of this compound (**Suppl. Fig. 9**). Incubation with 500 µM NEM significantly reduced HDAC activity to 20% and 35% in nuclear extracts generated from suspension cells and seedlings, respectively. 1 µM TSA was used as positive control (**Fig. 18**).

These data demonstrate that the thiol-groups of cysteine residues are critical for nuclear HDAC activity in *Arabidopsis*.

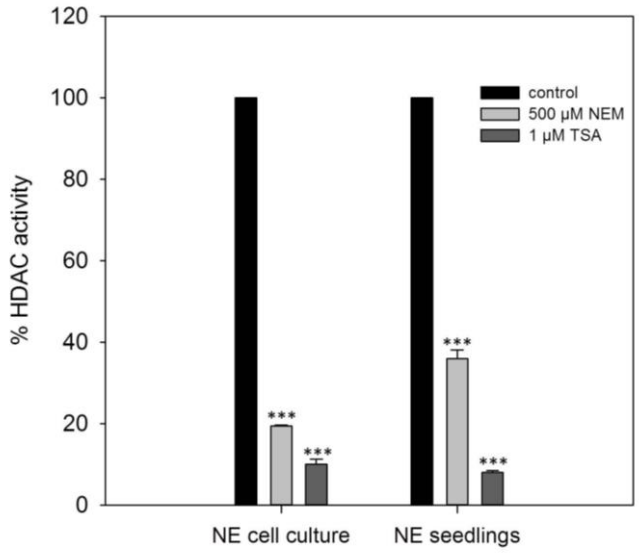

Figure 18: Inhibition of nuclear HDAC activity by NEM. Nuclear extracts (NE) from *Arabidopsis* suspension cells or liquid grown seedlings (7 days) were treated with 500 µM NEM, a chemical which alkylates thiol groups. 1 µM TSA was used as a positive control. Values are mean ± SEM of three independent preparations of nuclear extracts and normalized to control treatment. ***P < 0.001, Student´s t-test.

2.2.3 Reversible inhibition of nuclear HDAC activity by S-nitrosylation

Nuclear extracts from suspension cells and seedlings were incubated with different concentrations of either GSNO or SNAP. GSNO and SNAP strongly inhibited nuclear HDAC activity compared to water and GSH control (**Fig. 19A, C**). The dose response curve dropped sharply for inhibitor concentrations ranging from 10 – 50 µM and flattened for higher concentrations of GSNO and SNAP reaching saturation at 200 – 250 µM and a residual activity of around 40%. Addition of the reducing agent dithiothreitol (DTT) to nuclear extracts and protoplasts pretreated with 1 mM GSNO or SNAP restored HDAC activity in both systems demonstrating the reversibility – representing a critical prerequisite for signal transduction mechanisms - of the corresponding thiol-modification (**Fig. 19B, D**). Moreover, these results excluded that the reduction of HDAC activity was due to chemical side-effects of GSNO and SNAP.

To further strengthen these results, soil-grown seedlings were fumigated with 100 ppm NO or air (control) and HDAC activity was measured 0, 2, 4, 6 and 8 h after the start of the treatment. However, no clear differences of HDAC activity in total protein extracts generated from control and NO-fumigated plants could be detected in this experiment, probably reflecting low NO uptake by the plants and therefore very low intracellular SNO concentrations (**Suppl. Fig. 10**).

Together, these results clearly demonstrated a very high sensitivity of *Arabidopsis* HDAC activity towards S-nitrosylation. HDAC activity could not be completely abolished but reached saturation at 40% residual activity. This might indicate that not all nuclear HDACs were affected by S-nitrosylation. Another possibility is that S-nitrosylation did not completely abrogate the activity of the modified enzyme.

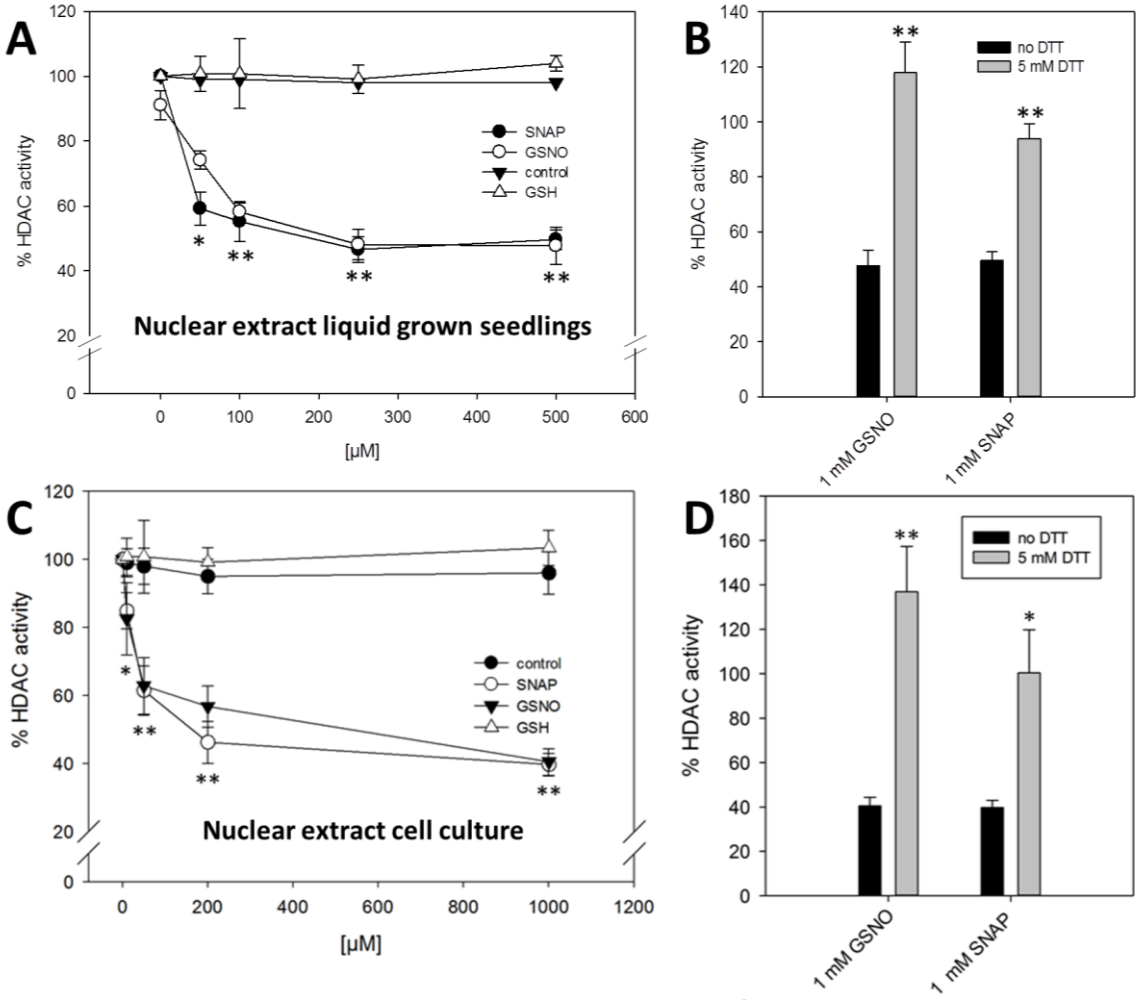

Figure 19: Reversible inhibition of nuclear HDAC activity by GSNO and SNAP. A and C) After pretreatment of nuclear extracts from *Arabidopsis* liquid grown seedlings (A) or cell cultures (C) with water (control), GSH, GSNO or SNAP, HDAC activity was measured. C and D) DTT restored HDAC activity after GSNO and SNAP treatment. Nuclear extracts were first incubated with GSNO and SNAP before addition of DTT. Subsequently, HDAC activity was measured. Values are normalized to control treatment. Values are mean ± SEM of three independent preparations of nuclear extract. * $P < 0.05$, ** $P < 0.01$, student´s t-test.

2.2.4 Inhibition of HDAC activity by oxidized glutathione and H_2O_2 in nuclear extracts and protoplasts

The effect of redox-modifications on HDAC activity was further investigated. Oxidized glutathione (GSSG) is capable of transferring a glutathione moiety to redox-sensitive thiol groups thus leading to a posttranslational modification called S-glutathionylation. S-glutathionylation is thermodynamically more stable than S-nitrosylation, however, due to the larger size of the glutathione, this modification is sterically constrained to freely accessible cysteines [6]. GSSG inhibited HDAC activity in nuclear extracts and protoplasts and this inhibition was reversible upon incubation with DTT (**Fig. 20**). Comparison with GSNO and SNAP treatment revealed that the effect of GSSG was significantly lower both in nuclear extracts (35% inhibition for 1 mM GSSG, 60% inhibition for 1 mM GSNO/SNAP) and

protoplasts (15% inhibition for 1 mM GSSG, 38% inhibition for 1 mM GSNO/SNAP), indicating that HDAC activity is more sensitive towards S-nitrosylation than S-glutathionylation.

H_2O_2 - another major player in the concert of redox-modifications - only showed very mild inhibition in nuclear extracts, which could not be significantly reverted by DTT. Together, these results suggested that HDAC activity in *Arabidopsis* might be regulated by redox-modifications, specifically by S-nitrosylation and S-glutathionylation, whereas oxidation of cysteine residues to sulfenic or sulfonic acid likely only plays a minor role.

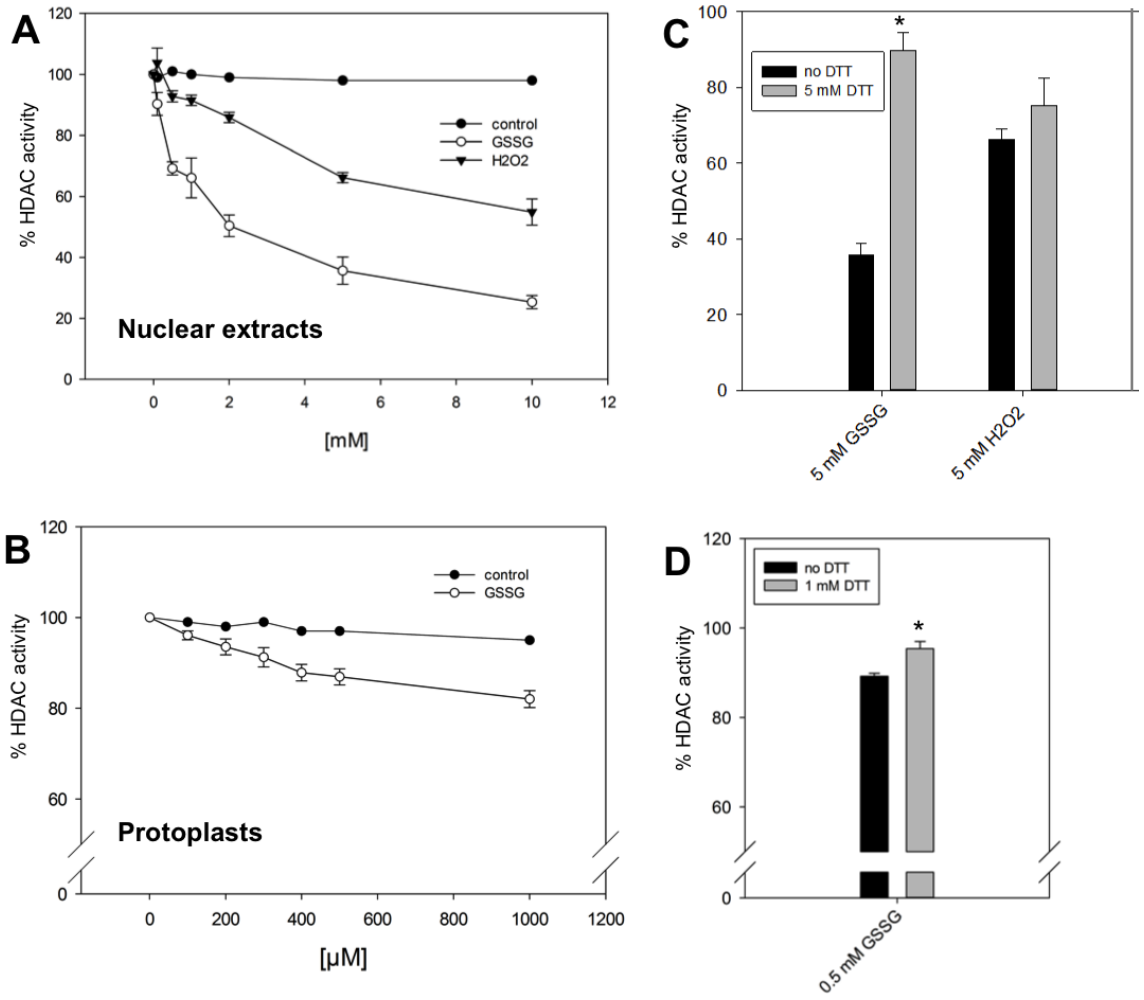

Figure 20: Inhibition of HDAC activity by GSSG and H_2O_2. A) Nuclear extracts from *A. thaliana* cell culture were incubated with different concentrations of GSSG and H_2O_2. B) Protoplasts from A. thaliana cell culture were treated with GSSG. C and D) DTT restored HDAC activity after GSSG but not H_2O_2 treatment. Nuclear extracts and protoplasts were incubated with DTT after GSSG and H_2O_2 addition. Values are expressed as percentage of HDAC activity in untreated nuclear extracts or protoplasts. Values are mean ± SEM of three independent preparations of nuclear extract or protoplasts. * $P < 0.05$, student´s t-test.

2.2.5 Insensitivity of HDAC activity towards S-nitrosylation in Hela nuclear extracts

In a neuronal cell line, nuclear HDAC activity was not affected by S-nitrosylation, whereas HDAC activity in the cytosolic fraction was inhibited by GSNO [142]. To determine whether the inhibition we observed was specific for plants, the effect of GSNO on HDAC activity in HeLa nuclear extracts was analyzed. In contrast to plant nuclear extracts no inhibitory effect of GSNO on HDAC activity was observed in HeLa nuclear extracts, pointing towards a possible plant specific inhibition mechanism (**Fig. 21**).

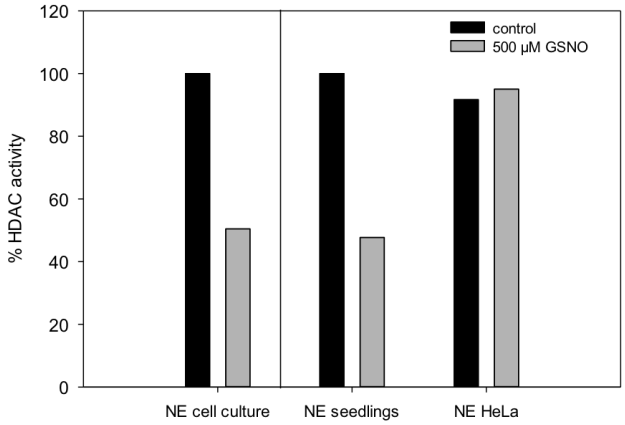

Figure 21: Comparison of GSNO sensitivity of HDAC activity in plant and animal nuclear extracts. Nuclear extracts (NE) containing 5 µg of protein were incubated with 500 µM GSNO and HDAC activity was measured. Shown is the mean of three technical replicates. Standard deviations are too small to be visible.

2.3 Identification of HDA6 as a candidate NO-regulated HDAC

The previous results clearly demonstrated that at least one nuclear HDAC can be inhibited by redox-modifications, specifically S-nitrosylation. The next steps aimed to identify possible candidate HDACs to be regulated by NO.

2.3.1 Homology based identification of HDA6 and HDA19 as putative NO-regulated HDACs

Apparently, only the activity of RPD3 and HDT-family members was measured in the HDAC activity assay, since HDAC activity in nuclear extracts could be completely abolished with TSA – a selective inhibitor of these two HDAC families. In contrast, in protoplasts, 20 % residual activity after TSA treatment were observed, which could be likely attributed to sirtuins, an HDAC class not inhibited by TSA (**Suppl. Fig. 11**). It has not been demonstrated up to date, whether HD-tuins really possess deacetylase activity, therefore we focused our search on the RPD3 family [143]. All members of the RPD3-superfamily contain cysteine residues and some of them are predicted to be nitrosylated using the bioinformatic prediction tool GPS-SNO [144] (for instance Cys273 in HDA6, which is also conserved in HDA19 and others). In many cases, S-nitrosylation of proteins is conserved across the kingdoms. We therefore

collected information about animal HDACs, which were regulated by S-nitrosylation and performed a homology search in *Arabidopsis*. Human HDAC2 was demonstrated to be nitrosylated at Cys262 and Cys274 close to the catalytic center [1, 145]. A BLAST search was performed identifying HDA6 and HDA19 as the closest homologs to human HDAC2. The HDAC domains of HDA6, HDA19 and HDAC2 were highly similar (HDAC2 vs HDA6 71% identity, HDAC2 vs HDA19 70% identity) whereas the C-terminal tails were divergent (**Suppl. Fig. 12**). Specifically, the cysteine residues shown to be nitrosylated in HDAC2 (Cys262 and 274 in HDAC2, Cys273 and 285 in HDA6, Cys269 and 281 in HDA19) lie within conserved regions (**Fig. 22A**) and one of them (Cys273 in HDA6) was predicted to be S-nitrosylated by GPS-SNO (see above).

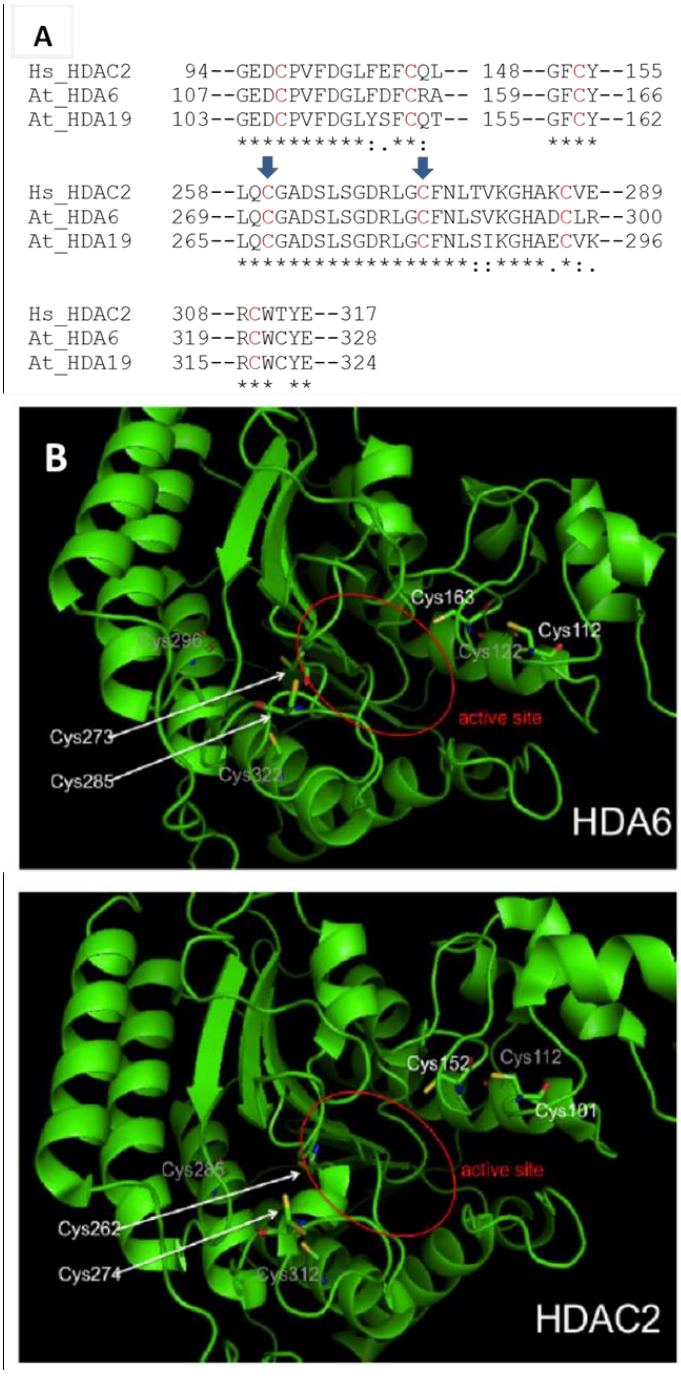

Figure 22: Comparison of HDA6, HDA19 and human HDAC2 sequences and structures. A) Sequence alignment of human HDAC2 and *A. thaliana* HDA6 and HDA19. Conserved cysteines are marked in red, cysteines which are nitrosylated in HDAC2 [1] are indicated with an arrow. Alignment was done using ClustalΩ. B) Structural comparison between human HDAC2 and *Arabidopsis* HDA6. The HDAC domain of HDA6 (amino acids 18 – 385, Uniprot entry Q9FML2) was modelled using the SwissProt Modelling server with human HDAC2 as template (pdb entry 4LY1). Conserved cysteine residues are shown as sticks. Cysteine residues, which are surface accessible or located within the active site are marked in white, a grey label indicates that this cysteine is not surface accessible. The structural comparison between HDAC2 and HDA19 looked very similar (**Suppl. Fig. 16**).

Moreover structural modeling of the HDAC domain of HDA6 and HDA19 using the crystal structure of HDAC2 as template revealed that conserved cysteines are located at the same positions within strikingly similar 3D-folds (**Fig. 22B**). Additionally, both proteins are constitutively located in the nucleus and ubiquitously expressed [97, 103, 146]. Together, this makes HDA6 and HDA19 promising candidates to be the NO-affected nuclear HDAC isoform(s).

2.3.2 Analysis of HDAC activity in *hda6* in response to NO treatment

Based on the results of the previous section an *hda6* cell suspension line was generated to determine whether NO sensitivity is altered upon knockout of HDA6. The *hda6 axe1-5* allele used to generate the cell culture contains an insertion resulting in a premature stop codon and the expression of a non-functional, C-terminally truncated version of HDA6 [96]. Obtained cell cultures exhibited similar growth kinetics and morphology to wild-type cells.

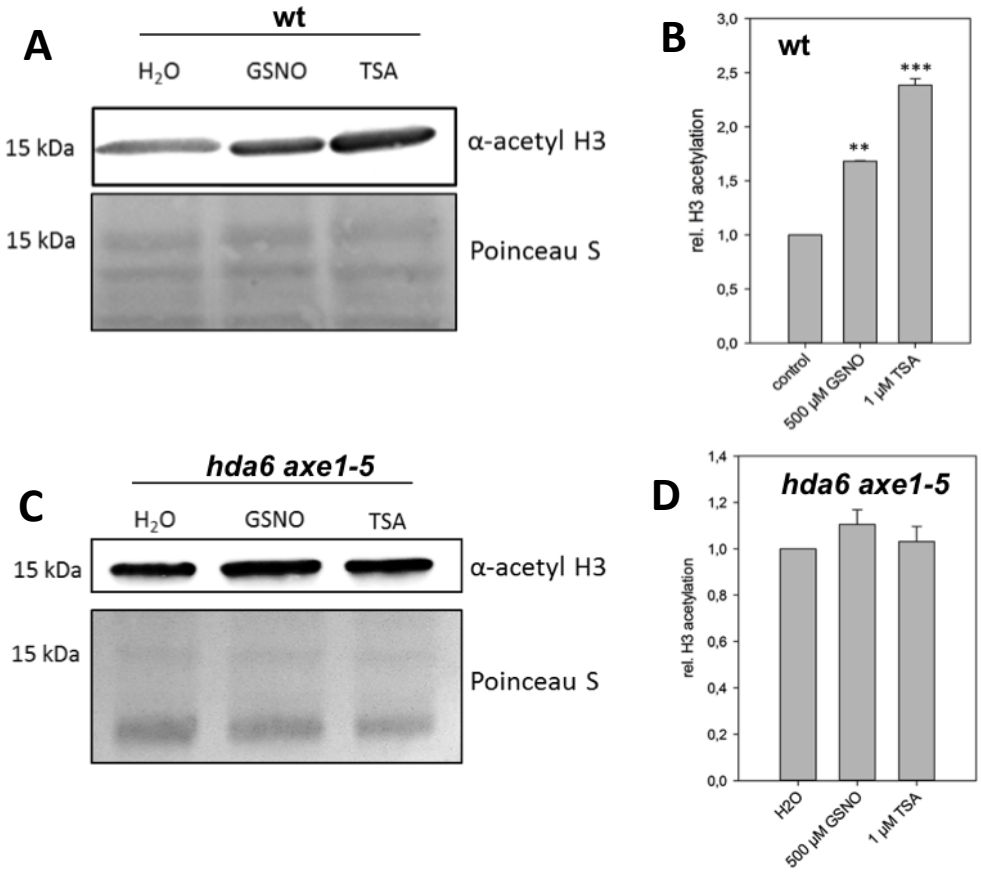

Figure 23: Comparison of H3 acetylation in wt and *hda6* suspension cells after GSNO treatment. A and C) Western-Blot analysis of GSNO- and TSA-treated wt and *hda6* cells. Nuclear extracts were separated by SDS-PAGE and blotted. The membrane was probed with an anti-acetyl H3 primary antibody and a secondary antibody coupled to HRP. Shown is one representative experiment. B and D) Quantification of A and C. Signal intensity was determined with Image J software. Shown is the mean ± SEM of three experiments. **P < 0.01, ***P < 0.001, student´s t-test. These experiments were done by Alexandra Ageeva under my supervision.

Consistent with previous results, wild-type cells showed a slight but significant increase in total H3ac level after GSNO treatment (500 µM), and a more pronounced, approximately 2.5 fold increase after TSA application (**Fig. 23A, B**). In contrast, GSNO treatment of *hda6* cells did not result in an accumulation of acetylated H3 (**Fig. 23C, D**). TSA treatment also did not increase H3 acetylation, indicating that HDA6 was the predominant TSA sensitive HDAC isoform in our cell culture system.

Nuclear extracts in previous experiments were isolated from protoplasts. However, no viable protoplasts from the *hda6* line could be generated. Therefore a different protocol for nuclei isolation was established. HDAC activity in wild-type nuclear extracts generated with this protocol was sensitive towards NO, but in contrast to previous results, TSA treatment could not completely abrogate HDAC activity (residual activity of 65 %), indicating the presence of TSA insensitive HDACs (i.e. sirtuins). HDAC activity in *hda6* nuclear extracts was around 50 % lower compared to wild-type nuclear extracts (**Suppl. Fig. 13**) and – consistent with the western blot results (**Fig. 23**) – was insensitive towards SNAP, NEM and TSA (**Fig. 24**).

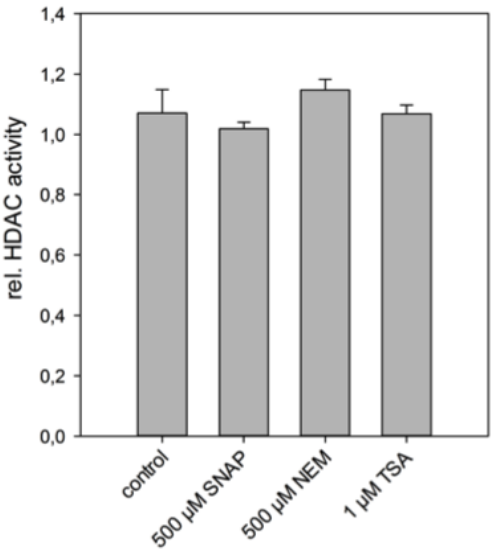

Figure 24: Insensitivity of HDAC activity in *hda6* suspension cells towards cysteine modifications and TSA. Nuclear extracts from *hda6* suspension cells were incubated with 500 µM SNAP, 500 µM NEM and 1 µM TSA and HDAC activity was measured over 90 min. Values are normalized to control treatment (water). Shown is the mean ± SEM of three independent preparations of nuclear extract.

Interestingly, different results were obtained in seedlings. Nuclear extracts prepared from an *hda6* line were as sensitive towards GSNO as wild-type seedlings (**Suppl. Fig. 14**). Moreover, HDAC activity from *hda6* seedlings was still inhibited by TSA, indicating that HDA6 was not the only TSA sensitive HDAC in nuclear extracts prepared from seedlings (**Suppl. Fig. 14**). These results indicate that besides HDA6, another NO sensitive HDAC isoform is expressed in seedlings.

2.3.3 Purification and S-nitrosylation of recombinant HDA6 in *E.coli*

Based on the sequence alignments and previous results, we decided to purify HDA6 and test whether this protein is S-nitrosylated *in vitro* and whether S-nitrosylation affects its activity.

Initial expression studies in a variety of *E. coli* strains under different expression conditions revealed a very low solubility of HDA6. Therefore, His_6-HDA6 and GST-HDA6 were expressed in E. coli BL21(DE3) cc4 ($HDA6^{E.coli}$) - a strain which contains additional chaperones, helping to produce proteins with low solubility - and purified using Ni-NTA or anti-GST affinity chromatography.

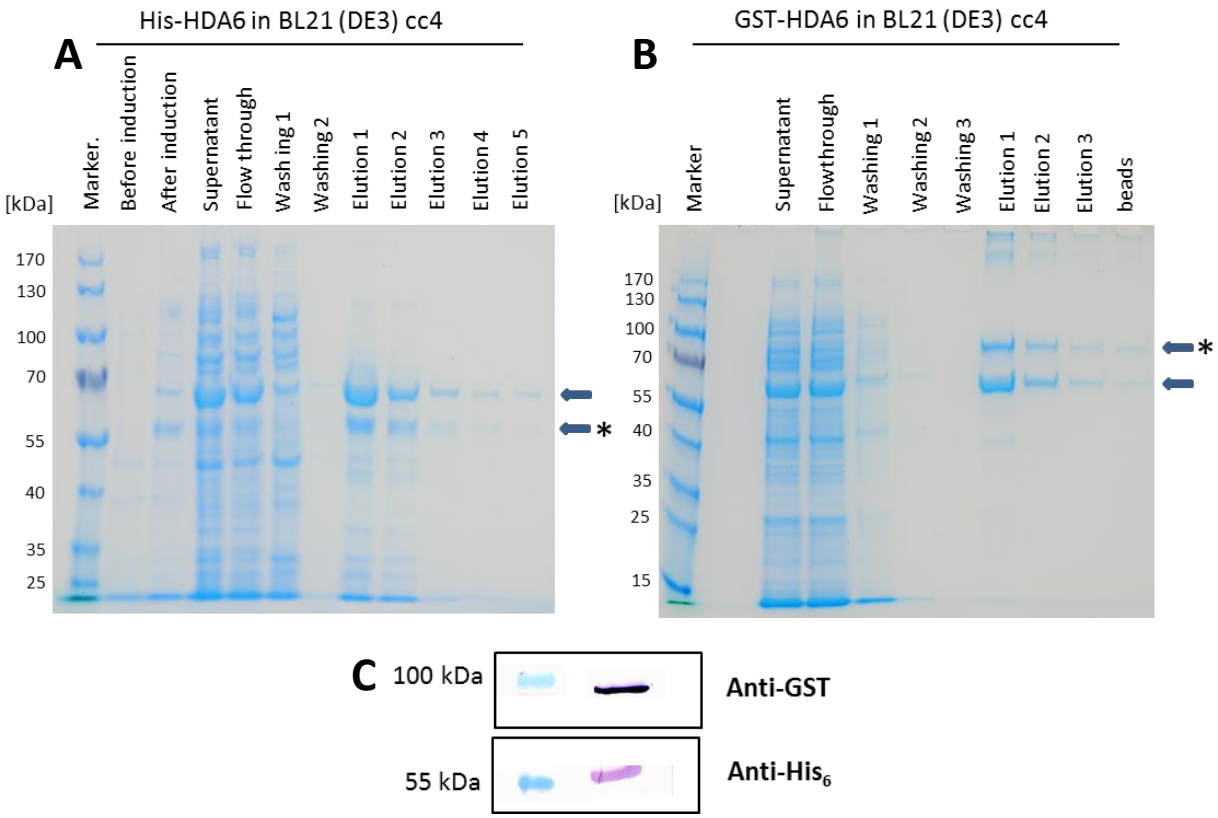

Figure 25: Recombinant purification of HDA6 in *E. coli* BL21 (DE3) cc4. A) Fractions of the different purification steps of His_6-HDA6 were separated by 12% SDS-PAGE. B) Fractions of the different purification steps of GST-HDA6 were separated by 12% SDS-PAGE. Bands marked with an arrow and asterisk correspond to His6-HDA6 (theoretical MW 53.7 kDa) and GST-HDA6 (theoretical MW 79 kDa), respectively. Bands marked with an arrow may represent the chaperone DnaK (theoretical MW 69 kDa). C) Western-Blot analysis. Elution fractions were blotted onto nitrocellulose and probed with anti-His_6 and anti-GST antibodies. The secondary antibody was coupled to alkaline phosphatase.

We obtained partially purified elution fractions containing the target proteins (His_6-HDA6 54 kDa, GST-HDA6 79 kDa, **Fig. 25**) as confirmed by Western Blot analysis using anti-His_6 and anti-GST antibodies (**Fig. 25C**). A second prominent band was found in the elution fractions which might correspond to DnaK (belongs to Hsp70 family, 69 kDa theoretical MW), a chaperone expressed in BL21 (DE3) cc4 to prevent aggregation of rather unsoluble proteins. This already suggests that HDA6 might contain hydrophobic stretches, which have to be shielded to prevent aggregation.

To investigate *in vitro* S-nitrosylation, His_6-HDA6 was chosen since the GST-tag contains cysteine residues, which might result in a false positive signal. *In vitro* S-nitrosylation of HDA6 was demonstrated using the biotin switch technique. This method allows for the selective conversion of S-nitrosylated to S-biotinylated thiols [147]. Equal amounts of recombinant His_6-HDA6 were incubated with GSH (250 µM, control) or different concentrations of GSNO (0, 1, 10, 100, 250 µM). After removal of excessive GSNO (or GSH) the samples were subjected to the biotin switch assay. Even for low concentrations of GSNO (10 µM) S-nitrosylated HDA6 was detected, indicating that this protein is very sensitive towards S-nitrosylation. No signal could be detected in water and GSH treated samples, demonstrating the specificity of the assay (**Fig. 26**).

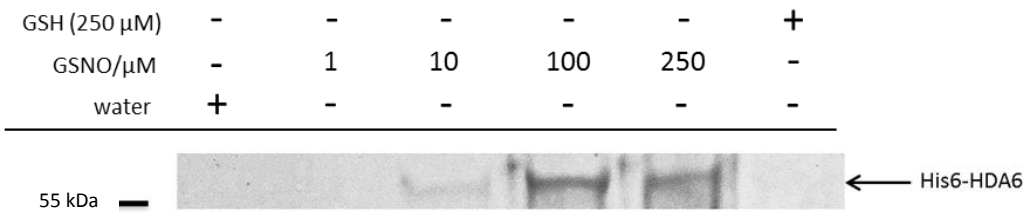

Figure 26: *In vitro* S-nitrosylation of HDA6. 5 µg of recombinant His_6-HDA6 (expressed in E. coli) were incubated with different concentrations of GSNO (or water and GSH as controls) for 30 min at room temperature. Excessive GSNO was removed by Zeba-Spin columns, and the eluates were subjected to the biotin switch assay using MMTS as blocking and ascorbate as reducing agent. After gelelectrophoresis and blotting, the membrane was probed with an anti-biotin antibody coupled to alkaline phosphatase. The assay was repeated twice with similar results.

We next tested recombinant HDA6 for its enzymatic activity. However, no deacetylase activity could be measured for His_6-HDA6 and GST-HDA6. This prompted us to speculate that HDA6 might need certain posttranslational modifications or was improperly folded in *E. coli*. Therefore insect cell expression was used to circumvent these problems.

2.3.4 Insensitivity of HDA6 activity towards S-nitrosylation

His_6-HDA6 was expressed in Sf5 insect cell cultures and purified using Ni-NTA affinity chromatography and subsequent gel-filtration as polishing step. The specific activity of HDA6 was determined as 329.8 $\pm$ 5.2 fmol min^{-1} μg^{-1} (**Fig. 27A**). Then HDA6 was incubated with different amounts of GSNO to analyze the influence of S-nitrosylation on the activity. However, no significant alterations of HDA6 deacetylase activity could be detected, indicating that S-nitrosylation did not affect the basal catalytic activity of HDA6 (**Fig. 27B**).

In summary, it was found that the inhibition of nuclear HDAC activity by GSNO, SNAP and NEM as well as the increase in total H3ac after GSNO treatment of cell-cultures was HDA6 dependent. However, the activity of recombinant HDA6 itself was not affected by cysteine modifying chemicals. This prompted us to speculate that the effect of S-nitrosylation of HDA6 might only be visible in the corresponding holocomplex. This hypothesis was

supported by several studies which demonstrated that recombinant HDACs are much less catalytically active than the same enzyme in its natural complex. Therefore, a purification strategy was initiated to purify the native HDA6 complex.

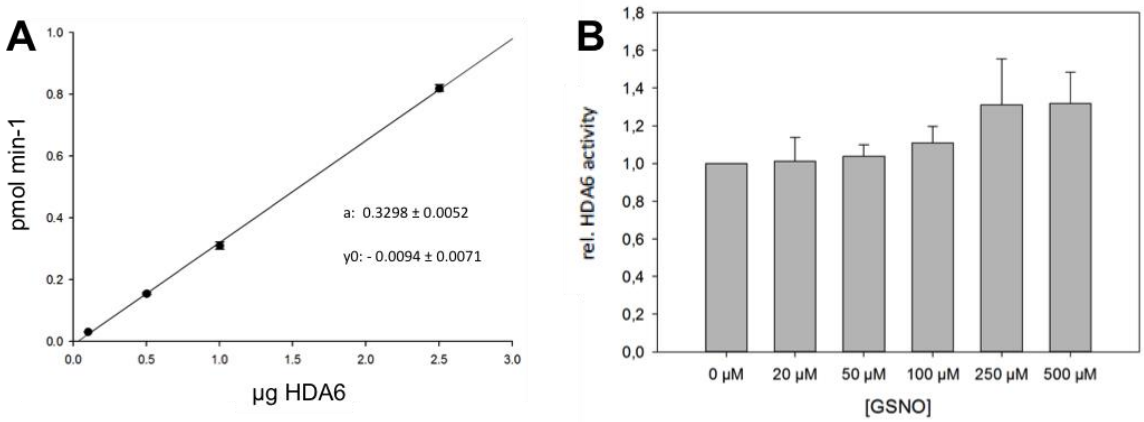

Figure 27: Analysis of HDA6 activity in response to GSNO treatment. HDA6 was expressed in Sf5 insect cells and purified by Ni-NTA affinity and subsequent size exclusion chromatography. A) HDAC activity was measured for different amounts of HDA6. Shown is the mean ± SEM of four HDA6 purifications (two preparations for C- and N-terminal His6-tag). B) 1 µg of recombinant HDA6 was incubated with different concentrations of GSNO and HDAC activity was measured. Shown is the mean ± SEM of four HDA6 preparations (two preparations for C- and N-terminal His6-tag). Values are normalized to the activity of untreated HDA6.

2.3.5 Purification of HDA6 in its native complex – initial steps

The easiest option to purify the native HDA6 complex would be a co-immunoprecipitation assay with an antibody directed against HDA6. However, so far no suitable antibody could be found. Therefore, HDAC activity from total protein extracts generated from seedlings was purified. Subsequent mass-spectrometric analysis would allow the identification of the fractions containing HDA6. In contrast to adult plants, seedling-extracts showed high HDAC activity, facilitating the purification procedure. Anion exchange chromatography was chosen as a first purification step, since almost all *Arabidopsis* HDACs exhibit pKa-values < 6. At a pH > 6, HDACs are negatively charged and thus should bind to the matrix of anion exchangers.

Total soluble proteins were extracted in extraction buffer (pH 6.5) and incubated with a DNA digesting enzyme, to solubilize DNA bound protein complexes. Extracts were loaded on a MonoQ column with a flow rate of approximately 1 mL/min. Bound proteins were eluted by stepwise increasing the sodium chloride concentration in the buffer (0 – 1 M NaCl). Each fraction (1 mL) was tested for HDAC activity and protein content. Fractions were then concentrated and analyzed by SDS-PAGE.

Three distinct HDAC activities could be identified in total soluble protein extracts from *Arabidopsis* seedlings. The first one eluted at 100 mM NaCl as a very sharp peak, the second small one at 250 mM, and the third rather broad one at 550 mM (**Fig. 28A**). Subsequent SDS-PAGE analysis revealed several protein bands, showing a similar pattern as the first and second HDAC activity peak (**Fig. 28B**). Protein concentration in fractions 10 - 16 were too low

for SDS-PAGE analysis. Initial experiments to test the main HDAC fractions for GSNO sensitivity resulted in inconsistent results among the replicates, probably due to oxidation processes during the purification procedure. We conclude that further streamlining of the protocol, as well as including additional chromatographic purification steps will be needed to identify the GSNO sensitive HDAC / HDAC-complex.

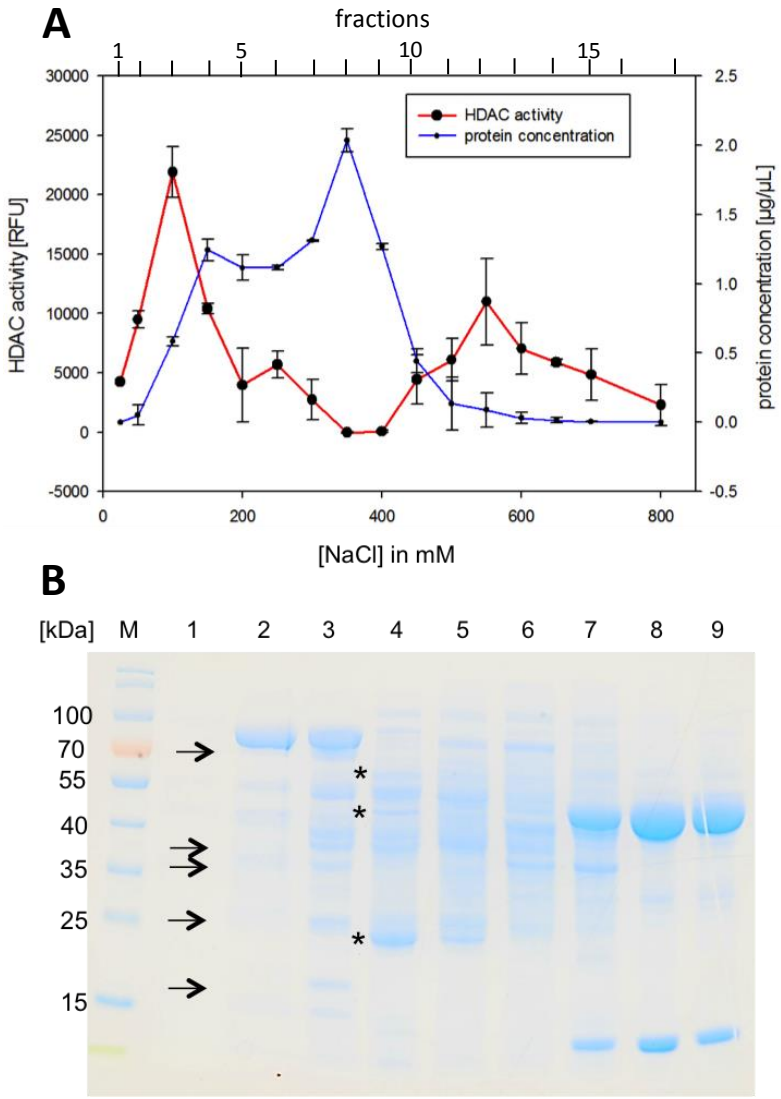

Figure 28: Separation of HDAC activity in *Arabidopsis* seedlings by anion exchange chromatography. A) Total protein extracts (pH 6.5) were loaded on a MonoQ column and bound proteins were eluted by a stepwise increase of salt concentration. HDAC activity was measured for every fraction and plotted as a function of the NaCl concentration in the elution buffer (red line). Protein concentration in each fraction was determined by Bradford-Assay (blue line). Shown is the mean ± SD of two independent experiments. B) Fractions 1 – 9 (25 – 400 mM NaCl) were concentrated and separated on a 12% SDS-PAGE and stained with Coomassie. Protein concentrations in fractions 10 – 16 were too low for SDS-PAGE analysis. Arrows and asterisks indicate bands which follow the HDAC activity pattern of the first and second peak, respectively.

2.3.6 Analysis of the salt stress response in wt and *hda6* after NO-pretreatment

The *hda6* mutant displayed increased susceptibility to salt stress [100]. Since NO positively modulates the salt stress response, we asked whether NO exerts parts of its beneficial effects through acting on HDA6. To test this, 5 day old wt and *hda6* seedlings were transferred to plates containing i) just MS and sucrose ii) 200 µM SNAP iii) 200 µM SNAP and 200 µM cPTIO. Two days later, seedlings were transferred to plates containing the above mentioned chemicals plus 150 mM NaCl. Root growth was chosen as readout for salt stress susceptibility/resistance.

Both lines showed similar root-growth rates before the treatments (day 0 to day 5). Consistent with several reports, pretreatment with SNAP resulted in reduced root-growth in both genotypes. Interestingly, the *hda6* mutant was slightly (but significant) more sensitive towards SNAP indicating a hypersensitivity towards NO. SNAP treated wild-type seedlings were more resistant to subsequent salt stress than nontreated and SNAP/cPTIO treated seedlings as indicated by much higher root-growth rates. This beneficial effect of NO was completely lost in the *hda6* mutant in which root-growth directly stopped after the start of salt stress. Importantly, these effects were reversible upon cPTIO treatment, demonstrating that the observed phenotype was due to NO (**Fig. 29**).

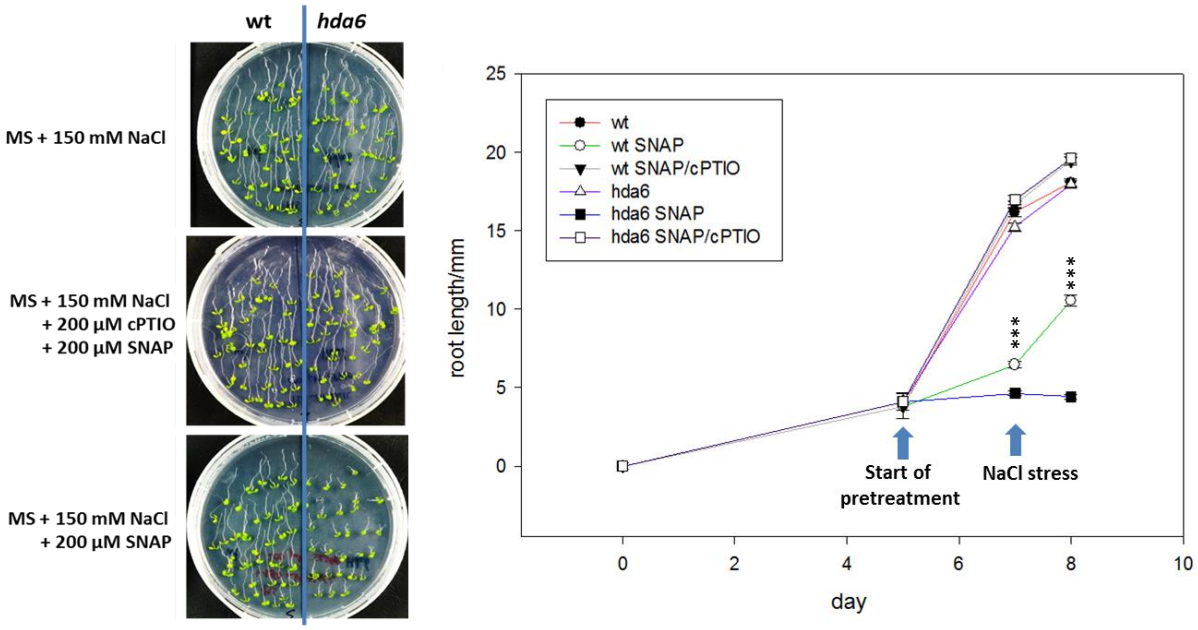

Figure 29: Salt stress response in wt and *hda6* after NO-pretreatment. Seedlings were grown on MS plates for 5 days and then transferred to plates containing i) 200 µM SNAP ii) 200 µM SNAP/200 µM cPTIO iii) just MS and 1% sucrose (pretreatment). Two days later seedlings were moved to plates containing 150 mM NaCl and the chemicals mentioned above. A) Representative image of seedlings grown for 1 day under salt stress, with the respective pretreatments indicated on the left. Shown is one replicate out of three. B) Quantification of root growth. Plates were photographed at the indicated time points and root length was measured using ImageJ software (n = 67 -118). Shown is the mean ± SEM of 67 – 118 individual roots grown on three different plates. *** P-value < 0.001, One way Anova (Holm-Sidak method, overall significance level 0.05).

3 Discussion

Although NO has been implicated in transcriptional reprogramming during the plant´s stress response, the molecular mechanisms remain largely elusive. In particular, the effect of NO on the chromatin structure has not been analyzed in plants. The aim of this work was to investigate the influence of NO on histone acetylation in *Arabidopsis*. GSNO treatment enhanced the H3K9/14ac in defense genes in *Arabidopsis* seedlings and induced a slight total increase in H3ac in suspension cells. Furthermore, NO inhibited HDAC activity in protoplasts and nuclear extracts, which was likely mediated by S-nitrosylation of HDAC-complexes. Finally, HDA6 was identified as a NO-targeted HDAC isoform. In summary, these data suggest a model in which NO participates in transcriptional regulation by inhibiting HDAC activity and thus increasing histone acetylation at defense genes.

3.1 H3K9/14 acetylation distribution shows strong similarities to other H3 acetylation marks.

In this work, the epigenomic profile of H3K9/14ac was mapped and analyzed for the first time in plants. Approximately 13000 H3K9/14ac sites were found in whole tissue samples of liquid grown *Arabidopsis* seedlings. More than 95% of the discovered sites were located in genic regions, and only a minority was found in intergenic regions. The mark was almost absent from repetitive regions like pericentromeric chromatin (**Fig. 6**). This is consistent with reports about similar histone acetylation marks. In *Physcomitrella*, H3K9ac (25000 sites) and H3K27ac were both primarily found within genic regions (92 and 96%, respectively [87]); in rice 86.2% of a total of around 30000 H3K9ac marks were annotated within genic regions [148]. In contrast, H3K9ac in maize was distributed more evenly throughout genic and intergenic regions [149]. Considering the small genome size of *Arabidopsis* (135 Mbp) compared to *Physcomitrella* (473 Mbp) and rice (430 Mbp) the detected number of 13000 H3K9/14ac sites (one site every 10.4 kbp) is well in the range of similar histone marks in the other species (one H3K9ac site every 18.9 kbp and 14.3 kbp in *Physcomitrella* and rice, respectively). However, in general these numbers are difficult to compare, since they strongly depend on the sequencing depth, which may vary in the different studies [131, 150].

Genome-wide distributions of H3K9ac and H3K14ac in mouse embryonic stem cells revealed a strong positive correlation between both modifications, i.e. both marks co-occurred in many gene regulatory regions. Moreover, the maxima of the corresponding distributions were located around 300 – 400 bp downstream of the TSS [128]. Similar observations were documented for H3K9ac and H3K27ac in *Physcomitrella*, in which both marks were

distributed sharply downstream of the TSS [87]. In strong accordance with this data, it was found in this study, that H3K9/14ac is primarily located within one kb of the 5´-end of the corresponding gene, showing a maximum in its distribution at 400 bp downstream of the TSS (**Fig. 7A**). Most of the detected peaks were located in exonic regions followed by triplex-forming sites (TTS, functional significance not clear) and promoter regions. Again this is in line with findings from other studies. For instance, in *Physcomitrella*, most of the H3K9ac and H3K27ac sites were found to be within promoters, coding sequences (which are the exons) and introns [87]. Interestingly, in *Physcomitrella* almost 20% of peaks were located in the 5´-UTR whereas in this work only 4% of the H3K9/14ac sites were found in these regions. This might indicate that the H3K9ac mark is broader or diffuser than the H3K9/14ac modification. In fact, the average length of the H3K9ac mark in the moss was around 800 bp (and even 1.2 kb in shoots of maize [151]), compared to 500 bp of the H3K9/14ac peaks in this study [87].

3.2 Histone acetylation is not sufficient to activate transcription

In general, histone acetylation is correlated with transcription of the decorated genes. However, recent publications suggest, that histone acetylation is not sufficient to activate transcription. Instead, genes are activated by transcription factors in tight interplay with histone acetylation changes. For instance, knockout of a maize HDAC (HDA101) lead to the hyperacetylation of several thousand genes but less than 2% of these genes were transcriptionally upregulated [152]. Another study reported that histone methylation changes induced by a weak salt-stress treatment did not merely reflect the transcriptional response [88]. In accordance with this, we found in initial qPCR experiments that several genes showing enhanced H3K9/14ac were also transcriptionally upregulated. Nevertheless, a significant proportion of the genes we tested did not show clear changes in the corresponding mRNA level, enforcing the notion that histone acetylation is not sufficient to activate transcription by its own. This might also partially explain why we could not detect a clear correlation of the ChIPseq data and the RNAseq data after GSNO treatment (**Suppl. Fig. 17**) although it has to be considered that fundamental experimental differences exist between both experiments [135].

3.3 NO/ROS dependent regulation of HDAC activity

Several lines of evidence suggest that NO and ROS negatively regulate HDAC activity in *Arabidopsis*. First, GSNO mainly increased histone acetylation in the ChIPseq study and the majority of genes found to be regulated by NO-induced histone acetylation also showed enhanced H3K9/14ac levels after TSA treatment, indicating that HDACs control the acetylation on these loci (**Fig. 9 and 12**). Moreover, it was found that SA-induced NO

inhibited total HDAC activity in protoplasts (**Fig. 15**). Furthermore, HDAC activity in protoplasts and nuclear extracts generated from different sources was strongly but reversibly reduced upon incubation with S-nitrosylating compounds (**Fig. 16** and **19**). Finally, cell cultures treated with GSNO showed slightly increased total H3ac (**Fig. 23**).

Interestingly, HDAC activity in the nuclear fraction of neurons could not be blocked by S-nitrosylation, whereas cytosolic HDAC activity was inhibited by GSNO in these cells [142]. Similarly we observed that nuclear extracts from Hela cells were insensitive towards GSNO. In contrast, HDAC activity in nuclear extracts generated from plants was strongly inhibited by S-nitrosylation (**Fig. 21**). Since *Arabidopsis* and human HDACs show strong sequence similarities, it seems likely that these differences are caused by the expression of different homologs in plant and Hela nuclear extracts. However, this difference might also point towards a plant specific inhibition mechanism.

In contrast to animals, reports about the connection between the redox-status of the cell and epigenetic changes are limited and rather indirect in plants. Heat-induced programmed cell-death (PCD) in maize seedlings was characterized by global histone hyperacetylation, which correlated with increasing O_2^- concentrations. In contrast, total H3K4me2 levels remained unchanged throughout the progression of PCD, suggesting that oxidative stress conditions might selectively affect histone acetylation [153]. It was furthermore demonstrated that heat treatment resulted in the decondensation of 45S and 5S rDNA loci, which was accompanied by DNA hypomethylation [154, 155]. However, the roles of histone acetylation and ROS/NO in this process were not investigated. Another study found that three different sugarbeet cell-lines, exhibiting different amounts of ROS, showed differential total histone acetylation as well as HDAC activity, indicating that these parameters might be connected by yet unknown molecular mechanisms [156]. Finally, silencing of rice HDT701 (a member of the plant specific HDT-family of HDACs) resulted in increased ROS production during PAMP-triggered immunity, indicating that HDT701 negatively regulated ROS production in the defense response [157]. This was likely accomplished by controlling the histone acetylation status and the expression of the SGT1-gene, which is part of the cytosolic defensome complex mediating the accumulation of ROS generated by NADPH oxidases [158].

In animals, HDACs seem to be the major epigenetic transducers of oxidative and nitrosative stress [159, 160]. For instance, Shimazu et al. demonstrated that under diets provoking oxidative stress conditions, mice produced D-b-hydroxybutyrate, a ketone-body, which acted as a specific class I HDAC inhibitor. Inhibition of HDAC1 and 2 by this compound increased global histone acetylation including two promoter regions of key oxidative stress responsive genes. This in turn led to increased transcript levels of these proteins and less susceptibility towards oxidative stress [161]. Further, HDACs are negative regulators of inflammation. They were recruited to inflammatory genes by glucocorticoid receptors, to control their expression. During oxidative and nitrosative stress, HDACs became inactivated and histone acetylation increased, resulting in uncontrolled expression of inflammatory genes [162].

Several studies in animals clearly demonstrate that HDACs are direct targets for redox-regulation. Interestingly, HDACs seem to be primarily targeted by NO-mediated PTMs, which confirms the observations in this work. Brain-derived neurotrophic factor induced NO production in nuclei of a neuronal cell line, which resulted in subsequent S-nitrosylation of HDAC2 at Cys262 and Cys274. S-nitrosylation did not affect the deacetylase activity of HDAC2. Instead this modification induced the dissociation of HDAC2 from the chromatin, resulting in enhanced histone acetylation on HDAC2 regulated genes [1]. One of these genes was brahma (Brm), which is a component of a chromatin-remodeling complex. By inducing the expression of brm and other neurotrophic genes, S-nitrosylation of HDAC2 induced chromatin remodeling and regulated neuronal development [145]. Another study reported, that application of NO-donors to dystrophin-deficient mice (dystrophin is a major muscular protein, its absence leads to a disease called Duchenne muscular dystrophy) resulted in the total inhibition of HDAC2 activity [124]. The different outcomes of S-nitrosylation on HDAC2 might be explained by modification of different cysteine residues in different tissues [163]. HDAC6 is a cytoplasmic HDAC controlling the acetylation of alpha-tubulin. HDAC6 was nitrosylated after stimulation with cytokines, which inhibited its activity and resulted in increased alpha-tubulin levels [125]. HDAC8 was demonstrated to undergo S-nitrosylation after incubation of the recombinant protein with NO donors. Similar to HDAC6, S-nitrosylation inhibited the deacetylase activity of HDAC8 [3]. In endothelial cells, S-nitrosylation of Protein phosphatase 2A induced the formation of a large protein complex consisting of HDAC4, HDAC5 and HDAC3 and the subsequent shuttling of this complex into the nucleus [126]. These studies imply that animal HDACs constitute central elements in redox-signaling cascades, which directly translate the production of NO and ROS into epigenetic responses.

Oxidative stress involves the production of several redox-active species apart from NO. Plasma-membrane located NADPH-oxidases generate superoxide, which subsequently becomes dismutated in the acidic milieu of the apoplast, resulting in the formation of the important redox-signaling molecule H_2O_2 [55]. H_2O_2 can oxidize susceptible cysteine residues to sulphinic, sulphenic or sulphonic acid, thereby affecting the function of the modified protein. Moreover, oxidative conditions shift the GSH-GSSG equilibrium towards oxidized glutathione (GSSG), which can lead to S-glutathionylation of proteins – another important redox-modification in plants and other species [6]. Further, NO and H_2O_2 enhanced the production of each other, resulting in a complex interplay of different redox-species [164]. This shows that NO rarely occurs as the only redox-active species in the cell, which prompted us to measure the effect of GSSG (promoting S-glutathionylation) and H_2O_2 on HDAC activity. S-glutathionylation and cysteine-oxidation by H_2O_2 also decreased total HDAC activity *in vitro* and in protoplasts. This was to be expected, since the chemical prerequisites for cysteines to be modified by either of these modifications are similar (low pKa, high nucleophilicity), although the steric constraints for the bulky GSH-moiety are higher than for the nitrosyl-moiety [6]. However, the inhibition caused by GSSG and H_2O_2 was much lower as compared

to GSNO or SNAP, suggesting that S-nitrosylation seems to be the prime redox-based mechanism for regulating HDAC activity.

In conclusion, this study established HDAC-complexes as targets of NO and possibly other ROS, thus providing the first molecular link between the production of NO/ROS and epigenetic changes in plants. The central role of HDACs at the interface between oxidative stress and chromatin changes seems to be conserved across the animal and plant kingdom, although details in the molecular mechanism might vary.

3.4 Redox regulation of the HDA6-complex

Redox-regulated cysteine residues are often conserved in different species. Therefore, information about S-nitrosylation of human HDACs was used to identify homologous proteins in *Arabidopsis*, with a focus on conservation of cysteines. With the exception of HDAC2, most of the studies conducted in human HDACs did not identify the cysteine residues which undergo S-nitrosylation. It was therefore decided to focus the analysis on HDAC2 homologs.

The closest *Arabidopsis* homologs of human HDAC2 are HDA6 and HDA19. The HDAC domains of HDAC2, HDA6 and HDA19 are highly similar (70% identity), whereas the C-terminal tails show low homology. The C-termini of HDA6 and HDA19 mediate the interaction with different interaction partners, for instance MET1 and FLD [99, 165]. In total, seven cysteine residues are conserved in all three proteins and all of them lie within the conserved HDAC-domain (**Suppl. Fig. 12**). Moreover, modeling of the 3D structures of the HDAC-domains of HDA6 and HDA19 and comparison with the crystal structure of HDAC2 revealed almost identical overall folds, in which the conserved cysteines are located at similar positions, within identical microenvironments (**Fig. 22**). The latter notice is of particular importance, since the surrounding amino acids (i.e. the microenvironment) play a crucial role in the determination of the pKa and thus the nucleophilicity of the corresponding cysteine, which in turn determines its susceptibility towards redox-modifications [166]. Moreover, hydrophobic pockets in close proximity to cysteines might enforce its S-nitrosylation, since they promote the formation of N_2O_3, a redox-species mediating de novo S-nitrosylation [57]. Two conserved cysteines were predicted to be S-nitrosylated using the prediction tool GPS-SNO (Cys152 and Cys262 in HDAC2, corresponding to Cys163/Cys273 in HDA6 and Cys159/Cys269 in HDA19) [144], and one of these (Cys262 in HDAC2) was demonstrated to be S-nitrosylated *in vivo* [1].

Cys262 and Cys274 of human HDAC2 (corresponding to Cys273/Cys285 in HDA6 and Cys269/Cys281 in HDA19) were demonstrated to be S-nitrosylated in response to BDNF-triggered NO synthesis in neurons [1]. Cys262 is located at the backside of the active center, whereas Cys274 is positioned at the entrance of the active site [167]. These residues are

conserved in a variety of species like *D. melanogaster* and *S. cerevisiae*. Unexpectedly, S-nitrosylation of Cys262 and Cys274 did not affect the deacetylase activity of HDAC2 but resulted in the dissociation from the chromatin [1]. Since HDAC2 itself does not possess DNA-binding activity (no DNA binding domain present) and is targeted to specific loci by interaction with sequence-specific DNA binding factors, this might indicate that S-nitrosylation of HDAC2 induced alterations in protein-protein interactions within the HDAC2 complex [168]. However, HDAC2 activity was measured after immunoprecipitating this protein from BDNF-stimulated (S-nitrosylated HDAC2) and non-stimulated cells (overnight). Since SNOs are very labile PTMs this procedure might have resulted in the loss of S-nitrosylation. Further, the HDAC2 mutant in which Cys262/Cys274 were substituted by alanines showed slightly reduced deacetylase activity, indicating that both cysteines might be involved in the catalytic process of HDAC2 (Fig. 3A in [1]). This is supported by another study, which demonstrated that application of NO-donors to dystrophin-deficient muscle cells resulted in the inhibition of HDAC2 activity by S-nitrosylation [124]. In summary, although HDAC2 has clearly been established as a target for S-nitrosylation, the effect of this modification on the HDAC2-complex is not entirely understood and probably affects the activity as well as the association of the HDAC2-complex with chromatin.

Is HDA6 (or HDA19) responsible for the reduction of HDAC activity after GSNO treatment? This question was answered by measuring HDAC activity in response to GSNO treatment in *hda6* suspension cells. Indeed, HDAC activity in this cell line could not be reduced by S-nitrosylation and cysteine-alkylation, indicating that HDA6 was the only nuclear redox-sensitive HDAC in our cell culture system (**Fig. 24**). Consistently, the slight increase in total H3ac after GSNO treatment observed in wild-type suspension cells was abolished in the *hda6* line (**Fig. 23**). However, from these experiments we cannot exclude that other HDACs might be targeted by S-nitrosylation since TSA treatment did not further reduce HDAC activity in nuclear extracts from *hda6* suspension cells, demonstrating that HDA6 was apparently the only RPD3-type HDAC in this system. Confirming this, HDAC activity in nuclear extracts from *hda6* seedlings (not suspension cells) could still be inhibited by GSNO, clearly demonstrating that HDA6 is not the only HDAC affected by S-nitrosylation in seedlings (**Suppl. Fig. 14**). In fact, the high sequence similarity of HDA6 and HDA19 suggests that both of these proteins might be targets of S-nitrosylation, although only HDA6 was further analyzed in this thesis.

Two alternative scenarios are conceivable how S-nitrosylation of HDA6 could decrease the activity of the HDA6 complex. First, S-nitrosylation might directly affect the deacetylase activity of HDA6 as reported for animal HDAC6 and HDAC8 [3, 125]. To test this hypothesis, HDA6 was produced in insect cells ($HDA6^{insect}$), since expression in *E. coli* resulted in inactive HDA6. This phenomenon was already described for other eukaryotic HDACs, which showed no or only very weak deacetylase activity after purification from *E. coli* – either due to missing posttranslational modifications or activating interaction partners [95]. $HDA6^{insect}$ was catalytically active but its activity was not inhibited by GSNO (**Fig. 27**). The second scenario considers the effect of S-nitrosylation on the whole HDA6-complex. *In vivo*, HDACs are subunits of large multi-protein repressor complexes whose activity is mainly regulated by

dynamic association/dissociation of partner proteins [95]. It was shown for HDACs from human and yeast that even the loss of one non-HDAC subunit strongly decreased the deacetylase activity of the complex [169]. Moreover, the catalytic activity of HDACs within these complexes is usually much higher as compared to the activity of recombinant HDACs [95]. This suggests an alternative model, in which S-nitrosylation of HDA6 induces structural changes within the repressor complex, resulting in a net decrease of HDAC activity. The complete dissociation of one subunit upon S-nitrosylation seems rather unlikely, since the inhibitory effect of GSNO could be restored by subsequent addition of DTT in nuclear extracts (**Fig. 19**).

As already indicated above, similar to other organisms, plant HDACs likely operate in large multi-protein repressor complexes, although no such complex has been purified and thoroughly characterized in plants up to now. For instance, HDA6 directly interacts with HDA5 and FLD to regulate the floral transition [102, 165]. Other examples include the complex formation with MET1 to regulate DNA-methylation/Histone-deacetylation at transposons and HDC1, a scaffolding protein likely regulating the activity of the associated HDACs [170]. Interestingly, RPD3-type HDACs were also demonstrated to interact with members of the plant-specific HDT-family of HDACs [171]. From our experiments, we cannot exclude that the inhibition of HDAC activity after GSNO treatment might result from the additional S-nitrosylation of other complex partners apart from HDA6. Our lab could already demonstrate that HDT3 was S-nitrosylated upon incubation of nuclear extracts with GSNO [127]. The function of HDT-proteins is not well investigated but evidence accumulates that members of this family do not possess HDAC activity but might instead serve as scaffolding platforms or regulators of HDAC activity [94]. This opens the possibility, that the GSNO mediated inhibition of HDA6-complex activity might be mediated by S-nitrosylation of not only HDA6 but possibly HDT3 (and others), thus pointing towards a plant specific inhibition mechanism.

3.5 NO induced changes in the H3K9/14 acetylation level of defense genes

The primary aim of the ChIPseq study was to identify NO-regulated H3K9/14ac sites, which was accomplished by comparison of the GSNO and the GSNO/cPTIO treatment. These sites were then annotated and the resulting gene list was searched for enriched GO-terms, in order to extract possible physiological implications of NO-regulated histone acetylation. A significant enrichment of genes associated with the defense response was identified (**Table 1**) which could reflect a possible function in the response to biotic stresses. Genes involved in different aspects of the plant immune system were identified (**Fig. 30**). The function of these genes during plant immunity is described in the following section.

AT5G15730 is a putative member of the family of leucine rich repeat (LRR) receptor serine/threonine kinases, which are generally involved in the initial recognition of microbe

associated molecular patterns (MAMPs) [172]. Binding of MAMPs to these receptors initiates a MAPK-signaling cascade, which leads to the induction of defense genes. MKK2 (MAPK kinase kinase 2) activates MPK4, which is a positive regulator of SA-mediated and a negative regulator of JA-mediated defense signaling. Accordingly, MKK2-oe plants were more resistant towards *Pseudomonas* (biotroph) but more susceptible towards *Alternaria* (necrotroph) infection [173]. Some pathogens evolved to suppress MAMP-triggered immunity by delivery of specific effector proteins. Plants in turn developed proteins (called R-proteins), which recognize these effectors and initiate the enhanced and exaggerated immune response often leading to local cell death around the infection site (hypersensitive response) [172]. Three of these plant R-proteins were identified in this ChIPseq study (AT3G25510, AT4G08450, AT5G11250), all of them belong to the TIR-NB-LRR class of intracellular effector recognition receptors. In response to pathogen attack, plants synthesize and secrete pathogenesis-related proteins (the products of PR-genes), which can have different biochemical activities like glucanase, chitinase, protease, or protease inhibitor activity. Two of these PR-genes showed NO-regulated H3K9/14ac. AT2G38870 belongs to the PR6-family and exhibits protease inhibitor activity. AIG2 is expressed early after infection with a *P. syringae* strain carrying the avrRpt2 avirulence gene but not after inoculation with a strain carrying the avrRPM1 gene [174]. Although parts of the structure of AIG2 (avrRPT2 INDUCED GENE 2) have been solved by NMR, the biochemical activity and biological function of this protein are still unknown [175]. Pathogen infection is often accompanied by localized cell-death around the infection site (hypersensitive response). BAG6 (BCL2 ASSOCIATED ATHANOGENE 6) limits cell-death spreading by affecting autophagy in response to *Botrytis cinerea* infection. BAG6 is proteolytically processed by an aspartyl-protease in response to infection, which results in the formation of autophagic structures and resistance to the fungus [176]. Thioredoxins are small proteins with two cysteine residues in the catalytic center, which can undergo reversible oxidation to a disulfide. Thioredoxins can reduce oxidized cysteines on proteins, thereby being oxidized to the respective disulfide. Oxidized thioredoxins are recovered by Thioredoxin-reductase, which uses NADPH as electron source. Thioredoxins play various roles in plant defense. One particularly well described example is the reduction of NPR1, which facilitates its nuclear translocation and the subsequent expression of PR-genes [15]. Transcriptional reprogramming in response to pathogen attack is governed by a complex network of transcription factors, which initiate or repress the transcription of defense related genes. One of the most important families of stress-related TFs are the plant-specific WRKY-proteins. WRKY-proteins are Zn-finger containing transcription factors, which bind to cis-elements called W-boxes. They can both activate or repress the transcription of defense-genes [177]. The functional importance of WRKY-proteins for plant immunity has been demonstrated extensively (for instance [178] [177]). Two members of the WRKY-family displayed increased H3K9/14ac after NO-treatment in this study. WRKY53 is involved in basal defense against *P. syringae*, possibly by modulation of SA-signaling [179]. WRKY27 is a negative regulator of resistance against the bacterial pathogen *R. solanacearum*. It is expressed in phloem companion cells and possibly represses the expression of Nia1 and Nia2, two enzymes, which are involved in nitrate assimilation and NO

production [180]. TGA2 and TGA5 are bZIP-transcription factors, which act as coactivators of NPR1 [181]. They bind to *ocs* elements (for instance *as-1*) and regulate the transcription of SA-dependent genes like PR1 in an NPR1-dependent manner [14]. TGA2 physically interacts with NPR1, which is dependent on the presence of SA and this interaction enhances the DNA-binding activity of TGA2 [182].

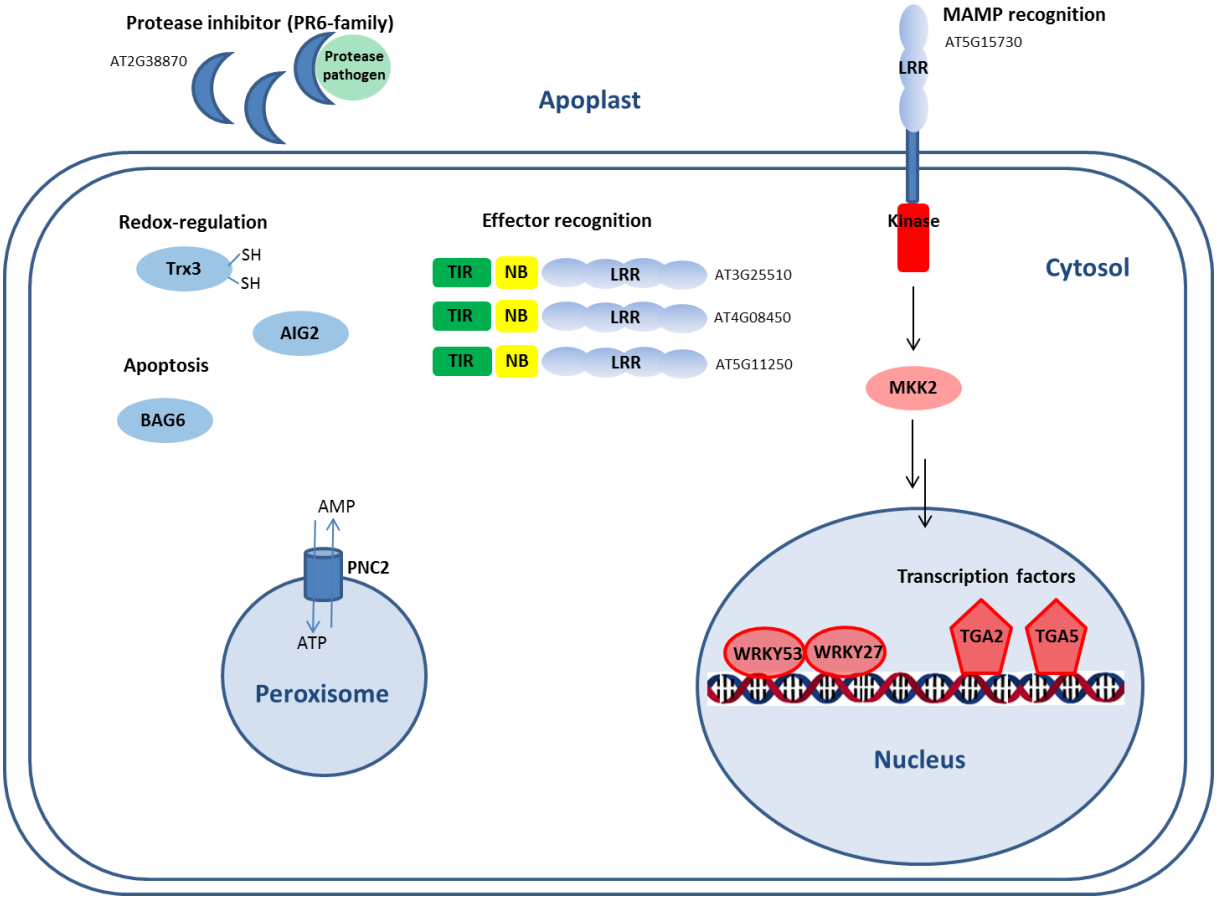

Figure 30: Graphical representation and functional categorization of the defense genes showing enhanced H3K9/14ac levels after NO treatment. Genes displaying NO-regulated H3K99/14ac are involved in MAMP-recognition, effector recognition, transcriptional regulation, redox-regulation, apoptosis, protease inhibition and peroxisomal transmembrane transport. If no gene names were available the corresponding ATG-numbers are depicted to specify the corresponding gene. See text for details.

We could furthermore demonstrate that SA and its functional analog INA induced endogenous NO-production resulting in NO-dependent inhibition of HDAC activity. This strengthens the hypothesis that NO-dependent inhibition of HDACs might play a functional role in the plant immune response since SA is the major plant defense hormone against biotrophic pathogens [183]. SA accumulation triggers the nuclear translocation of NPR1 where it initiates the transcription of PR-genes [185]. SA and NO production are intimately linked, since they reciprocally induced the synthesis of each other [17, 138-141]. Interestingly, it was demonstrated that HDA19 plays an essential role in the suppression of SA-biosynthetic genes and PR-genes during unchallenged conditions by deacetylation of the

corresponding promoters [104]. After pathogen attack, histone acetylation at these regions increased suggesting an inhibition of HDA19 activity or alternatively an activation/recruitment of HAT activity. Strikingly, increased histone acetylation at PR1 and PR2 gene was also observed after spraying with INA [104]. We identified HDA6 as one target for NO, which has up to now not been implicated in the immune response of *Arabidopsis*. However, as previously stated the very high sequence homology between the HDAC-domains of HDA6 and HDA19 (containing all conserved cysteine residues) makes it very likely that both homologs are targeted by NO. This argument is further supported by the fact that HDA6 and HDA19 share several interaction partners, like HDT3 and HDC1 [94, 170], indicating that both the HDA6 and HDA19 complex contain the same protein core. Our data might thus explain the observed increase in histone acetylation at SA-responsive loci by suggesting a mechanism in which SA stimulates NO-production which in turn leads to the deactivation of HDA19 (and possibly other HDACs), resulting in the hyperacetylation of those genes. This model can be expanded to any situation in which NO-signaling occurs. The temporally and spatially controlled production of NO as well as the presence or absence of NO-sensitive HDAC-complexes could then allow for the specific hyperacetylation of certain sets of stress-reponsive genes (for instance S-nitrosylation of HDA6 could enhance acetylation of salt-responsive genes). These NO-mediated histone acetylation changes could directly facilitate or enhance expression of the corresponding stress-related genes. However, these acetylation changes might also prime the chromatin for subsequent stresses. In this case, altered histone acetylation patterns would serve as a memory of the cell even when transcription has turned back to basal levels, enabling the cell to react more quickly upon subsequent stresses (**Fig. 31**). Since histone acetylation often enforces the establishment of activating histone methylation marks (for instance H3K4me3) in a self-reinforcing loop [186], the primed state would likely be characterized by hypermethylated and hyperacetylated histones and consequently a very open, relaxed chromatin structure. This enforces/accelerates subsequent binding of transcription factors upon repeated exposure to stress resulting in enhanced transcription kinetics of the corresponding genes. In support of this, a role for NO in the priming response of potato was already described [187]. In addition, several studies demonstrated priming-reagent induced histone acetylation and methylation changes (for instance [188]), however, the mechanism remained elusive. This work thus provides a new perspective for future investigations on how epigenetic marks are established in response to biotic and abiotic stresses in plants.

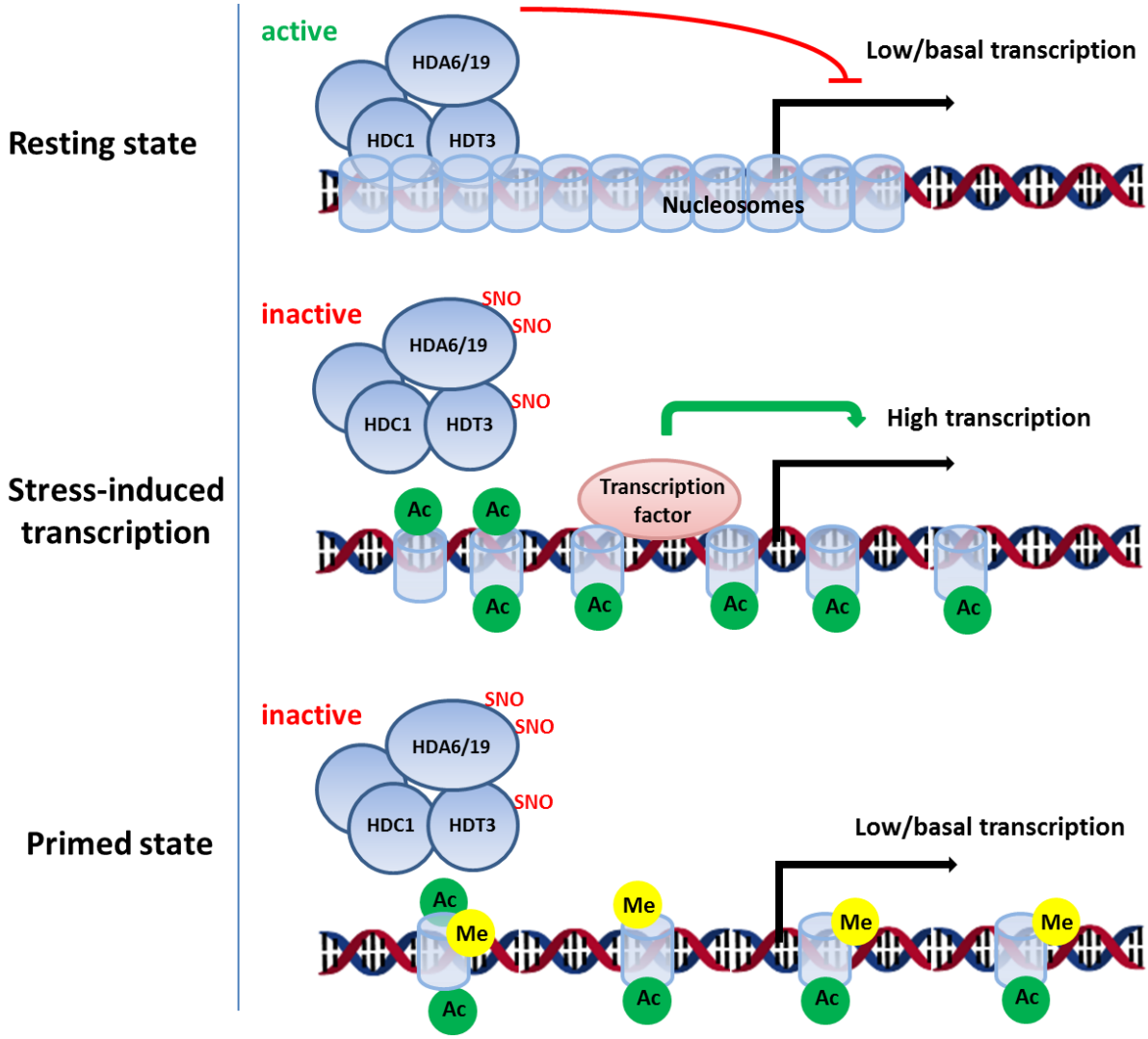

Figure 31: Schematic model of NO-induced epigenetic changes. In the resting state transcription of stress-inducible genes (see table 3.2) is low, due to HDAC mediated deacetylation of the chromatin. Upon formation of NO and ROS in response to biotic or abiotic stress, the HDA6/HDA19-complexes become inactivated/inhibited by S-nitrosylation, resulting in the acetylation of the chromatin. This induces transcription in tight interplay with activating transcription factors. In the post-stress phase transcription factors become inactivated and transcription is turned off. However, the permissive chromatin state might be maintained over a longer period allowing faster TF-binding and transcription-initiation upon subsequent stresses. This primed chromatin state is possibly characterized by hyperacetylated and hypermethylated histones, since histone acetylation enforces the establishment of other activating histone methylation marks.

4 Outlook

Epigenetically controlled stress-regulation and -memory is gaining more and more attention among the plant research community. Although many studies describe changes of epigenetic marks in response to abiotic and biotic stress, the underlying molecular mechanisms remain largely elusive. The key players in these processes have been identified by genetic approaches, but how these enzymes are regulated on a posttranscriptional and posttranslational level is completely unknown. This work links stress-induced changes in the histone acetylation level with NO-dependent inhibition of HDAC-complexes, thus providing a proof-of-principle example how environmental stress might be transduced into epigenetic changes. Preliminary results indicate that the observed changes in histone acetylation persist longer than the associated transcriptional activation. Future work will thus concentrate on two main issues: i) the role of NO-dependent inhibition of HDAC-activity during priming and systemic acquired resistance and ii) deciphering the exact molecular mechanism of NO-dependent inhibition of HDAC-complexes. In conclusion, this work suggests a new role of NO as a regulator of histone acetylation and provides a new perspective on how epigenetic changes are mediated in response to biotic and abiotic stresses in plants.

5 Material

5.1 Plant material

Plant line	background	description	source
Wild-type	Col-0	Wild-type line	
hda6 axe1-5	Col-0	Expresses a C-terminally truncated, non-functional variant of HDA6	[96]
hot5-2	Col-0	GSNOR knock-out line	[26]
nia1nia2	Col-0	Nitrate reductase 1 and 2 knock-out line	[189]
noa1	Col-0	NO associated 1 knock-out line	[190]
AtNOS	Col-0	Rat neuronal NO-synthase overexpression line	[191]

Suspension cell line	background	description
Wild-type	Col-0	Dark-grown suspension cell line generated from root tissue on callus inducing medium
hda6 axe1-5	Col-0	Dark-grown suspension cell line, expressing a C-terminally truncated, nonfunctional version of HDA6

5.2 Bacteria

strain	purpose	Chromosomal genotype	source
***E. coli* DH5α**	cloning	*fhuA2 lac(del)U169 phoA glnV44 Φ80' lacZ(del)M15 gyrA96 recA1 relA1 endA1 thi-1 hsdR17*	Lab
***E.coli* DB3.1**	Maintaining gateway vectors	*F- gyrA462 endA1 glnV44 Δ(sr1-recA) mcrB mrr hsdS20(r_B^-, m_B^-) ara14 galK2 lacY1 proA2 rpsL20(Sm^r) xyl5 Δleu mtl1*	Lab
***E.coli* BL21 (DE3) cc4**	Expression	*F^- ompT gal dcm lon $hsdS_B$(r_B^- m_B^-) λ(DE3 [lacI lacUV5-T7 gene 1 ind1 sam7 nin5])cc4*	A. Geerlof
***E.coli* BL21 (DE3) Rosetta2**	Expression	*F^- ompT $hsdS_B$(R_B^- m_B^-) gal dcm λ(DE3 [lacI lacUV5-T7 gene 1 ind1 sam7 nin5]) pLysSRARE (Cam^R)*	A. Geerlof
***E.coli* BL21 (DE3) pLysS**	Expression	*F^- ompT gal dcm lon $hsdS_B$(r_B^- m_B^-) λ(DE3) pLysS(cm^R)*	Lab

***E.coli* BL21 (DE3)**	Expression	*F^- ompT gal dcm lon hsdS_B(r_B^- m_B^-) λ(DE3 [lacI lacUV5-T7 gene 1 ind1 sam7 nin5])*	Lab

5.3 Kits

Kit	Company
QIAquick® PCR Purification Kit, No. 28104	Qiagen GmbH, Hilden, Germany
MinElute® PCR Purification Kit, No. 28004	Qiagen GmbH, Hilden, Germany
QIAprep® Spin Miniprep Kit, No. 27104	Qiagen GmbH, Hilden, Germany
QIAquick® Gel Extraction Kit, No. 28704	Qiagen GmbH, Hilden, Germany
RNeasy® Plant Mini Kit, No. 74904	Quiagen GmbH, Hilde, Germany
Gateway® BP Clonase™ Enzyme Mix, No.11789-013	Invitrogen, Karlsruhe, Germany
Gateway® LR Clonase™ Enzyme Mix, No.11791-019	Invitrogen, Karlsruhe, Germany
Epigenase HDAC Activity/Inhibition Direct Assay Kit (Fluorometric), No. P-4035-96	Epigentek, Farmingdale, NY/USA
InSitu HDAC Activity Fluorometric Assay Kit, No. K339-100	BioVision, Milpitas, California/USA
Plant ChIP-seq kit, No. C01010150	Diagenode, Liege, Belgium
MicroPlex Library Preparation kit v2, No. C05010014	Diagenode, Liege, Belgium
IPure Kit, No. C03010012	Diagenode, Liege, Belgium
SensiMix™ SYBR Low-Rox Kit, No. QT 625-05	BioLine, Luckenwalde, Germany
QuantiTect® Reverse Transcription Kit, No. 205311	Qiagen GmbH, Hilden, Germany
Extract-N-Amp™ Plant PCR Kit, No. SLBH0328	SIGMA-ALDRICH, St. Louis, USA
QuantiT Pico Green Assay, No. P7589	Invitrogen, Karlsruhe, Germany
Western Lightning *Plus* ECL Kit, No. NEL103001EA	Perkin Elmer, Waltham, Massachusetts
Mini-PROTEAN® TGX™ Precast Gels, No. 4561044	Biorad, Hercules, California/USA

5.4 Buffers and Solutions

Buffers supplied with Kits are not listed.

Buffer name	Composition
Phosphate buffered saline (PBS)	10 mM Na_2HPO_4, 1.8 mM KH_2PO_4, 2.7 mM KCl, 137 mM NaCl, pH 7.4
Tris-buffered saline (TBS)	50 mM Tris pH 7.5, 150 mM NaCl
TBS-T	0.5% (w/v) Tween in TBS
Blocking Buffer	5% BSA in TBST-T
Blot Buffer	1:7 Dilution of 10 x SDS-PAGE running buffer
Transfer buffer	80% (v/v) Blot buffer, 20% Methanol
AP buffer	100 mM Tris-HCl pH 9.5, 100 mM NaCl, 5 mM $MgCl_2$
BCIP solution	5% (w/v) BCIP in 100% DMF
NBT solution	5% (w/v) NBT in 70% DMF
NIBA (nuclei purification from protoplasts)	20 mM HEPES pH 7.4, 20 mM KCl, 13.8 % Hexylene glycol, 1% Triton X-100, 50 µM spermine, 125 µM spermidine, protease inhibitor tablet
NLB (nuclei lysis)	10 mM Tris pH 7.5, 500 mM NaCl, 1% Triton X-100, 10% glycerol, 1 mM $Na_4P_2O_7$, protease inhibitor cocktail
LB-buffer (nuclei isolation from tissue)	20 mM Tris pH 7.4, 25% glycerol, 20 mM KCl, 2 mM EDTA, 2.5 mM $MgCl_2$, 250 mM sucrose, 1 mM DTT, protease inhibitor cocktail
NRBT-buffer (nuclei isolation from tissue	20 mM Tris pH 7.4, 25% glycerol,, 2.5 mM $MgCl_2$, 0.2% Triton X-100, protease inhibitor cocktail
Enzyme solution (protoplast isolation)	0.4 M mannitol, 20 mM KCl, 20 mM MES pH 5.7, 10 mM $MgCl_2$, 0.1 % BSA, 2% Cellulase, 1% Macerocym
W5 (protoplast isolation)	20 mM MES pH 5.7, 154 mM NaCl, 125 mM $CaCl_2$, 5 mM KCl
Lysis-buffer Ni-NTA	50 mM phosphate pH 8.0, 300 mM NaCl, 10 mM imidazole, 0.1% Triton X-100
Wash buffer Ni-NTA	20 mM phosphate pH 8.0, 500 mM NaCl, 20 mM imidazole
Elution buffer Ni-NTA	20 mM phosphate pH 8.0, 500 mM NaCl, 500 mM imidazole
Lysis-buffer Anti-GST	20 mM phosphate pH 7.4, 300 mM NaCl, 10 mM EDTA, 1x complete protease inhibitor (Roche), 1 mg/mL lysozyme
Wash buffer Anti-GST	20 mM phosphate pH 7.4, 300 mM NaCl, 10 mM EDTA, 1x complete protease inhibitor (Roche)
Elution buffer Anti-GST	200 mM Tris pH 7.4, 40 mM reduced glutathione, 10 mM EDTA
Lysis-buffer (insect cells)	200 mM NaCl, 25 mM Tris pH 8.0, 20 mM imidazole, 10 mM $MgSO_4$, 10 µg/ml DNaseI (Serva), 1 mM protease inhibitor mix AeBSF-HCl (Roth), 0.01% thioglycerol, 0.5% NP40
Wash buffer Ni-NTA (insect cells)	200 mM NaCl, 25 mM Tris pH 8.0, 30 mM imidazole, 0.01% thioglycerol
Elution buffer Ni-NTA (insect cells)	200 mM NaCl, 25 mM Tris pH 8.0, 300 mM imidazole, 0.01%

	thioglycerol
Gelfiltration buffer	25 mM Tris pH 8.0, 100 mM NaCl, 0.01% thioglycerol
HEN buffer (biotin switch)	25 mM HEPES pH 7.7, 1 mM EDTA, 0.1 mM Neocuprine
HENS buffer (biotin switch)	25 mM HEPES pH 7.7, 1 mM EDTA, 0.1 mM Neocuprine, 1% SDS
MonoQ extraction buffer	50 mM Bis-Tris pH 6.5
MonoQ elution buffer	50 mM Bis-Tris pH 6.5, 2M NaCl
50x TAE running buffer	2.0 M Tris base , 5.71 % (v/v) glacial acetic acid, 50 mM EDTA
Coomassie R-250 staining solution	0.25% (w/v) Commassie Brilliant Blue R-250, 50% (v/v) methanol, 10% (v/v) glacial acetic acid
Coomassie R-250 destaining solution	30% (v/v) methanol, 10% (v/v) glacial acetic acid
Poinceau S solution	0.5% (w/v) Poinceau S, 1% acetic acid
10x SDS running buffer	250 mM Tris base, 2 M glycine, 1% (w/v) SDS
2x reducing sample buffer	100 mM Tris/HCl, pH 6.8, 4% (w/v) SDS, 0.2% (w/v) bromphenol blue, 20% (w/v) glycerol, 200 mM DTT
Triiodide solution (NO Analyzer)	35 mL glacial acetic acid, 325 mg iodine, 500 mg KI, 10 mL ddH_2O

5.5 Antibiotics

Antibiotic	Stock concentration	Working concentration
Ampicillin (Amp)	100 mg/mL in ddH_2O	100 µg/mL
Carbenicillin (Carb)	100 mg/ml in 20% (v/v) EtOH	100 µg/mL
Rifampicin (Rif)	50 mg/ml in DMF	50 µg/mL
Gentamycin (Gent)	25 mg/ml in ddH2O	25 µg/mL
Kanamycin (Kan)	50 mg/ml in ddH2O	50 µg/mL
Spectinomycin (Spec)	100 mg/ml in ddH2O	100 µg/mL

5.6 Media

All media were prepared with ddH_2O and autoclaved before use. Plant tissue culture grade chemicals were used.

Medium	Composition
LB	1% (w/v) tryptone 0.5% (w/v) yeast extract 0.5% (w/v) NaCl *Adjust to pH 7.0* 1.5% (w/v) agar for solid media
SOC	2% (w/v) tryptone 0.5% (w/v) yeast extract 0.05% (w/v) NaCl 2.5 mM KCl *Adjust to pH 7.0 and complement before use* 10 mM (final conc.) $MgCl_2$ (filter sterilized, 0.22 µm) 20 mM (final conc.) glucose (filter sterilized, 0.22 µm)
MS	4.05 g/L MS salts incl. MS vitamins 1% (w/v) sucrose 0.5 g/L MES hydrate *Adjust to pH 5.7 with KOH* 1.0% (w/v) phytoagar for solid media
AS	4.3 g/L MS salts incl. vitamins 3% (w/v) sucrose 0.0001% (w/v) (2,4-Dichlorophenoxy-) acetic acid *Adjust to pH 5.7 with KOH*

5.7 Chemicals and solutions

Common chemicals were from SIGMA, Merck or Roth with the highest available purity.

Chemical/solution	Company
S-nitrosoglutathione (GSNO), No. ALX-420-002	Enzo, Lörrach, Germany
S-nitroso-penicillamine (SNAP), No. BML-CN210-0100	Enzo, Lörrach, Germany
2-(4-Carboxyphenyl)-4,4,5,5-tetramethylimidazoline-1-oxyl-3-oxide (cPTIO), No. ALX-430-001	Enzo, Lörrach, Germany
N-ethyl-maleimide (NEM), No. 128-53-0	Sigma, St. Louis, USA
Salicylic acid (SA), No. S7401	Sigma, St. Louis, USA
Dichloro-isonicotinic acid (INA), No. 5398-44-7	Sigma, St. Louis, USA
Trichostatin A (TSA), No. T8552	Sigma, St. Louis, USA
Di-amino-fluorescein diacetate (DAF-FM DA), No. D2321	Sigma, St. Louis, USA
Bradford Reagent, No. 500-0006	Biorad, Germany
16% methanol-free formaldehyde solution, No. 28908	Sigma, St. Louis, USA

5.8 Enzymes

Enzyme	Company
Antarctic Phosphatase, No. M0289	New England Biolabs, Frankfurt, Germany
Phusion High Fidelity DNA Polymerase, No. M0530	New England Biolabs, Frankfurt, Germany
iProof High-fidelity™ Phusion Polymerase, No. 1725300	Biorad, Munich, Germany
Taq DNA Polymerase	Agrobiogen, Hilgertshausen, Germany
RNase A, No. 19101	Qiagen GmbH, Hilden, Germany
EcoRI, No. R0101	New England Biolabs, Frankfurt, Germany
ApaI, No. R0114	New England Biolabs, Frankfurt, Germany
HindIII, No. R0104	New England Biolabs, Frankfurt, Germany
XhoI, No. R0146	New England Biolabs, Frankfurt, Germany
NcoI, No. R0193	New England Biolabs, Frankfurt, Germany
Benzonase, No. E1014	SIGMA-ALDRICH, St. Louis, USA

5.9 Antibodies

Antibody	species	Dilution	Company
Anti-rabbit-IgG HRP conjugate, No. W401B	mouse	1:2500	Promega, Fitchburg, USA
Anti-rabbit-IgG AP conjugate, No. S373B	mouse	1:7500	Promega, Fitchburg, USA
Anti-mouse-IgG AP conjugate, No. S372B	rabbit	1:7500	Promega, Fitchburg, USA
Anti-His6-tagged protein, No. OB05	mouse	1:2000	Calbiochem, Darmstadt, Germany
Anti-GST tagged protein, No. G7781	rabbit	1:2000	Sigma, St. Louis, USA
Anti-Biotin HRP conjugate, No. ab19221	goat	1:5000	Abcam, Cambridge, Great Britain
Anti-acetyl-Histone H4, No. 06-866	rabbit	1:20000	Millipore, Darmstadt, Germany
Anti-acetyl-Histone H3, No. 06-599	rabbit	1:20000	Millipore, Darmstadt, Germany
Anti-acetyl-H3K9, No. ab4441	rabbit	1:5000	Abcam, Cambridge, Great Britain
Anti-acetyl-H4K5, No. ab51997	rabbit	1:20000	Abcam, Cambridge, Great Britain
Anti-acetyl-protein, No. A5463	rabbit	1:10000	Sigma, St. Louis, USA
Anti-H3K9/14 acetylation, No. C15410200	rabbit	1 µg/IP	Diagenode, Liege, Belgium

5.10 Resins, columns, membranes

Product	Company
ZebaSpin™ spin columns, No. 89882	Invitrogen, Waltham, USA
Ni-NTA resin, No. 17-5318-01	GE Healthcare, Freiburg, Germany
GT sepharose 4B, No. 17-0756-01	GE Healthcare, Freiburg, Germany
HisTrap FF columns 1 mL, No. 17-5255-01	GE Healthcare, Freiburg, Germany
HiTrap Q FF columns 1 mL, No. 17-1153-01	GE Healthcare, Freiburg, Germany
HiTrap DEAE sepharose FF columns 1 mL, No. 17-5055-01	GE Healthcare, Freiburg, Germany
Whatman Nitrocellulose membrane	GE Healthcare, Freiburg, Germany

5.11 Plasmids and vectors

Plasmid	Cloning procedure	Description
TEV_HDA6_pDONR221	HDA6 was first amplified from N_fus_HDA6_ pDONR221 using primers #5 and 2. The amplicon was purified and used as template for PCR with primers #6 and 2 (stepwise addition of the TEV and attB sites). The product was transferred into pDONR221 by BP reaction.	Full length coding sequence of HDA6 plus additional N-terminal TEV-site in pDONR221
N_fus_HDA6_pDONR221	HDA6 was amplified from cDNA using primers #1 and 2 and then transferred into pDONR221 by BP reaction.	Full length coding sequence of HDA6 for N-terminal fusions (start codon ATG removed)
C_fus_HDA6_pDONR221	HDA6 was amplified from cDNA using primers #3 and 4 and then transferred into pDONR221 by BP reaction.	Full length coding sequence of HDA6 for C-terminal fusions (stop codon removed)
HDA6_pDEST15	LR reaction of N_fus_HDA6_pDONR221 and pDEST15.	Expression plasmid (E.coli) for N-terminally GST-tagged HDA6
HDA6_pDEST17	LR reaction of N_fus_HDA6_pDONR221 and pDEST17.	Expression plasmid (E.coli) for N-terminally His6-tagged HDA6
HDA6_pDEST42	LR reaction of C_fus_HDA6_pDONR221 and pDEST42.	Expression plasmid (E.coli) for C-terminally His6-tagged HDA6
TEV_HDA6_pDEST15	LR reaction of TEV_HDA6_pDONR221 and pDEST15.	Expression plasmid (E.coli) for N-terminally GST-tagged HDA6, with an additional TEV site to

		cleave the GST-tag
His6_HDA6_pFastBac	HDA6 was amplified from N_fus_HDA6_ pDONR221 using primers #11 (contains His6-tag) and 12. The amplicon was digested with EcoRI and HindIII and ligated into pFastBac (cut with the same enzymes and dephosphorylated).	Expression plasmid (H5 cells) for N-terminally His-tagged HDA6
HDA6_His6_pFastBac	HDA6 was amplified from C_fus_HDA6_ pDONR221 using primers #9 and 10 (contains His6-tag). The amplicon was digested with EcoRI and HindIII and ligated into pFastBac (cut with the same enzymes and dephosphorylated).	Expression plasmid (H5 cells) for C-terminally His-tagged HDA6
HDA6_GS_His6_pFastBac	HDA6 was amplified from C_fus_HDA6_ pDONR221 using primers #9 and 14 (contains His6-tag and GS-linker). The amplicon was digested with EcoRI and HindIII and ligated into pFastBac (cut with the same enzymes and dephosphorylated).	Expression plasmid (H5 cells) for C-terminally His-tagged HDA6 with an additional $[GGGS]_2$ linker between the tag and HDA6
His6_TEV_ HDA6_ pFastBac	HDA6 was amplified from N_fus_HDA6_ pDONR221 using primers #13 (contains His6-tag and TEV site) and 10. The amplicon was digested with EcoRI and HindIII and ligated into pFastBac (cut with the same enzymes and dephosphorylated).	Expression plasmid (H5 cells) for N-terminally His-tagged HDA6 with an additional TEV cleavage site between the tag and HDA6
HDA6_HDAC_domain_pENTR_TEV	The HDAC domain of HDA6 was amplified from N_fus_HDA6_ pDONR221 using primers #7 and 8. The amplicon was transferred into pENTR_TEV using directed site-specific recombination (TOPO-Cloning).	HDAC domain of HDA6 for N-terminal fusions with an additional TEV site
TEV_HDA6_HDAC_domain_pETG41	LR reaction of HDA6_HDAC_domain_ pENTR_TEV with pETG41.	Expression plasmid (E.coli) for MBP-tagged HDAC domain of HDA6 with an additional TEV site to cleave the MBP tag
HDA6_Mut1_pDONR221	Site-directed mutagenesis of N_fus_HDA6_ pDONR221 using primers HDA6_Mut_1f and HDA6_Mut_1r [192].	HDA6 carrying Cys112 to Ala mutation
HDA6_Mut2_pDONR221	Site-directed mutagenesis of N_fus_HDA6_ pDONR221 using primers HDA6_Mut_2f and HDA6_Mut_2r [192].	HDA6 carrying Cys122 to Ala mutation

HDA6_Mut3_pDONR221	Site-directed mutagenesis of N_fus_HDA6_ pDONR221 using primers HDA6_Mut_3f and HDA6_Mut_3r [192].	HDA6 carrying Cys163 to Ala mutation
HDA6_Mut4_pDONR221	Site-directed mutagenesis of N_fus_HDA6_ pDONR221 using primers HDA6_Mut_4f and HDA6_Mut_4r [192].	HDA6 carrying Cys273 to Ala mutation
HDA6_Mut5_pDONR221	Site-directed mutagenesis of N_fus_HDA6_ pDONR221 using primers HDA6_Mut_5f and HDA6_Mut_5r [192].	HDA6 carrying Cys285 to Ala mutation
HDA6_Mut6_pDONR221	Site-directed mutagenesis of N_fus_HDA6_ pDONR221 using primers HDA6_Mut_6f and HDA6_Mut_6r [192].	HDA6 carrying Cys296 to Ala mutation
HDA6_Mut7_pDONR221	Site-directed mutagenesis of N_fus_HDA6_ pDONR221 using primers HDA6_Mut_7f and HDA6_Mut_7r [192].	HDA6 carrying Cys323 to Ala mutation
HDA6_Mut8_pDONR221	Site-directed mutagenesis of N_fus_HDA6_ pDONR221 using primers HDA6_Mut_8f and HDA6_Mut_8r [192].	HDA6 carrying Cys325 to Ala mutation
HDA6_Mut9_pDONR221	Site-directed mutagenesis of N_fus_HDA6_ pDONR221 using primers HDA6_Mut_9f and HDA6_Mut_9r [192].	HDA6 carrying Cys441 to Ala mutation
HDA6_pEarlyGate202	LR reaction of N_fus_HDA6_ pDONR221 with pEarlyGate202.	Binary vector carrying N-terminally FLAG-tagged HDA6

Vector	Company/source
pDONR221	Thermo Fisher Scientific, Freiburg, Germany
pDEST15	Thermo Fisher Scientific, Freiburg, Germany
pDEST17	Thermo Fisher Scientific, Freiburg, Germany
pDEST42	Thermo Fisher Scientific, Freiburg, Germany
pFastBac	Thermo Fisher Scientific, Freiburg, Germany
pENTR_TEV	Thermo Fisher Scientific, Freiburg, Germany
pETG41	Protein core facility (A. Geerlof)
pEarlyGate202	[193]

5.12 Primer

Primer used for cloning

#	name	Sequence 5´→ 3´
1	**fus-HDA6-f**	GGGGACAAGTTTGTACAAAAAAGCAGGCTTCGAGGCAGACGAAAGCGGCATCTCT
2	**fus-HDA6-r**	GGGGACCACTTTGTACAAGAAAGCTGGGTTTAAGACGATGGAGGATTCACGTC
3	**HDA6-fus-f**	GGGGACAAGTTTGTACAAAAAAGCAGGCTGAAGGAGATAGAATGGAGGCAGACGAAGCGGCATC
4	**HDA6-fus-r**	GGGGACCACTTTGTACAAGAAAGCTGGGTCAGACGATGGAGGATTCACGTC
5	**TEV-HDA6-f**	GCAGGCTTCGAGAATCTTTATTTTCAGGGCGAGGCAGACGAAAGCGGCATCTCT
6	**TEV-HDA6-f2**	GGGGACAAGTTTGTACAAAAAAGCAGGCTTCGAGAATCTTTATTTTCAGGGCGAGGCAGACGAAAGCGGCATCTCT
7	**HDA6-HDAC-domain-f**	CACCCGAGTCAGTTACTTCTACGAGCCG
8	**HDA6-HDAC-domain-r**	TCCAACAGCAACTGCAGTCTCATAAC
9	**EcoRI-HDA6-f**	AAAAAAGAATTCATGGAGGCAGACGAAAGCGGCATCTCT
10	**HindIII-H-HDA6-r**	AAAAAAAAGCTTTTATTAATGGTGATGGTAATGGTAAGACGATGGAGGATTCACGTC
11	**EcoRI-H-HDA6-f**	AAAAAAGAATTCATGCACCATCACCATCACCATGAGGCAGACGAAAGCGGCATCTCT
12	**HindIII-HDA6-r**	AAAAAAAAGCTTTTATTAAGACGATGGAGGATTCACGTC
13	**EcoRI-His-TEV-HDA6-f**	AAAAAAGAATTCATGCACCATCACCATCACCATGAGAATCTTTATTTTCAGGGCGAGGCAGACGAAAGCGGCATCTCT
14	**HindIII-His-GS-HDA6-r**	AAAAAAAAGCTTTTATTAATGGTGATGGTAATGGTAGGAGCCTCCGCCGGAGCCTCCGCCAGACGATGGAGGATTCACGTC

Primer used for Mutagenesis

Name	Mutation	Sequence 5´→ 3´
HDA6_Mut_1f	Cys112 to Ala	CAATGTCGGTGAGGATGCTCCTGTCTTCGACGG
HDA6_Mut_1r	Cys112 to Ala	CCGTCGAAGACAGGAGCATCCTCACCGACATTG
HDA6_Mut_2f	Cys122 to Ala	CTTTTTGATTTTGCCCGTGCTTCCGCCGGAGGTTC
HDA6_Mut_2r	Cys122 to Ala	CGGAAGCACGGGCAAAATCAAAAAGTCCGTCGAAG
HDA6_Mut_3f	Cys163 to Ala	GCGAGGCTTCTGGGTTTGCTTATGTAAACGACATCG
HDA6_Mut_3r	Cys163 to Ala	CGATGTCGTTTACATAAGCAAACCCAGAAGCCTCGC
HDA6_Mut_4f	Cys273 to Ala	GTTCTTCAGGCTGGTGCTGACTCCTTAAGTGGTGATCG
HDA6_Mut_4r	Cys273 to Ala	GTCAGCACCAGCCTGAAGAACAACTGCCTCTGGC
HDA6_Mut_5f	Cys285 to Ala	GGTTGGGTGCCTTCAACTTATCAGTCAAGGGTCAC

HDA6_Mut_5r	Cys285 to Ala	GACTGATAAGTTGAAGGCACCCAACCGATCACCAC
HDA6_Mut_6f	Cys296 to Ala	GTCACGCTGATGCCCTTCGGTTCTTAAGATCTTACAAC
HDA6_Mut_6r	Cys296 to Ala	GAACCGAAGGGCATCAGCGTGACCCTTGACTGATAAG
HDA6_Mut_7f	Cys323 to Ala	GTTGCCCGTGCCTGGTGTTATGAGACTGCAGTTG
HDA6_Mut_7r	Cys323 to Ala	CATAACACCAGGCACGGGCAACATTTCGAATAGTATAC
HDA6_Mut_8f	Cys325 to Ala	CCGTTGCTGGGCTTATGAGACTGCAGTTGCTGTTG
HDA6_Mut_8r	Cys325 to Ala	CAGTCTCATAAGCCCAGCAACGGGCAACATTTCG
HDA6_Mut_9f	Cys441 to Ala	GTTACTCAGCTCGTGGTGGCGCAACTACGGACAGG
HDA6_Mut_9r	Cys441 to Ala	CGCCACCACGAGCTGAGTAACCATGAAGAGGTTTATC

Primer for ChIP-qPCR

name	**Sequence**	**name**	**Sequence 5´→ 3´**
Peak1_positive_f	TGCTACTCTCAATCCGACCC	**LHCB3_exon_f**	AACTCCGTCTTACCTCACCG
Peak1_positive_r	GTGAGGTGAAGAACAGGGGA	**LHCB3_exon_r**	TCAGGGTCTGCGGATAAACC
Peak1_negative_f	CACCTCTGCACAACCTTTCC	**ANTR1_exon_f**	GCGAATCAGAAACGACGTCA
Peak1_negative_r	TGGGAAACTGAGGCTTGTGA	**ANTR1_exon_r**	TCCGGGTATTAGTTCGGAGC
Peak2_positive_f	GCTGTGGATTGGTGGGTTTT	**At3g53830_exon_f**	TACTTACCAGGAGCTGCGTC
Peak2_positive_r	CAGACAACCCTTCAGCAACC	**At3g53830_exon_r**	GAATCCACAACCACCACCAC
Peak2_negative_f	TCTATGGAGAGAGGATTCGACG	**At1g62510_exon_f**	TTGGATGAGGGTGCAACATG
Peak2_neagtive_r	CGCACTCGTTTTGGGACTC	**At1g62510_exon_r**	CGGCCTACTAAACGTAACCC
Peak3_positive_f	GAGCTCCTCCAATGTGCAAG	**COL2_exon_f**	ACGAAGCAACCTCTCGATCA
Peak3_positive_r	GCTAATAGAAAGACGCCGCC	**COL2_exon_r**	TTCCGCAAACCCACTAGCTA
Peak3_neagtive_f	AAACCGATCGACCAAACCAC	**DOG1_exon_f**	CCCCACTCATGCATCGAAAG
Peak3_negative_r	CCAGTCTGTGCATTTCCAAGA	**DOG1_exon_r**	ACAAGGAGCGGATTTCTTGC
Peak4_positive_f	TCGGGACTATCGTTGCTGAT		
Peak4_positive_r	CAGGGCCAAAGTAAGCAAGT		
Peak4_negative_f	ACTGAGAGGGAGAAGCGAAA		
Peak4_negative_r	TGTCATCGTTGCTCCAGgta		

5.13 Instruments

Instrument	Type	Company
Anion exchange column	MonoQ Fast-Flow 1 mL	GE Healthcare, Freiburg, Germany
Autoclave	D-150	Systec, Puchheim, Germany
Balance	PS600/C/2	Wägetechnik München, Munich, Germany
	CPA225D	Sartorius, Göttingen, Germany
	L2200P	Sartorius, Göttingen, Germany
Centrifuge	5417R	Eppendorf, Hamburg, Germany
	RC26+	Sorvall, Freiburg, Germany
	4K15C	SIGMA, St. Louis, USA
	Rotanta 460R	Hettich, Tuttlingen, Germany
Camera	Powershot G2	Canon, Tokyo, Japan
DNA Electrophoresis Unit		Peqlab, Erlangen, Germany
Electroporator	Gene Pulser Electroporation	Bio-Rad, Munich, Germany
FPLC system	ÄKTA Explorer 10S	GE Healthcare, Freiburg, Germany
Gel Documentation	MegaCapt	Vilber, Eberhardzell, Germany
Homogenizer	Silamat S6	Ivoclar vivadent, Ellwangen, Germany
Incubator	Innova4340	New Brunswick Scientific, Nürtingen, Germany
	G25	New Brunswick Scientific, Nürtingen, Germany
	INPlus	Memmert, Schwabach, Germany
Magnetic stirrer	IKA-Combimag Ret	IKA, Staufen, Germany
Microwave	Micromat	AEG, Frankfurt, Germany
Microscope	BX700	Olympus, Tokyo, Japan
NO-Analyzer	Sievers 280i	GE Healthcare, Freiburg, Germany
pH measurement	pH523	WTW, Weilheim, Germany
Protein Electrophoresis system	Mini-PROTEAN Tetra system	Bio-Rad, Munich, Germany
Protein Blotting system	SemiDry Electroblotter	Sartorius, Göttingen, Germany
Rotors (for RC26+)	SLA1500	Sorvall, Freiburg, Germany
	SS34	Sorvall, Freiburg, Germany

	SA600	Sorvall, Freiburg, Germany
Scanner	Image Scanner II	GE Healthcare, Freiburg, Germany
Shaker	Polymax 1040	Heidolph, Schwabach, Germany
Spectrophotometer	DU 640	Beckmann, Hamburg, Germany
	NanoDrop ND-1000	NanoDrop Technologies, Freiburg, Germany
	Infinite M1000 Pro	Tecan, Männedorf, Suisse
Thermal cycler	Mastercycler Nexus Gradient	Eppendorf, Hamburg, Germany
Real time thermal cycler	ABI 7500 Fast	Applied biosystems, Freiburg, Germany
Thermoblock	Thermomix Comfort	Eppendorf, Hamburg, Germany
UltraPure water system	UltraClear	Siemens, Munich, Germany
Ultrasonic bath	BioRuptor Pico	Diagenode, Liege, Belgium
Ultrasonic device	Sonopuls HD2070	Bandelin, Berlin, Munich
Transilluminator	UV Transilluminator	UVP, Inc, Jena, Germany
Vacuum concentrator	Univapo 150W	UniEquip, Planegg, Germany
Vortexer	Vortex-Genie 2	Scientific industries, New York, USA
waterbath	VWB12	VWR, Erlangen, Germany

5.14 Internet tools and software

www.expasy.org (Protein data, structural modeling)

http://primer3.ut.ee/ (Primer design for qPCR)

www.pubmed.com (literature)

http://chipseek.cgu.edu.tw/ (downstream analysis of ChIPseq data)

Vector NTI 9.1.0© 2004 Invitrogen Corporation

ImageJ 1.41 of the National Institutes of Health, USA

CLC genomics workbench, Quiagen

DiffBind (R package for quantitative analysis of ChIPseq datasets)

SigmaPlot 12 (Graphs)

Endnote (source management)

6 Methods

6.1 Plant cultivation

6.1.1 Cultivation on soil

Seeds were sown on soil mixed with sand in a 1 : 5 ratio to ensure proper aeration. After two days of stratification at 4°C, plants were grown under longday (16 h light/8 h dark) or shortday (10 h light/ 14 h dark) conditions. Temperatures were 20°C during the day and 16°C during the night, with relative humidities of 80 and 65 %, respectively. Plants were covered with plastic foil during the first week to ensure high humidity and proper growth. Plants were bottom-up watered twice a week.

6.1.2 Cultivation in liquid media

Seeds were thoroughly sterilized by first incubating them in 70% ethanol for 1 min and then in 50% bleach-solution (hypochlorite solution) for 10 min, followed by extensive washing with sterile water (5x 1 mL). After two days of stratification, approximately 20 µL of seeds (dry volume) were added to one 250 mL flask containing 70 mL of liquid 1x MS (including vitamins, 1% sucrose, buffered with MES at pH 5.7). Plants were grown for 7 to 10 days under continuous shaking (120 rpm) in short day conditions (10 h light/14 h dark, light intensity 130 µmol/sm^2).

6.1.3 Suspension cells

Cells were maintained in AS medium in the dark with continuous shaking (200 rpm) and subcultured every week.

6.2 Molecular biology techniques

6.2.1 RNA extraction and cDNA library synthesis

RNA was extracted from 50 – 100 mg of tissue using the RNeasy Plant Mini Kit (Quiagen) according to the manufacturer´s instructions. 1 µg of total RNA was then used as input for reverse transcription using the QuantiTect® Reverse Transcription Kit (Quiagen). Concentration and purity of cDNA was estimated by spectrophotometry (NanoDrop) and agarose gel electrophoresis.

6.2.2 PCR

Genes of interest were amplified from cDNA (50 ng) or plasmid (1 ng) using corresponding primer pairs and the appropriate annealing temperatures and elongation times in a total volume of 50 µL. In most of the cases the iProof Polymerase (Biorad) was used, which needs 15 – 30 seconds/kb. In difficult cases 2 – 4% of DMSO was added to melt possible secondary structures in the template. Sufficient amount of DNA was obtained after 25 – 30 cycles. PCR samples were purified by Gel-extraction and the concentration was measured by spectrophotometry (NanoDrop).

6.2.3 BP reaction

150 ng of donor vector (pDONR221) were incubated with 50 fmol of attB-sites containing PCR product (ensuring a molar 1:1 ratio) together with 1 µL BP Clonase and 1 µL BP clonase buffer in a total reaction volume of 5 µL overnight at 25°C (in a thermomixer with heated lid). BP reaction was stopped by adding Proteinase K and incubating for 10 min at 37°C. 1 -2 µL of the reaction was transformed into *E. coli* DH5 alpha. 4 colonies were picked and grown in two mL of LB medium at 37°C overnight. After plasmid purification the presence of the insert was verified by PCR.

6.2.4 LR reaction

100 ng of entry clone was incubated with an equal molar amount of destination vector and 1 µL of LR Clonase and 1 µL of LR Clonase buffer in a total reaction volume of 5 µL. After 3 -5 hours, LR reaction was stopped by incubating with Protease K (37°C, 10 min). 1 -2 µL of the reaction was transformed into E. coli DH5 alpha. 5 colonies were picked and grown in two mL of LB medium at 37°C overnight. The plasmid was isolated and the concentration was determined by spectrophotometry. Plasmids were sequenced (Eurofins MWG) and stored at – 20°C.

6.2.5 Restriction digest

Restriction sites were added at the 5´ends of the PCR primers to allow for subsequent conventional sticky end cloning. 1 µg of PCR product was incubated with 1 µL of each restriction enzyme in a total reaction volume of 30 µL using the appropriate buffer system. After 2 hours typically at 37°C, the sample was subjected to 1% agarose gel electrophoresis to deactivate the enzymes and purify the DNA by gel extraction.

6.2.6 Ligation

Vector and insert (both cut with the same restriction enzymes) were incubated in a molar 1:4 ratio together with 1 µL T4 Ligase and 1 µL T4 ligase buffer (containing ATP) in a total

reaction volume of 10 µL overnight at 16°C. 1 -2 µL of the reaction was transformed into E. coli DH5 alpha. 5 colonies were picked and grown in two mL of LB medium at 37°C overnight. The plasmid was isolated and the concentration was determined by spectrophotometry. Plasmids were sequenced (Eurofins MWG) and stored at – 20°C.

6.2.7 Transformation

1 – 2 µL of DNA sample (BP, LR, Ligation sample) were added to 500 µL of chemically competent cells. Mixing was achieved by gently tapping the reaction vessel. After 20 -30 min incubation on ice, a heat-shock was performed (45 seconds at 42°C) and after additional 2 min on ice, 50 µL of non-selective LB was added. After shaking for 1 h at 37°C, 10 – 200 µL of the transformation sample were plated on selective media and grown overnight at 37°C.

6.2.8 Purification of plasmid DNA

Plasmid DNA was purified using QIAprep® Spin Miniprep Kit (Quiagen) which is based on alkaline lysis according to the manufacturer´s instructions.

6.2.9 Agarose gelelectrophoresis

DNA samples were separated by size using 1 – 2 % agarose gels (1 – 2 g of highly pure agarose in 100 mL of TAE buffer) supplemented with ethidium bromide. Gels were run at 120 V for 30 – 45 min. DNA was visualized on a UV transilluminator (MegaCapt).

6.2.10 Extraction of DNA from gels

Gel extraction of DNA was performed using the QIAquick® Gel Extraction Kit (Quiagen) according to the manufacturer´s instructions.

6.3 Protein techniques

6.3.1 Determination of protein concentration

Protein concentration in extracts was estimated by Bradford Assay [194]. Briefly, 1 – 5 µL of protein extract were incubated with Bradford reagent (1:5 diluted) in a total reaction volume of 1 mL. After 10 min, the absorption at 595 nm was measured in a spectrophotometer. Standard curves were recorded by measuring the absorbance for different amounts of BSA (1, 2, 3,…, 10 µg).

For recombinant proteins, the specific absorbance at 280 nm was calculated and used for quantification. Alternatively, protein concentration was estimated by SDS-PAGE using BSA as standard.

6.3.2 SDS-PAGE

Proteins were separated by SDS-PAGE on precast 12% acrylamide gels (Mini-PROTEAN® TGX™ Precast Gels, BioRad) in standard SDS running buffer (25 mM Tris base, 0.2 M glycine, 0.1% (w/v) SDS) on a Mini-PROTEAN Tetra cell system. Typically, running times were 35 min at 200 V. Gels were stained with Coomassie (0.25% (w/v) Coomassie Brilliant Blue R-250, 50% (v/v) methanol, 10% (v/v) glacial acetic acid) for 1 h and destained overnight (30% (v/v) methanol, 10% (v/v) glacial acetic acid).

6.3.3 Western Blot

Proteins were separated on 12% polyacrylamide gels and transferred to a nitrocellulose membrane using a semi-dry western blot procedure. Briefly, the membrane and the gel were sandwiched by whatman paper wetted in Transfer buffer (80% (v/v) Blot buffer, 20% Methanol) and blotted for 45 – 60 min (depending on the size of the protein of interest) at 2.5 x a x b mA, where a and b represent the dimensions of the membrane. The membrane was stained by Poinceau Red solution to verify efficient transfer and blocked by incubation in Blocking buffer (5% BSA in TBST) for 1 h at RT under moderate shaking. The primary antibody (diluted in blocking buffer) was added and incubated overnight at 4°C with continuous shaking. The membrane was washed 3 times in 20 mL TBST and the secondary antibody (diluted in TBST) was added. After 1 h the membrane was washed 3 times with 20 mL TBST and one time with 20 mL TBS (5 min each). Signal was developed using the Western Lightning *Plus* ECL Kit (Perkin Elmer) according to the manufacturer´s instructions.

6.4 Nuclear extract preparation

6.4.1 Suspension cells

Nuclear extracts from A. thaliana suspension cells were prepared from protoplasts. Protoplasts were prepared as described in section 5.5. To isolate the nuclei, protoplasts were resuspended in 20 mL NIBA buffer (20 mM HEPES pH 7.4, 20 mM KCl, 13.8% Hexylene glycol, 1% Triton X-100, 50 µM spermine, 125 µM spermidine, protease inhibitor tablet) resulting in the lysis of the plasma membrane and most cellular organelles (but not nuclei). Suspensions were filtered through 30 µM nylon membranes and centrifuged (1000 g, 4°C, 12 min). The pellet was resuspended in a small volume of NIBA buffer and layered on top of a 1.5 M sucrose cushion. After centrifugation (10000 g, 4°C, 20 min) the pellet was washed four times with 0.5 mL of NIBA (10000 g, 4°C, 5 min).

To extract nuclear proteins the nuclei pellet was resuspendend in 340 µL NLB buffer (10 mM Tris pH 7.5, 500 mM NaCl, 1% Triton X-100, 10% glycerol, 1 mM $Na_4P_2O_7$, protease inhibitor cocktail) and subjected to sonification on a Bandelin Sonopuls HD2070 (25 seconds, 50% duty cycle, 10% power output; seven repetitions with one minute rest on ice between each cycle). After centrifugation (12000 g, 4°C, 15 min) the supernatant was recovered and protein concentration was determined by Bradford assay. Typical concentrations were 5 – 10 µg/µL. Nuclear extracts were stored in aliquots at – 80°C.

6.4.2 Seedlings

Seedlings (1 - 4 g) were ground to a fine powder in liquid nitrogen. If seedlings were grown in liquid MS, they were harvested in a sieve, extensively washed with tap water and dried in paper towels. The powder was resuspended in 2 mL of LB-buffer (20 mM Tris pH 7.4, 25% glycerol, 20 mM KCl, 2 mM EDTA, 2.5 mM $MgCl_2$, 250 mM sucrose, 1 mM DTT, PI) per gram of tissue and homogenization was achieved by vigorous vortexing. The homogenate was filtered through two layers of Miracloth and the filtrate was centrifuged (1500 g, 15 min, 4°C). The pellet containing nuclei and chloroplasts was resuspendend in 5 mL of NRBT-buffer (20 mM Tris pH 7.4, 25% glycerol, 2.5 mM $MgCl_2$, 0.2% Triton X-100, PI) first with inoculation needles and then by gentle shaking. After centrifugation (1000 g, 10 min, 4°C) the supernatant was discarded and the washing step of the pellet was repeated up to three times until the pellet appeared white or only slightly green. The nuclei were then resuspended in 1 x IP-buffer (SIGMA) and lysed by sonication (30 sec, 30% duty cycle, 40% power output, 5 times). After sonication the extracts were treated for 1 h with 50 units Benzonase (Sigma) at 4°C. After centrifugation (14000 rpm, 15 min, 4°C in benchtop centrifuge) the supernatant was recovered, protein concentration was estimated by Bradford assay, aliquoted and stored at – 80°C.

6.4.3 Protoplast isolation

Protoplasts were generated from *Arabidopsis thaliana* cell suspension cultures grown in the dark. Cell cultures were centrifuged at 2000 g for 10 min and the supernatant was discarded. Approximately 5 g of cells were resuspended in 20 mL of enzyme solution (0.4 M mannitol, 20 mM KCl, 20 mM MES pH 5.7, 10 mM $MgCl_2$, 0.1 % BSA, 2% Cellulase, 1% Macerocym) and incubated for 3 – 4 h at room temperature with gentle agitation (60 rpm). Every hour, cells were gently pipetted up and down to resuspend cell clumps. The reaction was stopped with 20 mL W5 solution (20 mM MES pH 5.7, 154 mM NaCl, 125 mM $CaCl_2$, 5 mM KCl) and the suspension was filtered through two layers of miracloth. Protoplasts were washed two times with 20 mL cold W5 (100 g, 3 min, 4°C). After the last centrifugation step cells were resuspended in 4 mL cold W5 to count them in a hemacytometer. The concentration of the protoplast suspension was adjusted to 10^6 cells/mL with W5.

6.5 Measurement of HDAC activity

6.5.1 Nuclear extracts

HDAC activity in protein extracts was measured using the Epigenase™ HDAC Activity/Inhibition Direct Assay Kit (Fluorimetric, Epigentek), according to the manufacturer´s instructions. Briefly, 0.5 – 10 µg of protein extract per well were incubated with 50 ng of substrate for 90 min at room temperature. Deacetylated product was immuno-detected and fluorescence at Ex/Em = 530/590 nm was measured on a fluorescence microplate reader (Tecan infinite 1000). After subtracting the blank, the RFU values were directly used for relative quantification. For absolute quantification standard curves were recorded as described in the manual. All chemicals were tested for interference with the assay by performing standard curves in the presence of this chemical. In most of the cases, effector chemicals were directly added into the wells because no interference could be detected. Since DTT interfered with the assay, protein samples were desalted (ZebaSpin™ columns) after incubation with DTT and then subjected to HDAC measurements.

6.5.2 Protoplasts

HDAC activity in protoplasts was measured using the *InSitu* HDAC Activity Fluorometric Assay Kit (BioVision) with some modifications. 10^5 protoplasts per well were incubated with 1 µl of substrate at room temperature in the presence or absence of effector chemicals (cPTIO was added 10 min before addition of the substrate). The reaction was stopped by adding fluorescence developer and mixing well by pipetting up and down to ensure proper lysis and homogenization of the cells. For each treatment one well was stopped directly after addition of the substrate (t = 0) a second well was stopped after 30 min (t = 30 min). After lysis, the plate was incubated for 30 min at 37°C to develop the signal. Fluorescence was measured at Ex/Em = 368/442 nm in a fluorescence microplate reader (Tecan infinite 1000). The difference in fluorescence between t = 0 and t = 30 min was used to quantify HDAC activity. All chemicals which were used (GSNO, SNAP, GSSG, SA, INA, cPTIO, DTT) were tested for interference with the assay by performing standard curves and by monitoring kinetics of the fluorescence development in the presence of this chemical.

6.6 Measurement of NO production in protoplasts

2 x 10^5 protoplasts were incubated with 15 µM DAF-FM DA for 15 min at room temperature in the dark. After centrifugation (100 g, 2 min, RT) protoplasts were resuspended in 200 µL W5 buffer. Then, 100 µM cPTIO or water (control) was added. After 10 min at room temperature, cells were centrifuged, resuspended in W5 and subsequently stimulated with 100 µM SA or INA. After 1 h, protoplasts were visualized using an Olympus BX700 microscope with a GFP filter set. For quantitative measurement of DAF-FM fluorescence, DAF-FM DA loaded protoplasts were stimulated with different concentrations of SA and INA

and split in wells of a black 96 well plate (Greiner, 12 technical replicates per treatment, 2 x 10^5 protoplasts/well). Fluorescence was measured on a Tecan Infinite 1000 every 10 min for a total of 20 cycles at Ex/Em = 485/535 nm.

6.7 Nitrosothiol / nitrite measurement

Nitrosothiols and nitrite was measured using the Nitric Oxide Analyzer Sievers 280i from GE Healthcare. The analyte is injected into a triiodide solution, which reduces SNOs and nitrite to NO. Then, NO is oxidized by ozone to give NO_2 (excited state) and O_2. During relaxation to its ground state NO_2 emits light which is detected in a photomultiplier. To selectively determine the SNO content, sulfanilamide is added to the analyte, which scavenges nitrite and prevents its reduction by triiodide.

100 mg of tissue was homogenized in 500 µL PBS and then incubated on ice for 10 min. After centrifugation at maximum speed in a tabletop microcentrifuge, 20 – 200 µL of the supernatant were injected into the triiodide solution (35 mL glacial acetic acid, 325 mg iodine, 500 mg KI, 10 mL ddH_2O). For SNO measurement, aliquots of the sample were diluted 1:9 with sulfanilamide and 200 µL were injected. A standard curve was recorded with sodium nitrite, and the values for nitrite and SNOs were calculated according to this standard curve.

6.8 Recombinant expression and purification

6.8.1 Expression and purification in E. coli

His6-HDA6 and GST-HDA6 were expressed in E. coli BL21 (DE3) cc4, an expression strain producing chaperones to enhance solubility of recombinant proteins (Quelle). 250 mL LB medium were inoculated with an overnight culture of the corresponding constructs transformed into the respective expression strain and grown at 37°C (200rpm) until OD_{600} reached 0.6 – 0.8. Then, the cultures were put on ice, IPTG was added to a final concentration of 1.0 mM and the cultures were incubated at 18°C overnight. Bacteria were pelleted at 4000 rpm for 20 min (SLA600 rotor).

For His6-HDA6, bacteria were resuspended in lysis buffer (50 mM phosphate pH 8.0, 300 mM NaCl, 10 mM imidazole, 0.1% Triton X-100) and lysed by sonication (3 min, 30% duty cycle, 60% power output, repeat three to four times). The lysate was cleared by centrifugation (16000 g, 60 min, 4°C). The supernatant was loaded on a preequilibrated HisTrap (1 mL) Fast flow (GE Healthcare) connected to a syringe. After extensive washing with Wash buffer 1 (15 CV with 20 mM phosphate, 500 mM NaCl, 20 mM imidazole, pH 8)

bound protein was eluted in 5 CV Elution buffer (20 mM phosphate, 500 mM NaCl, 500 mM imidazole, pH 8).

For GST-HDA6, bacteria were lysed in lysis buffer (20 mM phosphate pH 7.4, 300 mM NaCl, 10 mM EDTA, 1x complete protease inhibitor (Roche), 1 mg/mL lysozyme). After clearing, the supernatant (15 mL) was incubated with 0.5 mL of equilibrated GT-Sepharose 4B (GE Healthcare) for 30 min at 4°C. After washing three times with 15 mL Washing buffer (20 mM phosphate pH 7.4, 300 mM NaCl, 10 mM EDTA, 1x complete protease inhibitor (Roche)) for 30 min at 4°C, bound protein was eluted in 200 mM Tris pH 7.4 supplemented with 40 mM reduced glutathione and 10 mM EDTA. Elution was performed three times with 0.5 mL of elution buffer (1^{st} time: 30 min incubation, 2^{nd} and 3^{rd} time: 10 min incubation). In all steps, GT-beads were recovered by centrifugation at 500 g for 5 min. Fractions were analyzed for the presence of HDA6 on a precast 12% acrylamide gel (Biorad).

6.8.2 Expression and purification in H5 (insect) cells

Expression and purification was done by Dr. Georg Huber from the Protein Purification core facility. 150 ml H5 cells ($1x10^6$ cells/ml) were infected with MOI 1 and harvested 56h pi. Cells were resuspended in lysis buffer (200 mM NaCl, 25 mM Tris pH 8.0, 20 mM imidazole, 10 mM $MgSO_4$, 10 µg/ml DNaseI (Serva), 1 mM protease inhibitor mix AeBSF-HCl (Roth), 0.01% thioglycerol, 0.5% NP40) and sonicated on ice 3 x 1 min (Bandelin sonifier: duty cycle 30%, power 50%) with intermediate cooling. The lysate was centrifuged (30 min, 32000 g, 4°C) and the supernatant was cleared through a 0.45 µm-filter. The cleared lysate was applied to a 5 ml Ni-chelating resin (GE Healthcare) and washed (200 mM NaCl, 25 mM Tris pH 8.0, 30 mM imidazole, 0.01% thioglycerol). Bound proteins were eluted (200 mM NaCl, 25 mM Tris pH 8.0, 300 mM imidazole, 0.01% thioglycerol) and analyzed by SDS-PAGE followed by coomassie-staining. HDA6-positive fractions were pooled, concentrated by spin-concentrators (MWCO 10 kDa) and separated by gelfiltration (S200GL, GE Healthcare). HDA6-positive fractions were identified by Coomassie-stained SDS-PAGE, pooled and concentration was determined by photometric measurement using the specific extinction coefficient of HDA6 (ProtParam/ExPASY). Purity was >90% and yielded in 0.27mg/ml (5 ml in total).

6.9 Biotin switch

The biotin switch assay was performed as previously described [195] using 5 µg of recombinant protein. Briefly, the protein was incubated with GSNO in HEN buffer to S-nitrosylate cysteine residues. Then, free cysteines were blocked using MMTS and S-nitrosylated Cys were reduced by addition of ascorbate. The free thiol groups were then labeled using Biotin-HPDP and detected in a western blot.

6.10 Chromatin immunoprecipitation followed by deep sequencing (ChIPseq)

All steps were carried out as described detailed in the manual for the Plant ChIPseq Kit from Diagenode, with small modifications. Therefore, only short descriptions including adaptations of the protocol are given below. For all steps filter tips were used to avoid cross-contamination between samples. For both biological replicates all samples were treated in parallel, all libraries were done at the same day.

6.10.1 Treatments

Liquid grown A. thaliana seedlings (7 days old) were used to exclude contamination with bacterial and/or fungal DNA from soil. One flask (containing approximately two gram of tissue) per condition and time point was treated with water (control), 250 µM GSNO (stock 50 mM in water), 250 µM GSH (stock 100 mM in water), 250 µM GSNO/ 500 µM cPTIO (100 mM in water) or 5 µM TSA (10 mM in ethanol). Differences in the volume of added solvent between the treatments were equalized with sterile water. For the control treatment three time points were sampled (0, 3, 16 h), for all other treatments, two time points were sampled (3, 16 h). Since the light was switched off at 17.00 in the growth chamber used, treatments were started at this time to ensure that light mediated degradation of the compounds was kept to a minimum.

6.10.2 Crosslinking and harvesting

1 g of plant tissue was crosslinked on ice in 1% formaldehyde (methanol free 16% solution, SIGMA) for 15 min in an exsiccator connected to a vacuum pump. The vacuum was released after 5 min, the floating tissue was submerged and vacuum was applied for additional 10 min. Crosslinking was stopped by addition of glycine and subsequent vacuum infiltration for 5 min. After washing the X-linked tissue was snap-frozen and stored at – 80°C.

6.10.3 Chromatin isolation and shearing

The X-linked tissue was ground to a fine powder with mortar and pestle. The powder was homogenized in Extraction buffer 1, the nuclei were pelleted by centrifugation and subsequently washed 5 times with Extraction buffer 2 and once with Extraction buffer 3. To shear the chromatin, the nuclear pellet was resuspended in 300 µL of sonication buffer und subjected to sonication in a Bioruptor Pico (Diagenode). Settings were: 30 sec ON/OFF, 13 cycles, power high. After centrifugation the supernatant was recovered. 50 µL of this chromatin preparation were used per IP and to check shearing efficiency later, another 50 µL aliquot was saved. The remaining 200 µl were stored at – 80°C.

6.10.4 Immunoprecipitation

220 µL of magnetic beads were washed and incubated with 11 µg of anti-H3K9/14ac antibody (1 µg/IP) for 7.5 h at 4°C on a rotating wheel set at lowest speed (around 40 rpm) to couple the antibody to the beads. Per IP, 20 µL of the antibody coupled beads were incubated with 250 µL of chromatin (1:5 diluted) and 0.25 µL of protease inhibitor overnight at 4°C on a rotating wheel at 40 rpm. 10 µL of the diluted chromatin were saved as input control (4%). The next morning, the immune-complexes were captured and washed extensively with wash buffers 1 - 4.

6.10.5 Elution, reverse crosslinking and quantification of ChIPed DNA

Washed beads and input samples were incubated in 100µL and 90 µL Elution buffer (IPure-Kit, Diagenode) for 4 h at 65°C (1300 rpm), respectively. The DNA was purified using the IPure-Kit from Diagenode according to the manufacturer´s instructions. Elution was performed in two steps using 25 µL Buffer C each. Total elution volume was 50 µL. ChIPed DNA was quantified using the QuantiT Pico Green Assay (Invitrogen). Assay volume was 200 µL and fluorescence was measured on a Tecan Infinite 1000.

6.10.6 Library preparation

Individual libraries were prepared using the Microplex Library Preparation Kit v2 (Diagenode, 48 indices) with 1 ng of starting material and 11 cycles in the amplification step according to the manufacturer´s instructions. Equal volumes (10 µL) of each individual, indexed library were pooled and purified with AMPure Resin (Beckmann Coulter). An aliquot of the final library was sequenced on a HiSeq3000.

6.10.7 Bioinformatic analysis

Reads were demultiplexed, filtered (based on quality phred scores) and mapped to the Arabidopsis genome (TAIR10) only keeping uniquely mapped reads. Since we sequenced the final library for a total of four times (technical replicates), corresponding read sets were merged for further analysis. Peaks were called using stringent settings ($p < 0.01$) using the appropriate input control as background reference. Peak lists were exported in .bed format whereas read mappings were stored as .bam files. All steps were carried out using the CLC genomics workbench (Quiagen). Quantitative comparison of the treatments was done using the R package DiffBind. Briefly, a common list of peaks is generated from all the treatment peak lists. Then, (normalized) reads mapping to these peak regions are computed. Reads from the corresponding background control (input) are subtracted. In the next step, groups to be compared are defined (control vs GSNO, control vs cPTIO, control vs GSH, GSNO vs GSH,…). Based on a false discovery threshold, significantly regulated peaks between these groups are then calculated.

6.10.8 ChIPqPCR

To validate the results from the ChIPseq analysis, selected peak regions and differentially regulated peaks were confirmed by qPCR. Therefore, the ChIP´ed and input chromatin was diluted 1 : 10 in ddH_20 and four µL of these dilutions were used as input for qPCR. qPCR was performed on an ABI 7500 Fast Real time thermal cycler (Applied Biosystems) using the SensiMix™ SYBR Low-Rox Kit (BioLine) according to the manufacturer´s instructions. Ct-values were computed and expressed as % of the input using the following formula:

$$\% \text{ input} = \frac{(1+eff)^{40-Ct}}{(1+eff)^{40-Ctinput}*25} \ 100\%$$

where Ct and Ctinput are the Ct-values of the ChIP and input sample, respectively. (1 + eff) describes amplification efficiency.

7 References

1. Nott, A., et al., *S-Nitrosylation of histone deacetylase 2 induces chromatin remodelling in neurons.* Nature, 2008. **455**(7211): p. 411-5.
2. Chen, T.W., et al., *ChIPseek, a web-based analysis tool for ChIP data.* BMC Genomics, 2014. **15**: p. 539.
3. Feng, J.H., et al., *Expression, purification, and S-nitrosylation of recombinant histone deacetylase 8 in Escherichia coli.* Biosci Trends, 2011. **5**(1): p. 17-22.
4. Powis, G., M. Briehl, and J. Oblong, *Redox signalling and the control of cell growth and death.* Pharmacol Ther, 1995. **68**(1): p. 149-73.
5. Schmidt, R. and J.H. Schippers, *ROS-mediated redox signaling during cell differentiation in plants.* Biochim Biophys Acta, 2015. **1850**(8): p. 1497-1508.
6. Dalle-Donne, I., et al., *Protein S-glutathionylation: a regulatory device from bacteria to humans.* Trends Biochem Sci, 2009. **34**(2): p. 85-96.
7. Marshall, H.E., K. Merchant, and J.S. Stamler, *Nitrosation and oxidation in the regulation of gene expression.* FASEB J, 2000. **14**(13): p. 1889-900.
8. Kovtun, Y., et al., *Functional analysis of oxidative stress-activated mitogen-activated protein kinase cascade in plants.* Proc Natl Acad Sci U S A, 2000. **97**(6): p. 2940-5.
9. Considine, M.J. and C.H. Foyer, *Redox regulation of plant development.* Antioxid Redox Signal, 2014. **21**(9): p. 1305-26.
10. Rouhier, N., et al., *Involvement of thiol-based mechanisms in plant development.* Biochim Biophys Acta, 2015. **1850**(8): p. 1479-1496.
11. Golldack, D., et al., *Tolerance to drought and salt stress in plants: Unraveling the signaling networks.* Front Plant Sci, 2014. **5**: p. 151.
12. Cantrel, C., et al., *Nitric oxide participates in cold-responsive phosphosphingolipid formation and gene expression in Arabidopsis thaliana.* New Phytol, 2011. **189**(2): p. 415-27.
13. Huang, G.T., et al., *Signal transduction during cold, salt, and drought stresses in plants.* Mol Biol Rep, 2012. **39**(2): p. 969-87.
14. Lindermayr, C., et al., *Redox regulation of the NPR1-TGA1 system of Arabidopsis thaliana by nitric oxide.* Plant Cell, 2010. **22**(8): p. 2894-907.
15. Tada, Y., et al., *Plant immunity requires conformational changes [corrected] of NPR1 via S-nitrosylation and thioredoxins.* Science, 2008. **321**(5891): p. 952-6.
16. Delledonne, M., et al., *Nitric oxide functions as a signal in plant disease resistance.* Nature, 1998. **394**(6693): p. 585-8.
17. Durner, J., D. Wendehenne, and D.F. Klessig, *Defense gene induction in tobacco by nitric oxide, cyclic GMP, and cyclic ADP-ribose.* Proc Natl Acad Sci U S A, 1998. **95**(17): p. 10328-33.
18. Besson-Bard, A., et al., *Real-time electrochemical detection of extracellular nitric oxide in tobacco cells exposed to cryptogein, an elicitor of defence responses.* J Exp Bot, 2008. **59**(12): p. 3407-14.
19. Feechan, A., et al., *A central role for S-nitrosothiols in plant disease resistance.* Proc Natl Acad Sci U S A, 2005. **102**(22): p. 8054-9.
20. Kovacs, I., J. Durner, and C. Lindermayr, *Crosstalk between nitric oxide and glutathione is required for NONEXPRESSOR OF PATHOGENESIS-RELATED GENES 1 (NPR1)-dependent defense signaling in Arabidopsis thaliana.* New Phytol, 2015.
21. Yun, B.W., et al., *S-nitrosylation of NADPH oxidase regulates cell death in plant immunity.* Nature, 2011. **478**(7368): p. 264-8.
22. Garcia-Mata, C. and L. Lamattina, *Nitric oxide and abscisic acid cross talk in guard cells.* Plant Physiol, 2002. **128**(3): p. 790-2.
23. Bright, J., et al., *ABA-induced NO generation and stomatal closure in Arabidopsis are dependent on H2O2 synthesis.* Plant J, 2006. **45**(1): p. 113-22.

24. Camejo, D., et al., *Salinity-induced changes in S-nitrosylation of pea mitochondrial proteins.* J Proteomics, 2013. **79**: p. 87-99.
25. Beligni, M.V., et al., *Nitric oxide acts as an antioxidant and delays programmed cell death in barley aleurone layers.* Plant Physiol, 2002. **129**(4): p. 1642-50.
26. Lee, U., et al., *Modulation of nitrosative stress by S-nitrosoglutathione reductase is critical for thermotolerance and plant growth in Arabidopsis.* Plant Cell, 2008. **20**(3): p. 786-802.
27. Pagnussat, G.C., et al., *Nitric oxide is required for root organogenesis.* Plant Physiol, 2002. **129**(3): p. 954-6.
28. Fernandez-Marcos, M., et al., *Nitric oxide causes root apical meristem defects and growth inhibition while reducing PIN-FORMED 1 (PIN1)-dependent acropetal auxin transport.* Proc Natl Acad Sci U S A, 2011. **108**(45): p. 18506-11.
29. Hu, X., et al., *Nitric oxide mediates gravitropic bending in soybean roots.* Plant Physiol, 2005. **137**(2): p. 663-70.
30. He, Y., et al., *Nitric oxide represses the Arabidopsis floral transition.* Science, 2004. **305**(5692): p. 1968-71.
31. Beligni, M.V. and L. Lamattina, *Nitric oxide stimulates seed germination and de-etiolation, and inhibits hypocotyl elongation, three light-inducible responses in plants.* Planta, 2000. **210**(2): p. 215-21.
32. Corpas, F.J., et al., *Constitutive arginine-dependent nitric oxide synthase activity in different organs of pea seedlings during plant development.* Planta, 2006. **224**(2): p. 246-54.
33. Rockel, P., et al., *Regulation of nitric oxide (NO) production by plant nitrate reductase in vivo and in vitro.* J Exp Bot, 2002. **53**(366): p. 103-10.
34. Yamamoto-Katou, A., et al., *Nitrate reductase is responsible for elicitin-induced nitric oxide production in Nicotiana benthamiana.* Plant Cell Physiol, 2006. **47**(6): p. 726-35.
35. Srivastava, N., et al., *Nitric oxide production occurs downstream of reactive oxygen species in guard cells during stomatal closure induced by chitosan in abaxial epidermis of Pisum sativum.* Planta, 2009. **229**(4): p. 757-65.
36. Planchet, E., et al., *Nitric oxide emission from tobacco leaves and cell suspensions: rate limiting factors and evidence for the involvement of mitochondrial electron transport.* Plant J, 2005. **41**(5): p. 732-43.
37. Russwurm, M. and D. Koesling, *NO activation of guanylyl cyclase.* EMBO J, 2004. **23**(22): p. 4443-50.
38. Nelson, M.J., *The nitric oxide complex of ferrous soybean lipoxygenase-1. Substrate, pH, and ethanol effects on the active-site iron.* J Biol Chem, 1987. **262**(25): p. 12137-42.
39. Mathieu, C., et al., *Direct detection of radicals in intact soybean nodules: presence of nitric oxide-leghemoglobin complexes.* Free Radic Biol Med, 1998. **24**(7-8): p. 1242-9.
40. Herold, S. and A. Puppo, *Oxyleghemoglobin scavenges nitrogen monoxide and peroxynitrite: a possible role in functioning nodules?* J Biol Inorg Chem, 2005. **10**(8): p. 935-45.
41. Perazzolli, M., et al., *Arabidopsis nonsymbiotic hemoglobin AHb1 modulates nitric oxide bioactivity.* Plant Cell, 2004. **16**(10): p. 2785-94.
42. Millar, A.H. and D.A. Day, *Nitric oxide inhibits the cytochrome oxidase but not the alternative oxidase of plant mitochondria.* FEBS Lett, 1996. **398**(2-3): p. 155-8.
43. Navarre, D.A., et al., *Nitric oxide modulates the activity of tobacco aconitase.* Plant Physiol, 2000. **122**(2): p. 573-82.
44. Clark, D., et al., *Nitric oxide inhibition of tobacco catalase and ascorbate peroxidase.* Mol Plant Microbe Interact, 2000. **13**(12): p. 1380-4.
45. Ferrer-Sueta, G. and R. Radi, *Chemical biology of peroxynitrite: kinetics, diffusion, and radicals.* ACS Chem Biol, 2009. **4**(3): p. 161-77.
46. Bayden, A.S., et al., *Factors influencing protein tyrosine nitration--structure-based predictive models.* Free Radic Biol Med, 2011. **50**(6): p. 749-62.
47. Cecconi, D., et al., *Protein nitration during defense response in Arabidopsis thaliana.* Electrophoresis, 2009. **30**(14): p. 2460-8.

48. Gaupels, F., et al., *Detection of peroxynitrite accumulation in Arabidopsis thaliana during the hypersensitive defense response.* Nitric Oxide, 2011. **25**(2): p. 222-8.
49. David, A., et al., *Nitric oxide accumulation and protein tyrosine nitration as a rapid and long distance signalling response to salt stress in sunflower seedlings.* Nitric Oxide, 2015. **50**: p. 28-37.
50. Holzmeister, C., et al., *Differential inhibition of Arabidopsis superoxide dismutases by peroxynitrite-mediated tyrosine nitration.* J Exp Bot, 2015. **66**(3): p. 989-99.
51. Chaki, M., et al., *High temperature triggers the metabolism of S-nitrosothiols in sunflower mediating a process of nitrosative stress which provokes the inhibition of ferredoxin-NADP reductase by tyrosine nitration.* Plant Cell Environ, 2011. **34**(11): p. 1803-18.
52. Melo, P.M., et al., *Glutamine synthetase is a molecular target of nitric oxide in root nodules of Medicago truncatula and is regulated by tyrosine nitration.* Plant Physiol, 2011. **157**(3): p. 1505-17.
53. Alvarez, C., et al., *Inhibition of Arabidopsis O-acetylserine(thiol)lyase A1 by tyrosine nitration.* J Biol Chem, 2011. **286**(1): p. 578-86.
54. Monteiro, H.P., R.J. Arai, and L.R. Travassos, *Protein tyrosine phosphorylation and protein tyrosine nitration in redox signaling.* Antioxid Redox Signal, 2008. **10**(5): p. 843-89.
55. Spadaro, D., et al., *The redox switch: dynamic regulation of protein function by cysteine modifications.* Physiol Plant, 2010. **138**(4): p. 360-71.
56. Liu, X., et al., *Accelerated reaction of nitric oxide with O2 within the hydrophobic interior of biological membranes.* Proc Natl Acad Sci U S A, 1998. **95**(5): p. 2175-9.
57. Ridnour, L.A., et al., *The chemistry of nitrosative stress induced by nitric oxide and reactive nitrogen oxide species. Putting perspective on stressful biological situations.* Biol Chem, 2004. **385**(1): p. 1-10.
58. Hogg, N., *The biochemistry and physiology of S-nitrosothiols.* Annu Rev Pharmacol Toxicol, 2002. **42**: p. 585-600.
59. Folkes, L.K. and P. Wardman, *Kinetics of the reaction between nitric oxide and glutathione: implications for thiol depletion in cells.* Free Radic Biol Med, 2004. **37**(4): p. 549-56.
60. Nakamura, T. and S.A. Lipton, *Emerging role of protein-protein transnitrosylation in cell signaling pathways.* Antioxid Redox Signal, 2013. **18**(3): p. 239-49.
61. Malik, S.I., et al., *GSNOR-mediated de-nitrosylation in the plant defence response.* Plant Sci, 2011. **181**(5): p. 540-4.
62. Lindermayr, C., et al., *Differential inhibition of Arabidopsis methionine adenosyltransferases by protein S-nitrosylation.* J Biol Chem, 2006. **281**(7): p. 4285-91.
63. Romero-Puertas, M.C., et al., *S-nitrosylation of peroxiredoxin II E promotes peroxynitrite-mediated tyrosine nitration.* Plant Cell, 2007. **19**(12): p. 4120-30.
64. Wang, Y.Q., et al., *S-nitrosylation of AtSABP3 antagonizes the expression of plant immunity.* J Biol Chem, 2009. **284**(4): p. 2131-7.
65. Hara, M.R., et al., *S-nitrosylated GAPDH initiates apoptotic cell death by nuclear translocation following Siah1 binding.* Nat Cell Biol, 2005. **7**(7): p. 665-74.
66. Abat, J.K. and R. Deswal, *Differential modulation of S-nitrosoproteome of Brassica juncea by low temperature: change in S-nitrosylation of Rubisco is responsible for the inactivation of its carboxylase activity.* Proteomics, 2009. **9**(18): p. 4368-80.
67. De Michele, R., et al., *Nitric oxide is involved in cadmium-induced programmed cell death in Arabidopsis suspension cultures.* Plant Physiol, 2009. **150**(1): p. 217-28.
68. Eichten, S.R., R.J. Schmitz, and N.M. Springer, *Epigenetics: Beyond Chromatin Modifications and Complex Genetic Regulation.* Plant Physiol, 2014. **165**(3): p. 933-947.
69. Matouk, C.C. and P.A. Marsden, *Epigenetic regulation of vascular endothelial gene expression.* Circ Res, 2008. **102**(8): p. 873-87.
70. Lilley, D.M. and J.F. Pardon, *Structure and function of chromatin.* Annu Rev Genet, 1979. **13**: p. 197-233.
71. Guelen, L., et al., *Domain organization of human chromosomes revealed by mapping of nuclear lamina interactions.* Nature, 2008. **453**(7197): p. 948-51.

72. Pope, B.D., et al., *Topologically associating domains are stable units of replication-timing regulation.* Nature, 2014. **515**(7527): p. 402-5.
73. Kim, J.M., et al., *Chromatin changes in response to drought, salinity, heat, and cold stresses in plants.* Front Plant Sci, 2015. **6**: p. 114.
74. Roudier, F., F.K. Teixeira, and V. Colot, *Chromatin indexing in Arabidopsis: an epigenomic tale of tails and more.* Trends Genet, 2009. **25**(11): p. 511-7.
75. Pikaard, C.S. and O. Mittelsten Scheid, *Epigenetic regulation in plants.* Cold Spring Harb Perspect Biol, 2014. **6**(12): p. a019315.
76. Zilberman, D., et al., *Genome-wide analysis of Arabidopsis thaliana DNA methylation uncovers an interdependence between methylation and transcription.* Nat Genet, 2007. **39**(1): p. 61-9.
77. Law, J.A. and S.E. Jacobsen, *Establishing, maintaining and modifying DNA methylation patterns in plants and animals.* Nat Rev Genet, 2010. **11**(3): p. 204-20.
78. Agius, F., A. Kapoor, and J.K. Zhu, *Role of the Arabidopsis DNA glycosylase/lyase ROS1 in active DNA demethylation.* Proc Natl Acad Sci U S A, 2006. **103**(31): p. 11796-801.
79. Deal, R.B. and S. Henikoff, *Histone variants and modifications in plant gene regulation.* Curr Opin Plant Biol, 2011. **14**(2): p. 116-22.
80. Raisner, R.M., et al., *Histone variant H2A.Z marks the 5' ends of both active and inactive genes in euchromatin.* Cell, 2005. **123**(2): p. 233-48.
81. Jerzmanowski, A., *SWI/SNF chromatin remodeling and linker histones in plants.* Biochim Biophys Acta, 2007. **1769**(5-6): p. 330-45.
82. Bratzel, F., et al., *Keeping cell identity in Arabidopsis requires PRC1 RING-finger homologs that catalyze H2A monoubiquitination.* Curr Biol, 2010. **20**(20): p. 1853-9.
83. Xu, L., et al., *The E2 ubiquitin-conjugating enzymes, AtUBC1 and AtUBC2, play redundant roles and are involved in activation of FLC expression and repression of flowering in Arabidopsis thaliana.* Plant J, 2009. **57**(2): p. 279-88.
84. Luo, M., et al., *UBIQUITIN-SPECIFIC PROTEASE 26 is required for seed development and the repression of PHERES1 in Arabidopsis.* Genetics, 2008. **180**(1): p. 229-36.
85. Houben, A., et al., *Phosphorylation of histone H3 in plants--a dynamic affair.* Biochim Biophys Acta, 2007. **1769**(5-6): p. 308-15.
86. Demidov, D., et al., *Identification and dynamics of two classes of aurora-like kinases in Arabidopsis and other plants.* Plant Cell, 2005. **17**(3): p. 836-48.
87. Widiez, T., et al., *The chromatin landscape of the moss Physcomitrella patens and its dynamics during development and drought stress.* Plant J, 2014. **79**(1): p. 67-81.
88. Sani, E., et al., *Hyperosmotic priming of Arabidopsis seedlings establishes a long-term somatic memory accompanied by specific changes of the epigenome.* Genome Biol, 2013. **14**(6): p. R59.
89. Berr, A., S. Shafiq, and W.H. Shen, *Histone modifications in transcriptional activation during plant development.* Biochim Biophys Acta, 2011. **1809**(10): p. 567-76.
90. Berr, A., et al., *Chromatin modification and remodelling: a regulatory landscape for the control of Arabidopsis defence responses upon pathogen attack.* Cell Microbiol, 2012. **14**(6): p. 829-39.
91. Pandey, R., et al., *Analysis of histone acetyltransferase and histone deacetylase families of Arabidopsis thaliana suggests functional diversification of chromatin modification among multicellular eukaryotes.* Nucleic Acids Res, 2002. **30**(23): p. 5036-55.
92. Earley, K.W., et al., *In vitro specificities of Arabidopsis co-activator histone acetyltransferases: implications for histone hyperacetylation in gene activation.* Plant J, 2007. **52**(4): p. 615-26.
93. Dangl, M., et al., *Comparative analysis of HD2 type histone deacetylases in higher plants.* Planta, 2001. **213**(2): p. 280-5.
94. Luo, M., et al., *HD2 proteins interact with RPD3-type histone deacetylases.* Plant Signal Behav, 2012. **7**(6): p. 608-10.
95. Sengupta, N. and E. Seto, *Regulation of histone deacetylase activities.* J Cell Biochem, 2004. **93**(1): p. 57-67.

96. Murfett, J., et al., *Identification of Arabidopsis histone deacetylase HDA6 mutants that affect transgene expression.* Plant Cell, 2001. **13**(5): p. 1047-61.
97. Earley, K., et al., *Erasure of histone acetylation by Arabidopsis HDA6 mediates large-scale gene silencing in nucleolar dominance.* Genes Dev, 2006. **20**(10): p. 1283-93.
98. Probst, A.V., et al., *Arabidopsis histone deacetylase HDA6 is required for maintenance of transcriptional gene silencing and determines nuclear organization of rDNA repeats.* Plant Cell, 2004. **16**(4): p. 1021-34.
99. Liu, X., et al., *HDA6 directly interacts with DNA methyltransferase MET1 and maintains transposable element silencing in Arabidopsis.* Plant Physiol, 2012. **158**(1): p. 119-29.
100. Chen, L.T., et al., *Involvement of Arabidopsis histone deacetylase HDA6 in ABA and salt stress response.* J Exp Bot, 2010. **61**(12): p. 3345-53.
101. To, T.K., et al., *Arabidopsis HDA6 is required for freezing tolerance.* Biochem Biophys Res Commun, 2011. **406**(3): p. 414-9.
102. Luo, M., et al., *Regulation of flowering time by the histone deacetylase HDA5 in Arabidopsis.* Plant J, 2015. **82**(6): p. 925-36.
103. Zhou, C., et al., *HISTONE DEACETYLASE19 is involved in jasmonic acid and ethylene signaling of pathogen response in Arabidopsis.* Plant Cell, 2005. **17**(4): p. 1196-204.
104. Choi, S.M., et al., *HDA19 is required for the repression of salicylic acid biosynthesis and salicylic acid-mediated defense responses in Arabidopsis.* Plant J, 2012. **71**(1): p. 135-46.
105. Long, J.A., et al., *TOPLESS regulates apical embryonic fate in Arabidopsis.* Science, 2006. **312**(5779): p. 1520-3.
106. Krogan, N.T., K. Hogan, and J.A. Long, *APETALA2 negatively regulates multiple floral organ identity genes in Arabidopsis by recruiting the co-repressor TOPLESS and the histone deacetylase HDA19.* Development, 2012. **139**(22): p. 4180-90.
107. Tanaka, M., A. Kikuchi, and H. Kamada, *The Arabidopsis histone deacetylases HDA6 and HDA19 contribute to the repression of embryonic properties after germination.* Plant Physiol, 2008. **146**(1): p. 149-61.
108. Zhou, Y., et al., *HISTONE DEACETYLASE19 interacts with HSL1 and participates in the repression of seed maturation genes in Arabidopsis seedlings.* Plant Cell, 2013. **25**(1): p. 134-48.
109. Benhamed, M., et al., *Arabidopsis GCN5, HD1, and TAF1/HAF2 interact to regulate histone acetylation required for light-responsive gene expression.* Plant Cell, 2006. **18**(11): p. 2893-903.
110. Liu, C., et al., *HDA18 affects cell fate in Arabidopsis root epidermis via histone acetylation at four kinase genes.* Plant Cell, 2013. **25**(1): p. 257-69.
111. Xu, C.R., et al., *Histone acetylation affects expression of cellular patterning genes in the Arabidopsis root epidermis.* Proc Natl Acad Sci U S A, 2005. **102**(40): p. 14469-74.
112. Kang, M.J., et al., *Repression of flowering under a noninductive photoperiod by the HDA9-AGL19-FT module in Arabidopsis.* New Phytol, 2015. **206**(1): p. 281-94.
113. van Zanten, M., et al., *HISTONE DEACETYLASE 9 represses seedling traits in Arabidopsis thaliana dry seeds.* Plant J, 2014.
114. Wang, C., et al., *Arabidopsis putative deacetylase AtSRT2 regulates basal defense by suppressing PAD4, EDS5 and SID2 expression.* Plant Cell Physiol, 2010. **51**(8): p. 1291-9.
115. Konig, A.C., et al., *The Arabidopsis class II sirtuin is a lysine deacetylase and interacts with mitochondrial energy metabolism.* Plant Physiol, 2014. **164**(3): p. 1401-14.
116. Huang, X., U. von Rad, and J. Durner, *Nitric oxide induces transcriptional activation of the nitric oxide-tolerant alternative oxidase in Arabidopsis suspension cells.* Planta, 2002. **215**(6): p. 914-23.
117. Polverari, A., et al., *Nitric oxide-mediated transcriptional changes in Arabidopsis thaliana.* Mol Plant Microbe Interact, 2003. **16**(12): p. 1094-105.
118. Feng, J., et al., *S-nitrosylation of phosphotransfer proteins represses cytokinin signaling.* Nat Commun, 2013. **4**: p. 1529.

119. Lozano-Juste, J. and J. Leon, *Nitric oxide regulates DELLA content and PIF expression to promote photomorphogenesis in Arabidopsis.* Plant Physiol, 2011. **156**(3): p. 1410-23.
120. Terrile, M.C., et al., *Nitric oxide influences auxin signaling through S-nitrosylation of the Arabidopsis TRANSPORT INHIBITOR RESPONSE 1 auxin receptor.* Plant J, 2012. **70**(3): p. 492-500.
121. Serpa, V., et al., *Inhibition of AtMYB2 DNA-binding by nitric oxide involves cysteine S-nitrosylation.* Biochem Biophys Res Commun, 2007. **361**(4): p. 1048-53.
122. Tavares, C.P., et al., *S-nitrosylation influences the structure and DNA binding activity of AtMYB30 transcription factor from Arabidopsis thaliana.* Biochim Biophys Acta, 2014. **1844**(4): p. 810-7.
123. Viola, I.L., L.N. Guttlein, and D.H. Gonzalez, *Redox modulation of plant developmental regulators from the class I TCP transcription factor family.* Plant Physiol, 2013. **162**(3): p. 1434-47.
124. Colussi, C., et al., *HDAC2 blockade by nitric oxide and histone deacetylase inhibitors reveals a common target in Duchenne muscular dystrophy treatment.* Proc Natl Acad Sci U S A, 2008. **105**(49): p. 19183-7.
125. Okuda, K., A. Ito, and T. Uehara, *Regulation of Histone Deacetylase 6 Activity via S-Nitrosylation.* Biol Pharm Bull, 2015. **38**(9): p. 1434-7.
126. Illi, B., et al., *Nitric oxide modulates chromatin folding in human endothelial cells via protein phosphatase 2A activation and class II histone deacetylases nuclear shuttling.* Circ Res, 2008. **102**(1): p. 51-8.
127. Chaki, M., et al., *Identification of nuclear target proteins for S-nitrosylation in pathogen-treated Arabidopsis thaliana cell cultures.* Plant Sci, 2015. **238**: p. 115-26.
128. Karmodiya, K., et al., *H3K9 and H3K14 acetylation co-occur at many gene regulatory elements, while H3K14ac marks a subset of inactive inducible promoters in mouse embryonic stem cells.* BMC Genomics, 2012. **13**: p. 424.
129. Akaike, T., et al., *Antagonistic action of imidazolineoxyl N-oxides against endothelium-derived relaxing factor/.NO through a radical reaction.* Biochemistry, 1993. **32**(3): p. 827-32.
130. Bourque, S., et al., *Type-2 histone deacetylases as new regulators of elicitor-induced cell death in plants.* New Phytol, 2011. **192**(1): p. 127-39.
131. Bailey, T., et al., *Practical guidelines for the comprehensive analysis of ChIP-seq data.* PLoS Comput Biol, 2013. **9**(11): p. e1003326.
132. Chen, L., et al., *A novel statistical method for quantitative comparison of multiple ChIP-seq datasets.* Bioinformatics, 2015. **31**(12): p. 1889-96.
133. Gadjev, I., et al., *Transcriptomic footprints disclose specificity of reactive oxygen species signaling in Arabidopsis.* Plant Physiol, 2006. **141**(2): p. 436-45.
134. He, J.M., et al., *Role and interrelationship of Galpha protein, hydrogen peroxide, and nitric oxide in ultraviolet B-induced stomatal closure in Arabidopsis leaves.* Plant Physiol, 2013. **161**(3): p. 1570-83.
135. Begara-Morales, J.C., et al., *Differential transcriptomic analysis by RNA-Seq of GSNO-responsive genes between Arabidopsis roots and leaves.* Plant Cell Physiol, 2014. **55**(6): p. 1080-95.
136. Im, J.H. and S.D. Yoo, *Transient expression in Arabidopsis leaf mesophyll protoplast system for cell-based functional analysis of MAPK cascades signaling.* Methods Mol Biol, 2014. **1171**: p. 3-12.
137. Kojima, H., et al., *Fluorescent Indicators for Imaging Nitric Oxide Production.* Angew Chem Int Ed Engl, 1999. **38**(21): p. 3209-3212.
138. Gemes, K., et al., *Cross-talk between salicylic acid and NaCl-generated reactive oxygen species and nitric oxide in tomato during acclimation to high salinity.* Physiol Plant, 2011. **142**(2): p. 179-92.
139. Zottini, M., et al., *Salicylic acid activates nitric oxide synthesis in Arabidopsis.* J Exp Bot, 2007. **58**(6): p. 1397-405.

140. Hao, F., et al., *Nia1 and Nia2 are involved in exogenous salicylic acid-induced nitric oxide generation and stomatal closure in Arabidopsis.* J Integr Plant Biol, 2010. **52**(3): p. 298-307.
141. Sun, L.R., et al., *AtNOA1 modulates nitric oxide accumulation and stomatal closure induced by salicylic acid in Arabidopsis.* Plant Signal Behav, 2010. **5**(8): p. 1022-4.
142. Watson, P.M. and A. Riccio, *Nitric oxide and histone deacetylases: A new relationship between old molecules.* Commun Integr Biol, 2009. **2**(1): p. 11-3.
143. Grandperret, V., et al., *Type-II histone deacetylases: elusive plant nuclear signal transducers.* Plant Cell Environ, 2014. **37**(6): p. 1259-69.
144. Xue, Y., et al., *GPS-SNO: computational prediction of protein S-nitrosylation sites with a modified GPS algorithm.* PLoS One, 2010. **5**(6): p. e11290.
145. Nott, A., et al., *S-nitrosylation of HDAC2 regulates the expression of the chromatin-remodeling factor Brm during radial neuron migration.* Proc Natl Acad Sci U S A, 2013. **110**(8): p. 3113-8.
146. Wu, K., et al., *HDA6 is required for jasmonate response, senescence and flowering in Arabidopsis.* J Exp Bot, 2008. **59**(2): p. 225-34.
147. Jaffrey, S.R. and S.H. Snyder, *The biotin switch method for the detection of S-nitrosylated proteins.* Sci STKE, 2001. **2001**(86): p. pl1.
148. He, G., et al., *Global epigenetic and transcriptional trends among two rice subspecies and their reciprocal hybrids.* Plant Cell, 2010. **22**(1): p. 17-33.
149. Hu, Y., et al., *Cold stress selectively unsilences tandem repeats in heterochromatin associated with accumulation of H3K9ac.* Plant Cell Environ, 2012. **35**(12): p. 2130-42.
150. Landt, S.G., et al., *ChIP-seq guidelines and practices of the ENCODE and modENCODE consortia.* Genome Res, 2012. **22**(9): p. 1813-31.
151. Wang, X., et al., *Genome-wide and organ-specific landscapes of epigenetic modifications and their relationships to mRNA and small RNA transcriptomes in maize.* Plant Cell, 2009. **21**(4): p. 1053-69.
152. Yang, H., et al., *Genome-Wide Mapping of Targets of Maize Histone Deacetylase HDA101 Reveals Its Function and Regulatory Mechanism during Seed Development.* Plant Cell, 2016. **28**(3): p. 629-45.
153. Wang, P., et al., *Epigenetic Changes are Associated with Programmed Cell Death Induced by Heat Stress in Seedling Leaves of Zea mays.* Plant Cell Physiol, 2015. **56**(5): p. 965-76.
154. Santos, A.P., et al., *Abiotic stress and induced DNA hypomethylation cause interphase chromatin structural changes in rice rDNA loci.* Cytogenet Genome Res, 2011. **132**(4): p. 297-303.
155. Tomas, D., et al., *Differential effects of high-temperature stress on nuclear topology and transcription of repetitive noncoding and coding rye sequences.* Cytogenet Genome Res, 2013. **139**(2): p. 119-27.
156. Causevic, A., et al., *Relationship between DNA methylation and histone acetylation levels, cell redox and cell differentiation states in sugarbeet lines.* Planta, 2006. **224**(4): p. 812-27.
157. Ding, B., et al., *HDT701, a histone H4 deacetylase, negatively regulates plant innate immunity by modulating histone H4 acetylation of defense-related genes in rice.* Plant Cell, 2012. **24**(9): p. 3783-94.
158. Nakashima, A., et al., *RACK1 functions in rice innate immunity by interacting with the Rac1 immune complex.* Plant Cell, 2008. **20**(8): p. 2265-79.
159. Escobar, J., et al., *Redox signaling and histone acetylation in acute pancreatitis.* Free Radic Biol Med, 2012. **52**(5): p. 819-37.
160. Sundar, I.K., H. Yao, and I. Rahman, *Oxidative stress and chromatin remodeling in chronic obstructive pulmonary disease and smoking-related diseases.* Antioxid Redox Signal, 2013. **18**(15): p. 1956-71.
161. Shimazu, T., et al., *Suppression of oxidative stress by beta-hydroxybutyrate, an endogenous histone deacetylase inhibitor.* Science, 2013. **339**(6116): p. 211-4.
162. Adcock, I.M., et al., *Redox regulation of histone deacetylases and glucocorticoid-mediated inhibition of the inflammatory response.* Antioxid Redox Signal, 2005. **7**(1-2): p. 144-52.

163. Nott, A. and A. Riccio, *Nitric oxide-mediated epigenetic mechanisms in developing neurons.* Cell Cycle, 2009. **8**(5): p. 725-30.
164. Zhao, J., *Interplay among nitric oxide and reactive oxygen species: a complex network determining cell survival or death.* Plant Signal Behav, 2007. **2**(6): p. 544-7.
165. Yu, C.W., et al., *HISTONE DEACETYLASE6 interacts with FLOWERING LOCUS D and regulates flowering in Arabidopsis.* Plant Physiol, 2011. **156**(1): p. 173-84.
166. Stamler, J.S., *Redox signaling: nitrosylation and related target interactions of nitric oxide.* Cell, 1994. **78**(6): p. 931-6.
167. Lauffer, B.E., et al., *Histone deacetylase (HDAC) inhibitor kinetic rate constants correlate with cellular histone acetylation but not transcription and cell viability.* J Biol Chem, 2013. **288**(37): p. 26926-43.
168. Fischle, W., et al., *A new family of human histone deacetylases related to Saccharomyces cerevisiae HDA1p.* J Biol Chem, 1999. **274**(17): p. 11713-20.
169. You, A., et al., *CoREST is an integral component of the CoREST- human histone deacetylase complex.* Proc Natl Acad Sci U S A, 2001. **98**(4): p. 1454-8.
170. Perrella, G., et al., *Histone deacetylase complex1 expression level titrates plant growth and abscisic acid sensitivity in Arabidopsis.* Plant Cell, 2013. **25**(9): p. 3491-505.
171. Luo, M., et al., *HD2C interacts with HDA6 and is involved in ABA and salt stress response in Arabidopsis.* J Exp Bot, 2012. **63**(8): p. 3297-306.
172. Jones, J.D. and J.L. Dangl, *The plant immune system.* Nature, 2006. **444**(7117): p. 323-9.
173. Brader, G., et al., *The MAP kinase kinase MKK2 affects disease resistance in Arabidopsis.* Mol Plant Microbe Interact, 2007. **20**(5): p. 589-96.
174. Reuber, T.L. and F.M. Ausubel, *Isolation of Arabidopsis genes that differentiate between resistance responses mediated by the RPS2 and RPM1 disease resistance genes.* Plant Cell, 1996. **8**(2): p. 241-9.
175. Lytle, B.L., et al., *Solution structure of Arabidopsis thaliana protein At5g39720.1, a member of the AIG2-like protein family.* Acta Crystallogr Sect F Struct Biol Cryst Commun, 2006. **62**(Pt 6): p. 490-3.
176. Li, Y., et al., *Aspartyl Protease-Mediated Cleavage of BAG6 Is Necessary for Autophagy and Fungal Resistance in Plants.* Plant Cell, 2016. **28**(1): p. 233-47.
177. Pandey, S.P. and I.E. Somssich, *The role of WRKY transcription factors in plant immunity.* Plant Physiol, 2009. **150**(4): p. 1648-55.
178. Kim, K.C., et al., *Arabidopsis WRKY38 and WRKY62 transcription factors interact with histone deacetylase 19 in basal defense.* Plant Cell, 2008. **20**(9): p. 2357-71.
179. Hu, Y., Q. Dong, and D. Yu, *Arabidopsis WRKY46 coordinates with WRKY70 and WRKY53 in basal resistance against pathogen Pseudomonas syringae.* Plant Sci, 2012. **185-186**: p. 288-97.
180. Mukhtar, M.S., et al., *The Arabidopsis transcription factor WRKY27 influences wilt disease symptom development caused by Ralstonia solanacearum.* Plant J, 2008. **56**(6): p. 935-47.
181. Kim, H.S. and T.P. Delaney, *Over-expression of TGA5, which encodes a bZIP transcription factor that interacts with NIM1/NPR1, confers SAR-independent resistance in Arabidopsis thaliana to Peronospora parasitica.* Plant J, 2002. **32**(2): p. 151-63.
182. Fan, W. and X. Dong, *In vivo interaction between NPR1 and transcription factor TGA2 leads to salicylic acid-mediated gene activation in Arabidopsis.* Plant Cell, 2002. **14**(6): p. 1377-89.
183. Boatwright, J.L. and K. Pajerowska-Mukhtar, *Salicylic acid: an old hormone up to new tricks.* Mol Plant Pathol, 2013. **14**(6): p. 623-34.
184. Cao, H., et al., *The Arabidopsis NPR1 gene that controls systemic acquired resistance encodes a novel protein containing ankyrin repeats.* Cell, 1997. **88**(1): p. 57-63.
185. Kinkema, M., W. Fan, and X. Dong, *Nuclear localization of NPR1 is required for activation of PR gene expression.* Plant Cell, 2000. **12**(12): p. 2339-2350.
186. Zhang, T., S. Cooper, and N. Brockdorff, *The interplay of histone modifications - writers that read.* EMBO Rep, 2015. **16**(11): p. 1467-81.

187. Floryszak-Wieczorek, J., et al., *Nitric oxide-mediated stress imprint in potato as an effect of exposure to a priming agent.* Mol Plant Microbe Interact, 2012. **25**(11): p. 1469-77.
188. Jaskiewicz, M., U. Conrath, and C. Peterhansel, *Chromatin modification acts as a memory for systemic acquired resistance in the plant stress response.* EMBO Rep, 2011. **12**(1): p. 50-5.
189. Cookson, S.J., L.E. Williams, and A.J. Miller, *Light-dark changes in cytosolic nitrate pools depend on nitrate reductase activity in Arabidopsis leaf cells.* Plant Physiol, 2005. **138**(2): p. 1097-105.
190. Guo, F.Q., M. Okamoto, and N.M. Crawford, *Identification of a plant nitric oxide synthase gene involved in hormonal signaling.* Science, 2003. **302**(5642): p. 100-3.
191. Shi, H.T., et al., *Increasing nitric oxide content in Arabidopsis thaliana by expressing rat neuronal nitric oxide synthase resulted in enhanced stress tolerance.* Plant Cell Physiol, 2012. **53**(2): p. 344-57.
192. Zheng, L., U. Baumann, and J.L. Reymond, *An efficient one-step site-directed and site-saturation mutagenesis protocol.* Nucleic Acids Res, 2004. **32**(14): p. e115.
193. Earley, K.W., et al., *Gateway-compatible vectors for plant functional genomics and proteomics.* Plant J, 2006. **45**(4): p. 616-29.
194. Bradford, M.M., *A rapid and sensitive method for the quantitation of microgram quantities of protein utilizing the principle of protein-dye binding.* Anal Biochem, 1976. **72**: p. 248-54.
195. Lindermayr, C., G. Saalbach, and J. Durner, *Proteomic identification of S-nitrosylated proteins in Arabidopsis.* Plant Physiol, 2005. **137**(3): p. 921-30.

8 Appendix

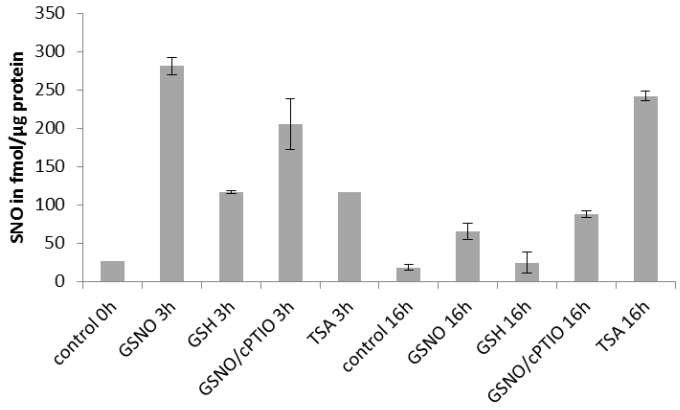

Supplemental Figure 1: **S-Nitrosothiol levels in liquid grown *Arabidopsis* seedlings after GSNO, GSH, GSNO/cPTIO and water (control) treatment.** Seedlings were treated with 250 µM GSNO, 250 µM GSH, 250 µM GSNO / 500 µM cPTIO or water and total S-nitrosothiol levels were determined after 3 and 16 h. SNOs were reduced with triiodide and the emitted NO was photochemically detected by its reaction with ozone.

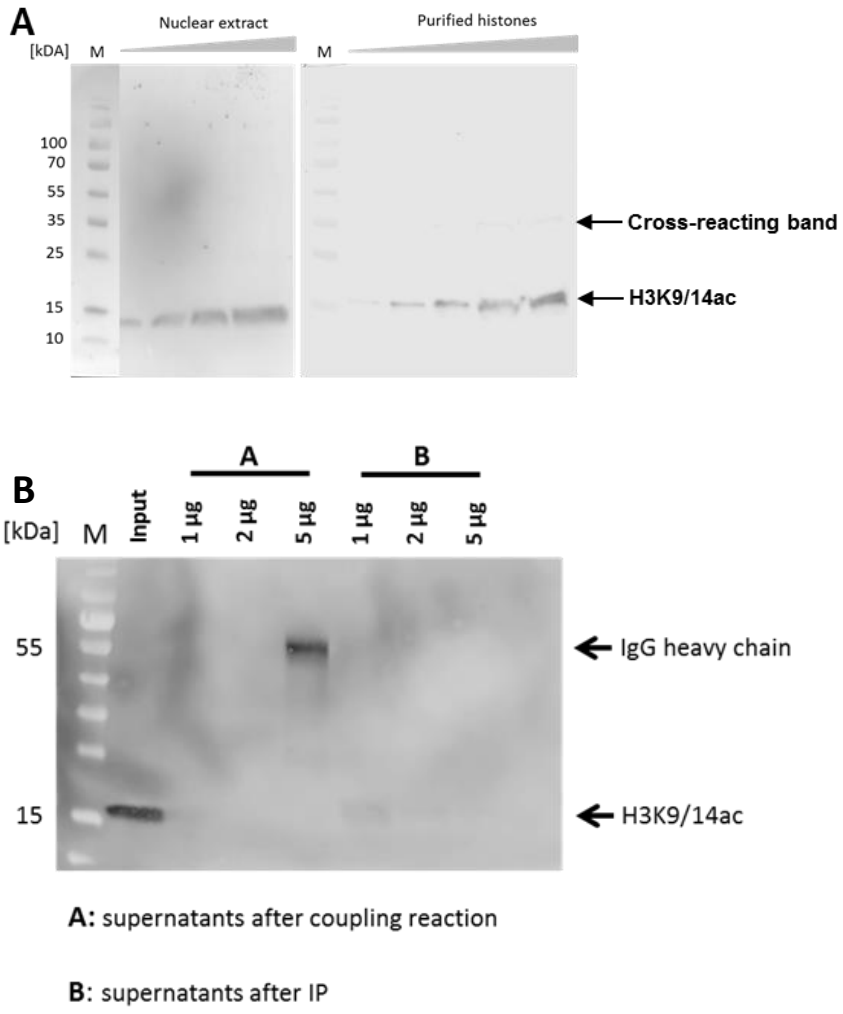

Supplemental Figure 2: **Antibody quality control and titration**. Different quantities of nuclear extracts and purified histones were separated by 12 % SDS-PAGE, blotted on nitrocellulose and probed with an anti-H3K9/14ac antibody (Diagenode). Secondary antibodies were anti-rabbit-IgG-HRP (Promega, nuclear extracts) and anti-rabbit-AP (Promega,

purified histones). The antibody was highly specific and only very weakly cross-reacted with H1, fulfilling the ENCODE criteria for ChIPseq antibodies. B) Titration experiment to determine the optimal amount of antibody. 1, 2 and 5 µg of anti-H3K9/14ac antibody were coupled to magnetic beads and aliquots of the supernatants after the coupling reaction (to assess the success of the coupling reaction) as well as after the immunoprecipitation (to check whether all antigen was immunoprecipitated) were probed with the same antibody. Sheared chromatin (input) was used as positive control. In these experiments chromatin was isolated from 2 g of starting material, for subsequent experiments only 1 g of material was used. Therefore, although a slight band is visible in lane 6, 1 µg of antibody was sufficient to immunoprecipitate all of the antigen present in the sample prepared from 1 g of tissue.

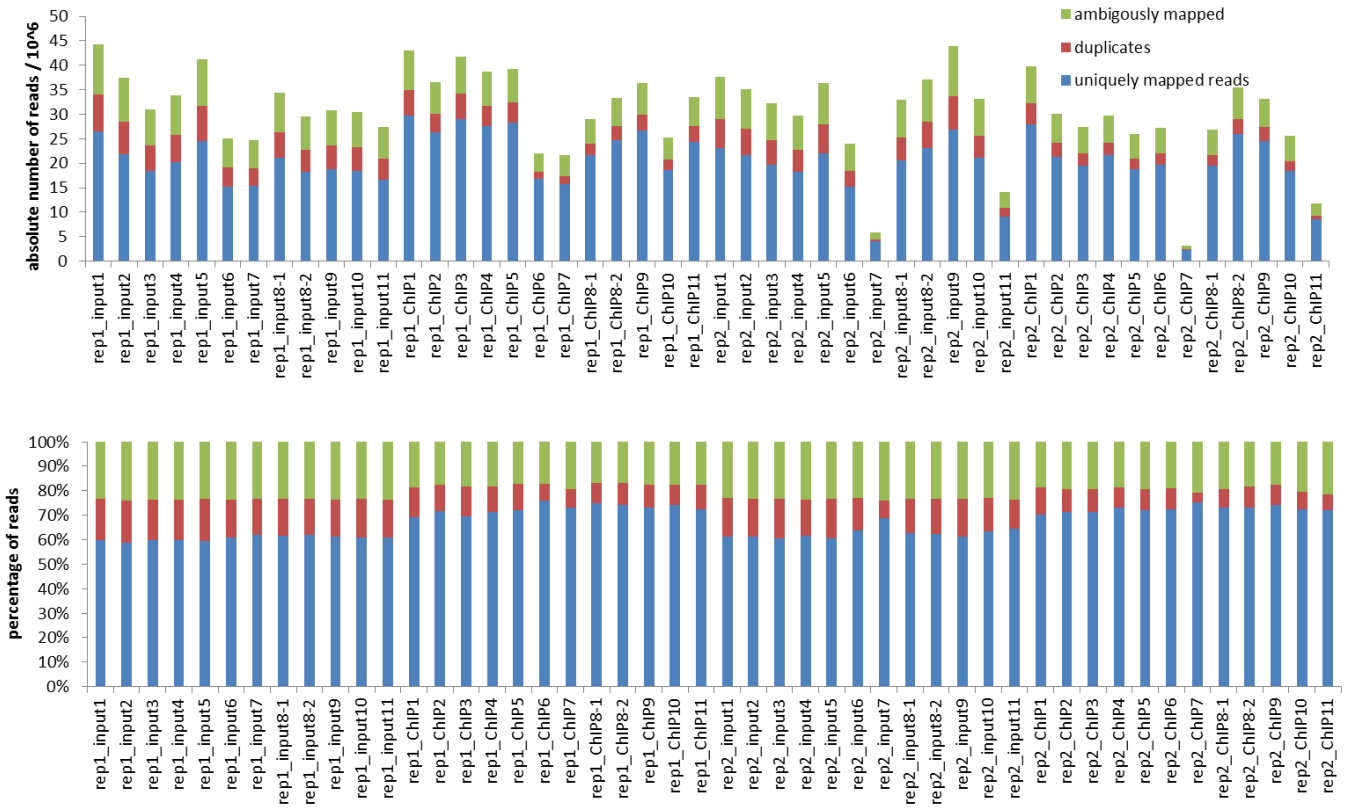

Supplemental Figure 3: **Summary of read mapping**. Raw reads generated by an Illumina HiSeq were aligned to the *Arabidopsis* reference genome (TAIR10) using the mapping tool of the clc genomics workbench (Quiagen) with default settings. Reads that mapped to more than one position and duplicate reads originating from PCR artefacts were excluded from further analysis. 15 -30 million uniquely mapping high quality reads per sample were obtained. Due to the low number of reads rep2_ChIP7 and rep2_input7 (corresponding to control treatment after 16h) could not be used for further analysis.

treatment	name	# reads	# peaks	RSC	NSC	peaks/reads
control t = 0	rep1_ChIP1	29683571	12784	1.009	1.131	0.000431
control t = 3	rep1_ChIP2	26258106	13882	1.060	1.198	0.000529
GSNO t = 3	rep1_ChIP3	29101321	13521	1.055	1.174	0.000465
GSH t = 3	rep1_ChIP4	27597269	12979	1.038	1.174	0.000470
cPTIO t = 3	rep1_ChIP5	28241039	13573	1.054	1.185	0.000481
TSA t = 3	rep1_ChIP6	16785680	13627	1.021	1.242	0.000812
control t = 16	rep1_ChIP7	15793934	6838	1.006	1.176	0.000433
GSNO t = 16	rep1_ChIP8-1	21722687	13484	1.068	1.241	0.000621
GSNO t = 16	rep1_ChIP8-2	24695272	14182	1.072	1.232	0.000574
GSH t = 16	rep1_ChIP9	26653757	13802	1.056	1.187	0.000518
cPTIO t = 16	rep1_ChIP10	18674559	10701	1.010	1.197	0.000573
TSA t = 16	rep1_ChIP11	24318293	14758	1.005	1.149	0.000607
control t = 0	rep2_ChIP1	27871262	439	0.897	1.084	0.000016
control t = 3	rep2_ChIP2	21377496	9136	0.986	1.157	0.000427
GSNO t = 3	rep2_ChIP3	19585686	7885	0.993	1.163	0.000403
GSH t = 3	rep2_ChIP4	21740591	11754	1.042	1.207	0.000541
cPTIO t = 3	rep2_ChIP5	18765809	8657	1.014	1.192	0.000461
TSA t = 3	rep2_ChIP6	19730422	11119	0.973	1.170	0.000564
control t = 16	rep2_ChIP7	2331035	1200	0.391	1.203	0.000515
GSNO t = 16	rep2_ChIP8-1	19546017	8572	0.999	1.167	0.000439
GSNO t = 16	rep2_ChIP8-2	25941867	9316	0.976	1.120	0.000359
GSH t = 16	rep2_ChIP9	24542001	13436	1.070	1.226	0.000547
cPTIO t = 16	rep2_ChIP10	18479068	6031	1.016	1.179	0.000326
TSA t = 16	rep2_ChIP11	8469745	385	0.717	1.119	0.000045

Supplemental Figure 4: Summary of peak calling parameters. The number of called peaks correlates with the number of reads in each sample. The relative strand cross-correlation (RSC) describes the ratio between the fragment-length peak and the read-length peak in the cross-correlation plot. Successful ChIP-experiments have RSC values greater than 0.8. The normalized strand coefficient describes the ratio between the fragment-length peak and the background cross-correlation values. This value should be greater than 1,05 for ChIP-seq experiments (CLC genomics workbench).

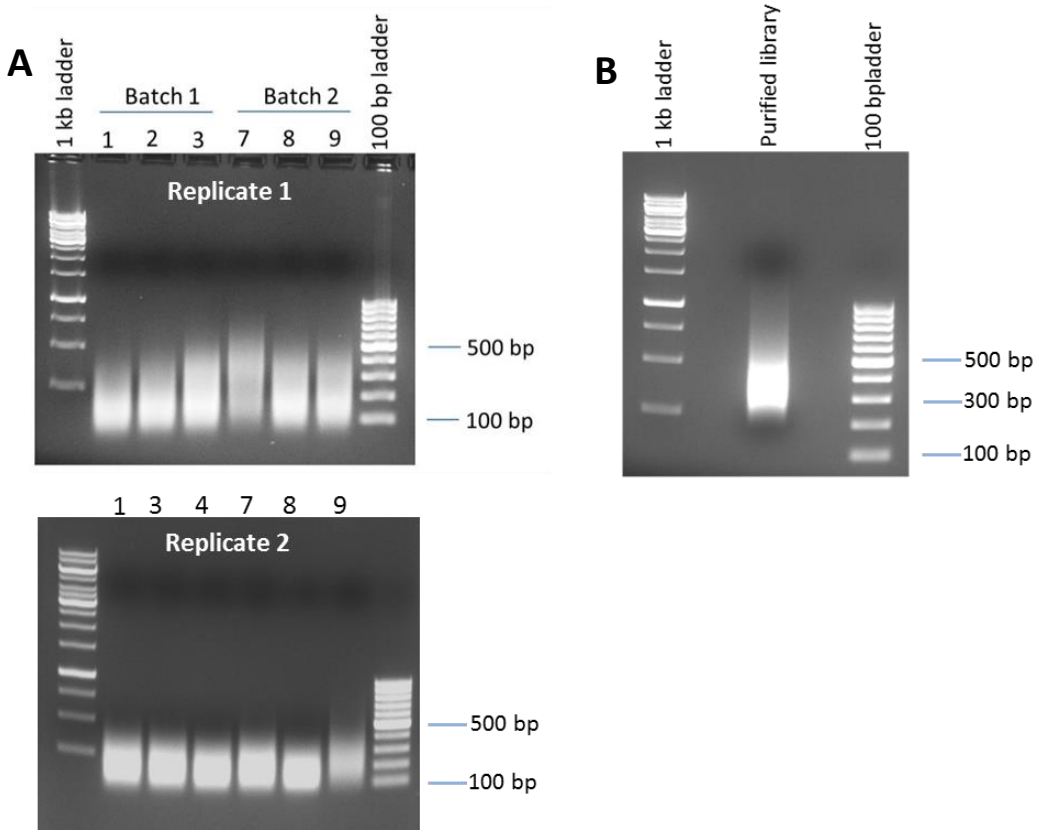

Supplemental Figure 5: Shearing and library preparation. A) Aliquots of sheared chromatin were separated on a 1.5% agarose gel and stained with ethidium bromide, revealing that the length of the fragments was between 100 and 500 bp, with a maximum at 200 bp. This length distribution was optimal for ChIPseq [150]. B) An aliquot of the final pooled library (consisting of 48 individual libraries, see Fig.1, additional technical replicates from GSNO treated sample) was separated on a 1.5% agarose gel and stained with ethidium bromide. Fragments had an average length of around 350 bp (200 bp DNA fragment + 150 bp adapters), demonstrating that library preparation was successful.

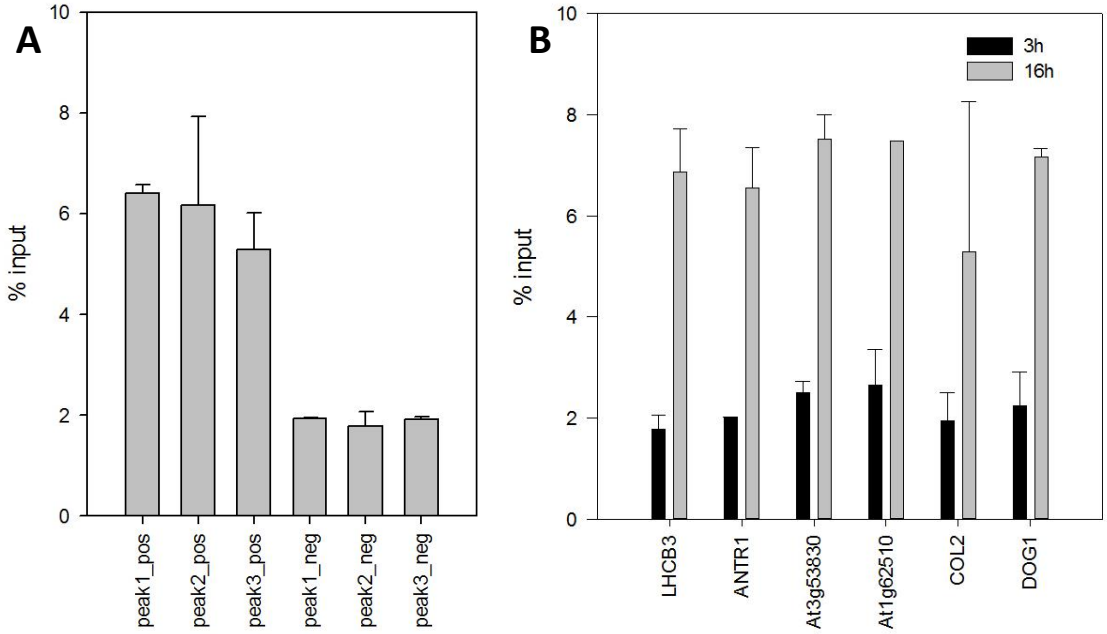

Supplemental Figure 6: Verification of Peak calling and quantitative analysis by ChIP-qPCR. A) In order to validate the peak calling algorithm, three predicted peak (Peak_pos) and adjacent non-peak (peak_neg) regions were chosen and primer sets to amplify these regions by qPCR were designed. B) To test the accuracy of the quantitative analysis, differentially regulated peaks in control_3h vs. control_16h were identified using DiffBind. The predicted sites were then confirmed using qPCR and peak-specific primer sets. All of the six candidates tested showed strongly increased H3K9/14ac levels after 16h of treatment – as determined by DiffBind. Values are expressed as % of the input. Shown is the data for two biological replicates, with two technical replicates each.

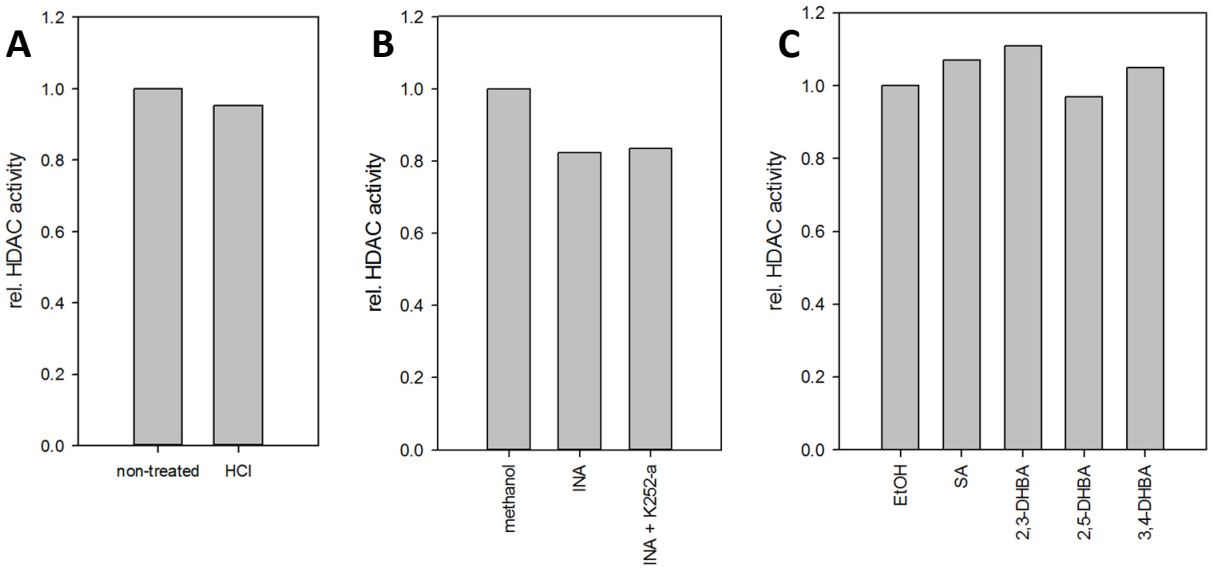

Supplemental Figure 7: HDAC assay control experiments. A) Protoplasts were incubated with diluted HCl at a pH similar to a SA/INA solution and HDAC activity was determined. B) Protoplasts were incubated with 500 µM INA and 500 µM INA + 100 nM K-252-a (kinase inhibitor) and HDAC activity was determined. C) Nuclear extracts were incubated with SA and different SA-derivatives and HDAC activity was measured. DHBA: Di-hydroxybenzoic acid.

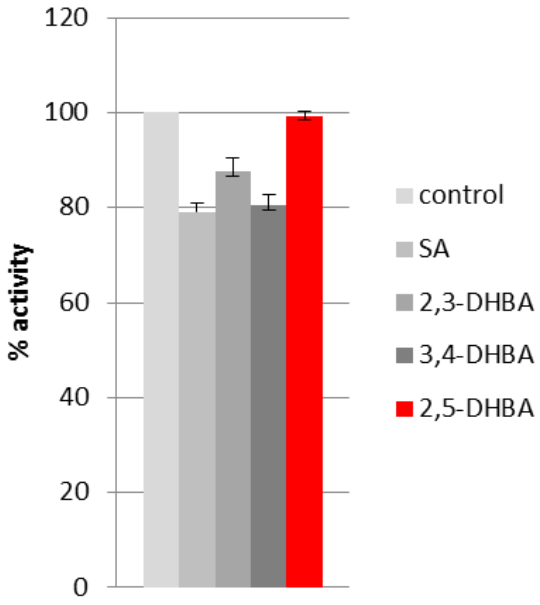

Supplemental Figure 8: Differential effect of SA derivatives on HDAC activity in protoplasts. Protoplasts were incubated with 500 µM SA, 2,3-dihydroxybenzoic acid (DHBA), 3,4-DHBA and 2,5-DHBA and HDAC activity was measured. 2,5-DHBA did not inhibit HDAC activity, indicating that the chemical structure of the inducer was critical. Shown is the mean ± SEM of three independent protoplast preparations.

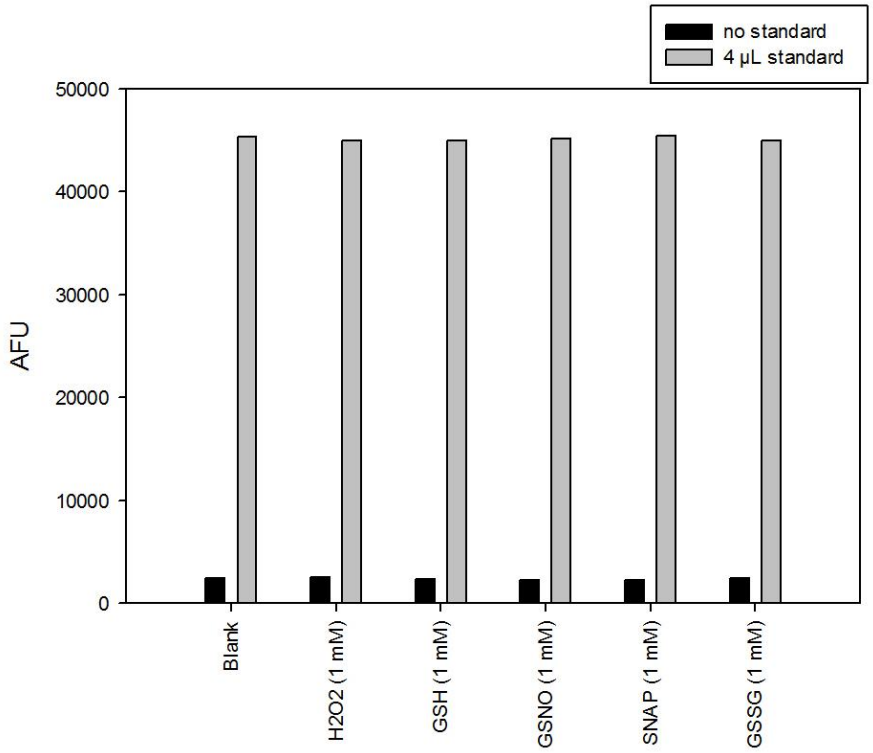

Supplemental Figure 9: Analysis of interference of H_2O_2, GSH, GSNO, SNAP and GSSG with the HDAC assay. The substrate (no standard, black bars) and deacetylated product (standard, grey bars) of the assay were incubated with the indicated chemicals and the assay was performed as described. Interference of a substance would alter the signal strength compared to Blank (no chemical present). AFU: arbitrary fluorescence units.

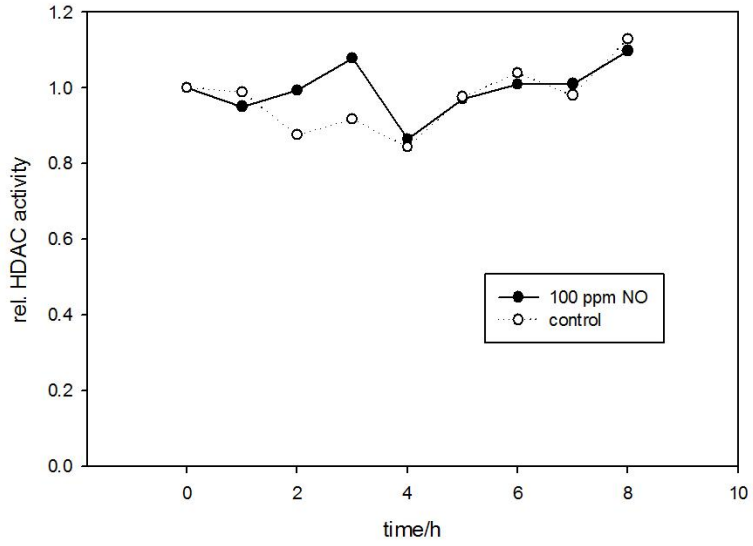

Supplemental Figure 10: HDAC activity after fumigation with 100 ppm NO. 2 week old soil-grown Arabidopsis plants were fumigated with 100 ppm NO and air (control) and after 0, 2, 4, 6 and 8 hours tissue was harvested and protein extracts were generated. HDAC activity in these extracts was measured as described. Shown is the relative HDAC activity (normalized to t = 0 h) as a function of the fumigation time. The experiment was only done once.

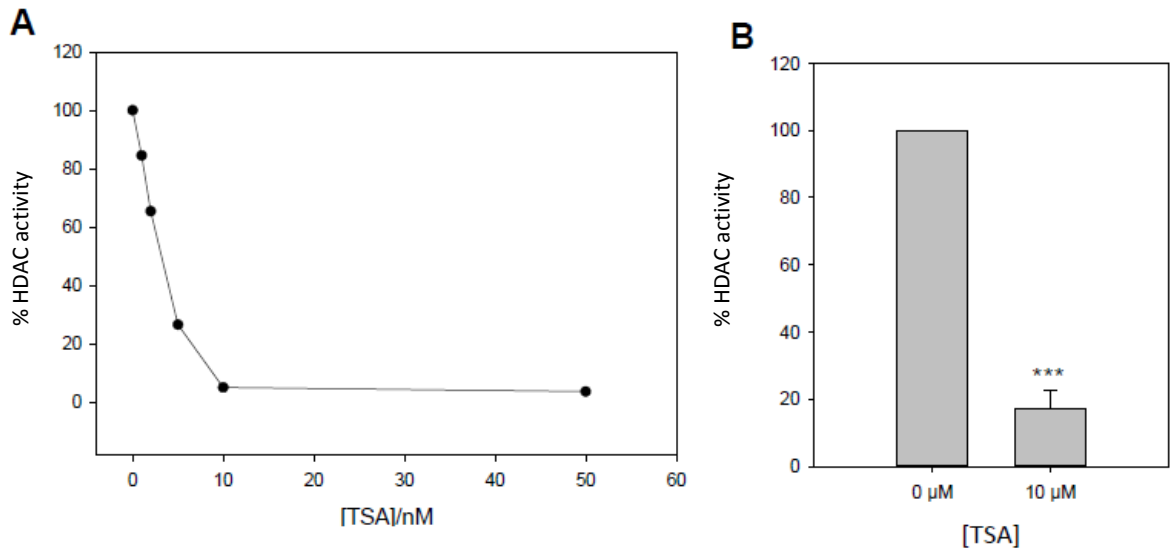

Supplemental Figure 11: Inhibition of HDAC activity by Trichostatin A. Nuclear extracts (A) and protoplasts (B) were incubated with TSA, a potent and specific HDAC inhibitor before measuring HDAC activity. Values are normalized to control treatment (DMSO) set as 100%. In A, one representative experiment is shown (n = 2). Values in B are mean ± SEM of three independent protoplast preparations. *** $P < 0.001$, student´s t-test.

Supplemental Figure 12: Alignment of human HDAC2 and Arabidopsis HDA6 and HDA19. Alignments were performed using ClustalΩ. The HDAC domain is depicted in green, conserved cysteines are marked in red, catalytically important residues are blue. Triangles indicate cysteines which were demonstrated to be nitrosylated in HDAC2 [1].

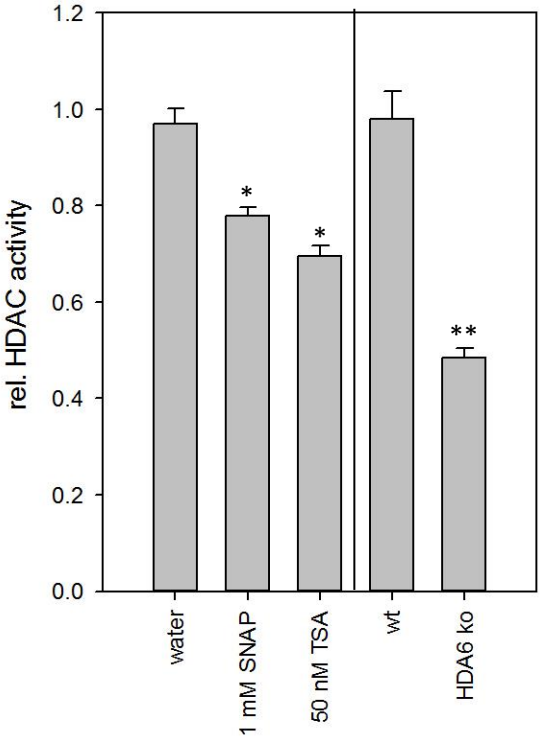

Supplemental Figure 13: HDAC activity in nuclear extracts of wt and *hda6* cell culture. Nuclear extracts were prepared according to section 5.4.2 and HDAC activity was measured as described. Values are normalized to water treatment or wt. Shown is the mean of two independent experiments with three technical replicates each. *P-value < 0.05, **P-value < 0.01.

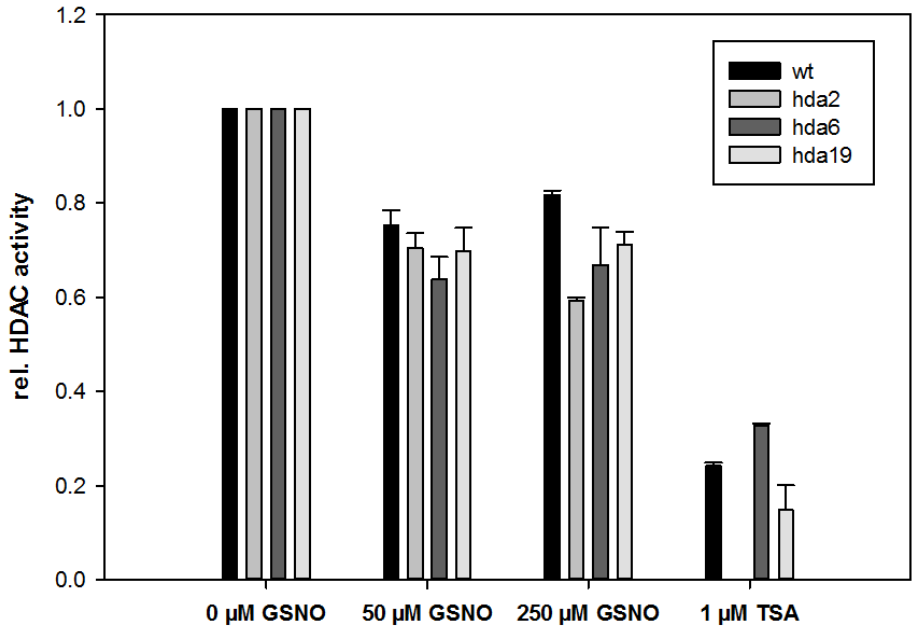

Supplemental Figure 14: Sensitivity of HDAC activity to GSNO in different HDAC mutants. Nuclear extracts from wt, *hda2*, *hda6* and *hda19* seedlings were incubated with GSNO or TSA and HDAC activity was measured. TSA was used as positive control. Shown is the mean of two technical replicates.

Motif logo	P-value	% of peaks with this motif	% of background with this motif	Similar motifs (score)
	E-168	48.71	37.16	ARR10 (0.84) AGP1 (0.82) ZmHOX2a (0.75)
	E-147	32.64	23.01	REL (0.58) AG (0.56) TRP (0.56) SEP3 (0.56) DOF2 (0.54)
	E-116	44.06	34.61	CBF (0.58) DCE (0.50)
	E-116	25.59	17.76	HMG (0.50)
	E-101	14.63	9.01	DCE (0.59) P(MYB) (0.54) PCF (0.54) RAV1 (0.51)
	E-80	39.43	31.76	AGP1 (0.64) HOX2a (0.62)
	E-62	29.04	22.90	ABI4 (0.73) MED (0.72) DCE (0.68)
	E-53	28.21	22.56	ABI4 (0.78) DCE_S_II (0.56) DCE_S_III (0.51)
	E-50	27.86	22.39	ABI4 (0.78) NtERF2 (0.73) GC-box (0.58)
	E-32	1.62	0.65	DOF2 (0.66) MNB1A (0.64) PBF (0.63) AGP1 (GATA) (0.61) DOF3 (0.56) ZmHOX2a (0.56) ARR10 (0.53)

Supplemental Figure 15: Motif analysis of H3K9/14ac peak regions. All identified ChIPseq peaks were subjected to the motif analysis tool of the ChIPSeek software. Shown are the consensus sequences of the identified motifs, the corresponding P-values, the percentage of peaks with this motif, and transcription factor binding sites, which show similarity to the identified motif. Names in red mark TFs with scores > 0.7.

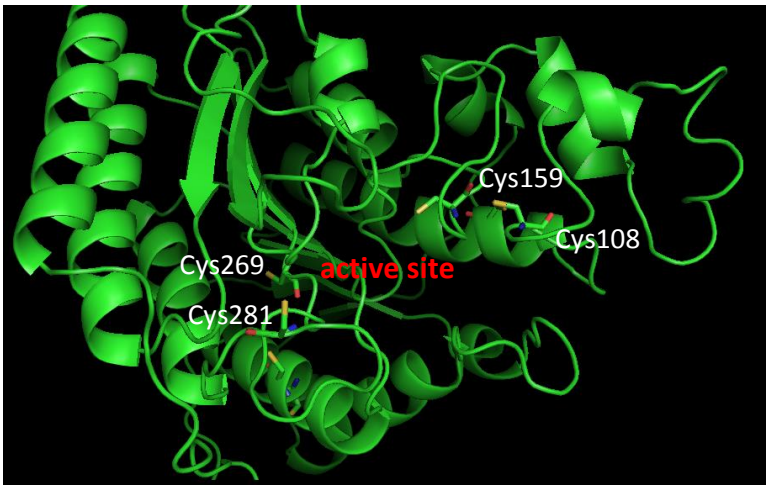

Supplemental Figure 16: Structural model of HDA19. The HDAC-domain of HDA19 was modelled using the Swiss-Prot modeling server with human HDAC2 as template (pdb entry 4LY1) and visualized with Pymol. Conserved and surface accessible cysteines are shown as sticks. The overall fold and the position of cysteines are identical to HDAC2 and HDA6.

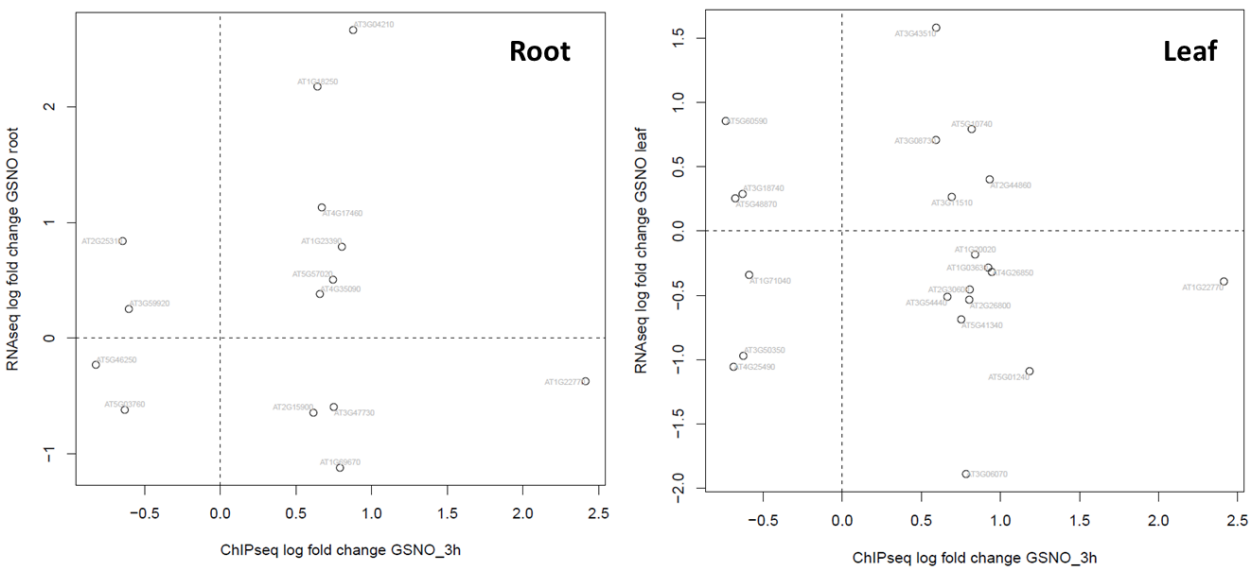

Supplemental Figure 17: Correlation analysis of H3K9/14ac and gene expression. The ChIPseq-results were compared to an RNAseq-dataset, in which *Arabidopsis* plants grown in hydroponic culture were treated with 1 mM GSNO and the transcriptomic changes were analysed separately in the root and leave. Several genes which were up- or downregulated displayed increased or decreased histone acetylation levels, respectively.

Supplemental References

"winter": www.encountersnorth.org

"flood": www.sumtercountyfl.gov

"desert": www.en.wikipedia.org

"infected Arabidopsis": www.pseudomonas-syringae.org

"root": www.noble.org

"flower": www.wikipedia.org

"gravitropism": www.pnas.org

"germination": www.mpipz.mpg.de

"stomata": www.jxb.oxfordjournals.org

Acknowledgements

First I would like to thank Prof. Jörg Durner for giving me the opportunity to work in his institute and his continuous scientific support and critical comments during this project. The freedom to integrate own ideas into this thesis greatly supported the development as an independent researcher and will be very valuable for later stages of my career.

Further, I would like to thank Dr. Christian Lindermayr for his continuous optimism and support during the PhD-thesis. The provided confidence created a very nice and relaxed working atmosphere and allowed the creative solution of scientific problems.

Special thanks go to Dr. Georg Huber from the Protein Purification Core Facility for his help with the expression of HDA6 in insect cells and the interesting and relaxing discussions and chats. I am also very grateful to Elisabeth Georgii, who helped a lot with the ChIPseq analysis.

I would also like to thank Prof. Brigitte Poppenberger-Sieberer for participation in my thesis committee. Her comments always helped to put a new perspective on my work.

Moreover, I thank all lab members and colleagues for a relaxing working atmosphere and support during scientifically and personally difficult phases.

In particular I feel grateful to you, dear Felicitas. Your happy and optimistic character as well as your great support and patience during hard-working days gave me the confidence to continue and finish this thesis. I really enjoyed every day – even the weekends – working with you.

Finally, I would like to thank my whole family for their trust and optimism during my studies and this PhD-thesis. It is a great feeling to know that decisions you make are supported by your family, no matter how the decisions look like.

Curriculum

Wilhelm Alexander Mengel
Hörwarthstraße 33
80804 München

email: w.alexandermengel@google.com
Mobil: 0170 3040787
Tel.: 089 46138150

2011/12 – 2015/11: **PhD thesis**, Institute of biochemical plant pathology
Helmholtz-centre munich (TU munich)
Title: Nitric oxide affects histone acetylation by inhibiting histone deacetylase activity in *Arabidopsis*.

2011/06 – 2011/11: **PhD thesis**, Department of biochemistry
LMU Munich, group of Prof. Karl-Peter Hopfner

2010/08 – 2011/01: **Master thesis**, Department of cell biology (Prof. Axel Ullrich)
Max-Planck institute for biochemistry, Martinsried

2010/05 – 2010/06: **Master exams** in biochemistry (grade: 1.0), cell biology (1.0) and structural biology (1.0)

2010/03: **Internship**, Institute of biochemical plant pathology
Helmholtz-centre munich, Lab of Dr. Christian Lindermayr

2009/09: **Internship**, Department of Botany
LMU munich, lab of Prof. Ute Vothknecht

2009/03: **Internship**, Department of biochemistry
LMU munich, lab of Prof. Patrick Cramer

2009/03 – 2011/01: **Master studies** in Biochemistry, LMU munich (entrance exam: 1.0)

2008/09 – 2008/12: **Bachelor thesis**, Department Translational Research in Psychiatry
Max-Planck institute of Psychiatry, Lab of Prof. Christoph Turck

2007/06 – 2011/01: **Scholarship**: “Studienstiftung des deutschen Volkes”

2005/09 – 2009/03: **Bachelor studies** Chemistry and Biochemistry, LMU munich

2005/05: **Bavarian Abitur** (final grade 1.0)

2003/09 – 2005/05: **Grammar school** Otto-von-Taube in Gauting

1996/09 – 2003/07: **Grammar school** in Starnberg

1992/09 – 1996/07: **Primary school** Ferdinand-Maria in Starnberg

1989/09 – 1992/07: **Evangelic kindergarden** in Starnberg

1985/08/22: Birth in Starnberg

Conferences:

2012/07: 4th International Plant NO club, Edinborough, UK

2014/07: 5th International Plant NO club, Munich, Germany, **Poster**

2014/08: 25th International Conference on Arabidopsis Research, Vancouver, Canada, **Poster and oral presentation**

Publications:

Leitner L, Shaposhnikov D, Mengel A, Descot A, Julien S, Hoffmann R, Posern G. "MAL/MRTF-A controls migration of non-invasive cells by upregulation of cytoskeleton-associated proteins." *J. Cell Sci*., 2011, **124**(Pt 24):4318-31

Mengel A, Chaki M, Shekariesfahlan A, Lindermayr C. "Effect of nitric oxide on transcription – S-nitrosylation of nuclear proteins." *Front Plant Sci.,* 2013, **4**:293

Chaki M, Shekariesfahlan A, Ageeva A, Mengel A, von Toerne C, Durner J, Lindermayr C. "Identification of nuclear target proteins for S-nitrosylation in pathogen-treated Arabidopsis thaliana cell cultures." *Plant Sci*., 2015, **238**: 115-126